# A STUDY OF THE MICROSTRUCTURE AND WEAR OF HIGH SPEED STEELS

ABDEL-MONEM EL-RAKAYBY

THESIS SUBMITTED FOR THE DEGREE OF

DOCTOR OF PHILOSOPHY

DEPARTMENT OF AERONAUTICAL AND MECHANICAL ENGINEERING

UNIVERSITY OF SALFORD

FEBRUARY 1986

TO MY COUNTRY ;

WHO ESTABLISHED THE

FIRST CIVILISATION

ON THE EARTH 7000

YEARS AGO . . . .

TO EGYPT, WITH LOVE.

# C O N T E N T S


page

List of Tables..... : i

List of Figures..... : ii

Acknowledgements..... : ix

Synopsis..... : x

1. INTRODUCTION : 1

2. METALLURGY OF HIGH SPEED STEELS : 4

2.1 Historical Background..... : 4

2.2 Heat Treatment of High Speed Steels..... : 5

2.2.1 Annealed high speed steels..... : 5

2.2.2 Hardening of high speed steels..... : 8

2.2.3 Tempering of high speed steels..... : 10

2.3 Techniques Used in Investigating High Speed Steels ..... : 17

2.3.1 Studies of the physical and mechanical properties ..... : 17

2.3.2 Microscopic observations..... : 18

2.3.3 Crystallography..... : 18

2.3.4 Chemical analysis..... : 20

3. WEAR OF HIGH SPEED STEELS : 21

3.1 General..... : 21

3.2 Classical Models of Wear..... : 22

3.3 Wear and Material Hardness..... : 24

3.4 Metallurgical Aspects of Wear..... : 27

3.5 Wear and Precipitated Carbides..... : 29

4. EXPERIMENTAL WORK : 37

4.1 General..... : 37

4.2 Metallurgical Investigations..... : 38

4.2.1 Sample preparation..... : 39

4.2.2 Hardness measurements..... : 40

4.2.3 Optical observations..... : 41

4.2.3.1 Volume fraction and size distribution of the primary carbides..... : 41

4.2.4 Electron probe microanalysis..... : 42

4.2.5 Electron microscopy..... : 42

4.2.5.1 Thin foil preparation..... : 44

4.2.5.2 Carbon extraction replica..... : 45

4.2.5.3 Other replicas..... : 45

4.2.6 Microanalysis..... : 46

4.3 Wear Testing..... : 50

5. RESULTS : 52

5.1 Results of Metallurgical Investigations..... : 52

5.2 Wear Results..... : 58

6. DISCUSSION : 60

6.1 Identification of Secondary Hardening Carbides in High Speed Steels..... : 60

6.2 Shape, Size, Composition and Distribution of Secondary Hardening Carbides ..... : 67

6.3 Sequence of Carbide Precipitation in High Speed Steels ..... : 71

6.4 Primary Carbides in High Speed Steels ..... : 74

6.5 Wear of High Speed Steels ..... : 77

7. CONCLUSIONS : 83

RECOMMENDATIONS FOR FUTURE WORK : 85

REFERENCES : 87

# LIST OF TABLES

Table(1): Some reported values for lattice parameters of high speed steel carbides in the pure form and as precipitated in steels, in Angstrom units [Å]

Table(2): Percentage of excess carbides existing as $M_6C$ and MC in hardened high speed steels.

Table(3): Chemical composition of high speed steels.

Table(4): Austenitising temperatures of different high speed steels.

Table(5): Chemical composition of workpiece.

Table(6): Chemical composition of secondary hardening carbides extracted from different steels tempered to their peak hardness.

Table(7): Chemical composition of different carbides precipitated in M42.

Table(8): Chemical composition of secondary MC carbides precipitated in the three steels examined.

Table(9): Some reported chemical compositions for MC carbide precipitated in different high speed steels.

Table(10): some reported chemical compositions for $M_6C$ carbide precipitated in different high speed steels.

# LIST OF FIGURES

Fig.(1): Volume percent of carbides in some quenched and annealed high speed steels.

Fig.(2): Amounts of undissolved carbides against austenitising temperature for M2 high speed steel.

Fig.(3): Schematic diagram for tempering high speed steels.

Fig.(4): Chart of the hardening cycle of M1 and M15.

Fig.(5): Rods extracted from round specimens by electro-errosion technique and discs sliced from the rods.

Fig.(6): Signals resulting from the interaction of a high energy electron beam with a crystalline material.

Fig.(7): EPMA chart showing constant molybdenum content across the standard Fe-Mo binary alloy specimen.

Fig.(8): Characteristic EDX spectrum obtained from the standard Fe-Mo binary alloy.

Fig.(9): Optical micrographs of workpiece microstructure .

(a) core and hardened surface.

(b) non-hardened core.

(c) hardened surface.

Fig.(10): Chart of Talysurf measurement of wear scar depth.

Fig.(11): Variation of hardness with tempering temperature.

Fig.(12): Carbon replica micrographs showing heterogeneous precipitation of secondary hardening carbides after tempering:

(a),(b) M42 for 2+2 hours at 430°C.

(c) M1 for 2+2 hours at 480°C.

Fig.(13): Carbon replica micrographs showing secondary hardening carbide precipitation after tempering to peak hardness. (a),(b) M42 and (c) M15.

Fig.(14): Thin foil micrographs showing secondary hardening carbide precipitated in M42 tempered to peak hardness.

Fig.(15): Carbon replica micrographs showing successful extraction of secondary hardening carbides from M42 tempered to its peak hardness.

(a) low magnification. (b) high magnification.

(c) area free from carbide precipitation.

Fig.(16): Convergent beam single crystal diffraction patterns of secondary hardening carbides extracted from :

(a) M42, zone axis [011].

(b) M42, zone axis $[\bar{1}14]$.

(c) M15, zone axis $[\bar{2}33]$.

Fig.(17): Characteristic EDX spectrum obtained from secondary hardening carbide of M42 using window-less detector.

Fig.(18): Variation of chemical composition of secondary hardening carbide with tempering temperature for: (a) M42 and (b) M1.

Fig.(19): Electron micrographs showing cementite needles precipitated in M42 .

(a) carbon replica from specimen tempered at 480°C.

(b) carbon replica from specimen tempered to peak hardness.

(c) thin foil tempered to peak hardness.

Fig.(20): Characteristic EDX spectrum of cementite extracted from M42.

Fig.(21): Variation of chemical composition of cementite with temperature.

(a) Fe, (b) Cr, (c) Co and (d) Mo.

Fig.(22): Electron micrographs showing hexagonal $M_2C$ needles and $M_{23}C_6$ particles precipitated after tempering for 2+2 hours at 700°C.

(a) and (b) carbon replica from M42.

(c) carbon replica from M15.

(d) thin foil from M1.

Fig.(23): Carbon replica micrographs showing the precipitation of secondary MC carbide after tempering for 24 hours at 700°C.

(a) M42 , (b) M1 and (c) M15.

Fig.(24): Carbon replica micrographs showing the microstructure of M42 after tempering for 24 hours at 800°C, which is similar to that of other steels examined.

(a) low magnification. (b) high magnification.

Fig.(25): Single crystal diffraction patterns of carbides present in annealed M42 which are similar to other steels examined.

(a) MC, zone axis $[\bar{1}11]$.

(b) $M_6C$, zone axis [011].

(c) $M_{23}C_6$, zone axis [$\bar{1}$23].

Fig.(26): Characteristic EDX spectrum obtained from secondary hardening carbide of M42.

Fig.(27): Characteristic EDX spectrum obtained from primary MC carbide extracted from M42.

Fig.(28): Characteristic EDX spectrum obtained from primary $M_6C$ carbide precipitated in M42.

Fig.(29): Characteristic EDX spectrum obtained from $M_{23}C_6$ carbide precipitated in M42.

Fig.(30): EDX spectrum showing the background of a carbon replica.

Fig.(31): Window-less EDX spectrum showing the background of an aluminium replica.

Fig.(32): Carbides produced in high speed steels after tempering for 2+2 hours at different temperatures.

Fig.(33): Variation of chemical composition of primary carbides with tempering temperatures.

(a) $M_6C$ carbide precipitated in M42.

(b) MC carbide precipitated in M15.

Fig.(34): Optical micrographs showing the tempered microstructure of:

(a) M42 and (b) M15.

Fig.(35): SEM micrographs of M42 microstructure which is typical of that of other steels examined.

(a) as quenched.

(b) as tempered to peak hardness.

(c) as annealed for 24 hours at 800°C.

Fig.(36): Thin foil micrographs showing primary carbides.

(a) MC carbide in M15.

(b) $M_6C$ carbide in M42.

Fig.(37): EPMA X-ray scans showing alloying element distributions in tempered M42 specimen.

(a) microstructure x2000 (b) Mo (c) V (d) Co and (e) Cr.

Fig.(38): EPMA X-ray scans showing alloying element distributions in tempered M15 specimen.

(a) microstructure x2000, (b) V, (c) W, (d) Co and (e) Cr.

Fig.(39): Optical micrographs showing selective etching of carbides.

(a) M42 specimen etched for $M_6C$ carbide.

(b) M15 specimen etched for MC carbide.

Fig.(40): Variation of volume fraction of carbides with tempering temperature.

(a) $M_6C$, (b) MC and (c) $M_6C$ + MC.

Fig.(41): Variation of average carbide particle size with tempering temperature.

(a) MC carbide. (b) $M_6C$ carbide.

Fig.(42): Particle size distribution of MC carbide

precipitated in M15.

Fig.(43): Particle size distribution of $M_6C$ carbide precipitated in M42.

Fig.(44): Relation between average particle size and carbide volume fraction.

Fig.(45): Relation between wear volume and sliding distance for samples tempered for 2+2 hours at 530°C.

Fig.(46): Variation of wear resistance with tempering temperature.

Fig.(47): Effect of tempering temperature on wear resistance and hardness of M42.

Fig.(48): Relation between wear resistance and hardness.

Fig.(49): SEM micrographs of wear surface of M42 tempered to peak hardness showing primary carbides fixed in their initial places.

(a) and (b) etched samples.

(c) unetched sample.

Fig.(50): SEM micrographs showing the flat surfaces of worn primary carbides in M42 sample tempered to peak hardness, worn surface being etched.

Fig.(51): SEM micrographs showing cracks in primary carbides in samples tempered to peak hardness.

Fig.(52): SEM micrographs showing worn surface of over-tempered high speed steels.

(a) primary carbides torn out the surface.

(b) and (c) primary carbide abrading the surface.

(d) loose primary carbides and the abraded surface .

## ACKNOWLEDGEMENTS

The author expresses his deepest gratitude to his supervisor Dr. B. Mills, who originated the topic of the present work, for his valuable guidance and encouragement during the present work.

Appreciation is also due to the Egyptian Army for their financial support.

The author's thanks are also due to Mr. G. France and Mr. H. Pendelbury for their technical and practical advice.

The author expresses his deepest gratitude to Dr. G.W. Lorimer, Mr. G. Cliff, Mr. I. Brough and Mr. F. Kneol, of the Department of Metallurgy and Material Science, University of Manchester, the first for giving access to the use of the electron microscope and fruitful discussions and the others for their invaluable technical and practical help.

Thanks are also due to Miss. D. Chesco, of the University of Surrey, for help with the window-less X-ray detection techniqe.

The encouragement, warm feelings and continuous moral support of my parents, the bless of my life, were very much appreciated during the course of this work.

The help, encouragement, patience and love of my wife, who was always behined any success in my life, are very much appreciable.

# SYNOPSIS

The present work describes the successful extraction of the secondary hardening carbides of high speed steels, which allowed the identification of these carbides by crystallographic and microanalysis techniques. The secondary hardening carbide of high speed steels was found to be the cubic $M_2C$ carbide and not the MC carbide as previously claimed. The secondary MC carbide was found to precipitate in the over-tempered state well beyond peak hardness. The sequence of secondary carbide precipitation has been determined. The relation between wear resistance and hardness of high speed steels has been found to be non-linear due to microstructural changes at and beyond peak hardness. However, primary carbides of the MC and $M_6C$ types of carbides were found to be stable during tempering of these steels. It has been shown that the primary carbides did not contribute to the wear resistance of steels tempered to peak hardness. However, the primary carbides were found to contribute to the wear rate of over-tempered steels due to their abrasive role.

# CHAPTER ONE

## INTRODUCTION

During previous extensive studies of high speed steels, the identification of the secondary hardening carbide, the sequence of secondary carbide precipitation during tempering and the relation between wear resistance and microstructure are not yet satisfactorily clear. The present work describes a study of three high speed steels in the region of secondary hardening. The study included a metallurgical investigation and wear testing. The metallurgical investigation was concerned with the identification of the secondary carbides and their sequence of precipitation. A Philips 400 T electron microscope fitted with an EDAX 9100 microanalysis machine was used in the present work. Both thin foils and carbon and non-carbon replicas were used, however, thin foils were found to be less useful than replicas in identifying carbides. The secondary hardening carbides were successfully extracted for the first time in the present work. Crystallographic, microanalysis data and studies of the kinetics of carbide precipitation proved that cubic $M_2C$ carbide was the secondary hardening carbide in high speed steels and not MC carbide as was previously considered to be the case. The cubic $M_2C$

carbide did not coarsen after peak hardness. It dissolved into the matrix and other carbides precipitated. The identification and the sequence of precipitation of these carbides has been determined in the present work. It was found that the secondary MC carbide precipitated in the over-tempered stage well after peak hardness.

The volume fraction, average particle size and particle size distribution of primary carbides were determined over the secondary hardening region using a Quantimet 720. Selective etching techniques were adopted to show each single primary carbide specie at a time. The chemical composition of primary carbides has been determined over the secondary hardening region using electron probe microanalysis (EPMA) and by microanalysing the particles extracted by replicas and from thin foils using an EDAX machine.

Primary carbides showed no variation in composition during the tempering of the steels and were quite stable. The secondary hardening of high speed steels could not be attributed to the primary carbides.

The wear tests were carried out on a crossed-cylinder wear testing machine. The wear surfaces were studied using scanning electron microscopy. It was found that the secondary hardening of high speed steels was associated with a peak in the wear resistance of the steels. It was also found that the wear resistance of steels tempered after peak hardness was always

lower than that for steels tempered up to peak hardness and having the same hardness. This was attributed to the significant changes which occured in the microstructure of high speed steels when tempered after peak hardness. It was found that in samples tempered to peak hardness, primary carbides had the same wear rate as the matrix and hence made no contribution to the wear resistance of the material. In over-tempered steels, primary carbides were easily torn from the surface and acted as abrasive particles which abraded the high speed steel surface contributing to an increase in the wear rate.

The present study suggests that steels free from massive primary carbides should be produced which will display secondary hardening and will have improved wear resistance beyond peak hardness.

# CHAPTER TWO

# METALLURGY OF HIGH SPEED STEELS

## 2.1 Historical Background

The first high speed steel was developed from air hardening alloy steels which were available at the end of the 19th century [1].

In 1907, Taylor [2] reported that the best high speed steel contained 18.91% tungsten, 0.23% vanadium, 5.47% chromium and 0.67% carbon. This led to the development of what was considered to be the standard high speed steel for many years, containing 18% tungsten, 4% chromium and 1% vanadium, or what is now known as T1 high speed steel.

Molybdenum was used as a replacement for tungsten, or in addition to tungsten in the early steels, but during the first world war, it was necessary to replace tungsten by molybdenum for strategic reasons. During the 1930's tungsten was replaced by molybdenum which resulted in the development of types M1 and M2 high speed steels. These molybdenum steels together with the classical T1 high speed steel formed the base of other high speed steels in which the vanadium and cobalt content were altered.

## 2.2 Heat Treatment of High Speed Steels

High speed steel is subjected to two basic heat treatments :

1- A hardening (austenitising and quenching) heat treatment which results in a hardened martensitic matrix rich in carbon and other alloying elements, some retained austenite and some residual (undissolved) carbides.

2- A tempering heat treatment, which results in stress relief, transformation of retained austenite with multiple tempering and most importantly, the precipitation of secondary carbides responsible for the secondary hardening of the steel.

### 2.2.1 Annealed high speed steels

The microstructure of annealed high speed steel consists of a ferritic matrix and excess alloy carbides. The η carbide ($M_6C$) was the first carbide to be discovered in annealed high speed steel in 1928, having an fcc crystal structure of lattice parameter 11.04 Å and a chemical composition in the range from $Fe_3W_3C$ to $Fe_4W_2C$ [3].

It is now well established that annealed high speed steels contain the three types of fcc carbides; $M_6C$, $M_{23}C_6$ and MC (or $M_4C_3$) [1,4-7].

Since the steel contains several carbide forming elements, these alloy carbides contain more than one of those elements rather than being pure carbides. So, they are designated as

$M_6C$, $M_{23}C_6$ and MC, where "M" stands for the metallic atoms in the carbide.

Annealed high speed steel carbides may be classified as follows :

1- $M_6C$, a tungsten or molybdenum rich carbide corresponding to the double η carbide. It's composition was firstly reported as $W_{3-2}Fe_{3-4}C$ [3,8]. However, other workers reported the composition of $\eta_2$ double carbide as $Mo_4Fe_2C$ [9,10]. Generally η carbide is classified as $\eta_1$ or $\eta_2$ according to its composition; i.e. ;

$\eta_1 = A_4B_2C - A_3B_3C$

$\eta_2 = A_2B_4C$

where A is an atom of the elements (Ni, Co, Fe, Mn, Cr, V and Ti), and B corresponds to the elements (Mo, W, Nb, Ta and Hf) [9].

The lattice parameter of $\eta_2$ carbide is always larger than that of the $\eta_1$ carbide for the same elements [9,10]. However, it has been reported that the lattice parameter of $M_6C$ carbide varies with composition [11].

2- $M_{23}C_6$, an fcc carbide corresponds to the pure $Cr_{23}C_6$ carbide of lattice parameter 10.638 Å [12]. The double carbide role of $M_{23}C_6$ is also reported [13]; the following reaction occurs due to the addition of tungsten or molybdenum to iron in solution :

$$Cr_{23}C_6 \xrightarrow{(+Mo/W)} (Fe,Cr)_{21}(Mo/W)_2C_6 \xrightarrow{(+Mo/W)} M_6C$$

The transformation of $M_{23}C_6$ to $M_6C$ is also reported to occur

in chromium steels containing molybdenum and/or tungsten [14].

3- MC ($M_4C_3$), this carbide corresponds to the pure cubic vanadium carbide VC, usually reported as $V_4C_3$ because it has not been detected in its stoichiometric form as VC in steels. On surveying the literature [15-20],it is clear that this carbide is a very stable one; it forms directly out of the matrix without the prior formation of any previous metastable phases, and does not transform to any other form of carbides at high temperatures. This carbide dissolves limited quantities of other elements. The lattice parameter of this fcc carbide is reported to be 4.16 Å for $V_4C_3$ carbide [20]. Since the high speed steel carbides are not pure carbides, their composition and lattice parameter will depend on the composition of the steel [11,21]. Some reported values for lattice parameters of $M_{23}C_6$, $M_6C$ and MC carbides are shown in Table (1) . Kayser and Cohen [6], reported that all high speed steels contain the same amount of $M_{23}C_6$ in the annealed state (9-11% by volume). The amount of MC and $M_6C$ depended on the chemical composition of the steel, such that the total amount of carbides present in all annealed high speed steels was found to be 26-33% by volume. This value is also confirmed for T1 and M2 high speed steels [22]. Generally the amount of MC carbide increases as the vanadium content increases unless the steel has a very large amount of tungsten which competes effectively to form $M_6C$ carbide as in the case of M1 and T2

high speed steels; M1 contains 1.75% tungsten and 1.25% vanadium and forms more MC carbide than T2 which contains 18% tungsten and 2.02% vanadium [6]. Fig.(1) shows the amount of each carbide in the annealed and quenched states for some high speed steels [6]. However, lower values for the amounts of carbides present in M2 high speed steel have been reported [5,23].

2.2.2 Hardening of high speed steels

In 1920, Scott [24] working on high speed steels, reported that the purpose of heating the steels was to dissolve some carbides which during tempering should precipitate. He also reported that secondary hardening occured only if austenitising was carried out at high temperatures (>1100 °C). It is also known that the higher the austenitising temperature, the greater the amount of dissolved carbides and the richer in carbon and alloying elements is the austenite [1,5,6,22,23,25]. The amount of retained austenite also increased with an increase in austenitising temperature [1,26]. The retention of austenite affects the hardness of the as quenched steel, however, Payson [1], reported that up to 20-25% by volume of retained austenite was acceptable, if the percentage was greater than 20-25 %, the hardness dropped drastically.

The high hardening temperature affects the grain size of other steels, however, high speed steels and tool steels in general

are insensitive to grain coarsening [1].

As seen from the previous section, the carbides present in the annealed high speed steels are, MC, $M_6C$ and $M_{23}C_6$. On heating up to austenitising temperature, these carbides dissolve either totally or partially into the austenitic matrix. Kayser and Cohen [6], found that all $M_{23}C_6$, 1-3% by volume MC and 7-10% by volume of $M_6C$ dissolved as a result of commercial austenitising, as shown in Fig. (1). The dissolution of $M_{23}C_6$ at high austenitising temperature has recently been confirmed for M2 high speed steel, while the amounts of dissolved MC and $M_6C$ depended on austenitising temperature as shown in Fig. (2) [5,23].

Rapid cooling of austenite rich in carbon and alloying elements results in the formation of highly alloyed martensite and the residual carbides which have not been dissolved during the hardening process in the form of MC and $M_6C$ together with some retained austenite. The amounts of residual carbides present in some as-quenched high speed steels are shown in Table (2),[25]. It is clear from this table and Fig.(1), that the majority of residual carbides was the $M_6C$ carbide except in molybdenum high speed steels containing great amounts of vanadium when MC becomes the predominant carbide [25]. The mechanism of austenite to martensite transformation and the retention of austenite is well explained by Cohen [26] and Payson [1,27]. The drawbacks of retention of some austenite

are overcome by multiple tempering as will be shown in the next section.

### 2.2.3 Tempering of high speed steels

The correlation between the change in hardness and the change in microstructure was first pointed out by Bain and Jeffries [28].

As mentioned previously, the precipitation of secondary carbides is the most important process in the tempering of high speed steels and alloy steels in general. Only one of those carbides is responsible for the secondary hardening of high speed steel.

Payson [27], simplified the mechanism of tempering of high speed steel in terms of two mechanisms, Fig.(3) :

1- softening mechanism, due to the decomposition of martensite.

2- strengthening mechanism, due to the precipitation of fine secondary carbides.

The result of tempering such steels is to give more ductility without loss in hardness which is the exact requirement for tempering alloy and high speed steels.

Tempering of carbon steels is classified into three stages [18] :

1- decomposition of martensite and precipitation of $\varepsilon$ carbide

2- transformation of retained austenite.

3- precipitation of cementite.

In certain alloy steels, a fourth stage of tempering occurs at higher temperatures when alloy carbides precipitate and replace cementite. The precipitation of such alloy carbides is usually associated with a significant increase in hardness. This increase in hardness is known as secondary hardening and the alloy carbide responsible for secondary hardening is known as the secondary hardening carbide.

Cohen and Koh [29], working on high speed steels were the first to document the stages of tempering of the hardened martensitic matrix containing carbon and alloying elements in solution. They reported that secondary hardening occured due to the precipitation of secondary carbides from the retained austenite. Somewhat revised since, the stages of the tempering process have been described by Payson [1].

The role of retained austenite in secondary carbide precipitation is underestimated since the sub-zero treated steel showed the same effect of secondary hardening as in ordinary hardened steel which contained retained austenite [30]. The presence of up to 20% by volume of retained austenite would not affect the hardness of the as-quenched steel, and after double tempering the steel, the retained austenite transformed. This austenite-free steel showed secondary hardening [1], and the effect on the red hardness of alloy martensite caused by the transformation of retained

austenite was generally not important [27]. It is the carbide precipitation out of the martensitic matrix which is of the most importance in the secondary hardening and red hardness of high speed steels, and a great deal of work has been carried out on the subject of carbide precipitation in high speed steels and alloy steels as well.

Payson [27], directly attributed secondary hardening in ferrous alloys to the coherent precipitation of alloy carbides. This was based on the interpretation of electron diffraction data. He established that the inflection in the hardness-tempering temperature curve for molybdenum steels was associated with the first detection of the $Mo_2C$ carbide, and the secondary hardness increased with the simultaneous increase in intensity of the $Mo_2C$ pattern and decrease in the intensity of the $Fe_3C$ pattern. He also concluded that the onset of secondary hardening was associated with the formation of coherent zones of alloy carbides, this conclusion was supported by broad X-ray lines, indicating lattice strain, noticed prior to peak hardness.

In vanadium steels, it is well established that $V_4C_3$ is the only carbide which replaces $Fe_3C$ and causes secondary hardening. Generally it is the only carbide reported to occur in tempered and annealed vanadium steels [18,19,27,31,34]. In chromium steels, $Cr_7C_3$ was the carbide which replaced $Fe_3C$. However, in the presence of enough Cr and/or other alloying

elements especially molybdenum and tungsten, $Cr_{23}C_6$ formed and replaced $Cr_7C_3$ [18,19,27,31,35]. It is also reported that $M_6C$ was detected as the final stage of precipitation in some chromium steels [14]. The chromium carbides are of less importance in giving the steel a considerable secondary hardening. They may give the steel a constant hardness up to a certain limit of tempering, then a drastic fall in the hardness occurs. This is probably due to the rapid rate of coarsening of $Cr_7C_3$ as a result of the ease with which chromium diffuses in ferrite. However, additions of other carbide forming elements to the steel or increases in the chromium content to 12% by weight, enhanced the secondary hardening of chromium steels [19].

In molybdenum steels, $Mo_2C$ is reported as the secondary carbide which replaced cementite and caused secondary hardening of the steel [18,19,27,34-36]. But during the early stages of formation, Irani and Honeycombe [37], observed streaks on some spots of the diffraction pattern of the matrix of a foil tempered prior to peak hardness. Those streaks were not observed in the as-quenched steel. They concluded that those streaks were due to the formation of zones rich in molybdenum and carbon, similar to those observed earlier in Al-Cu systems [38]. They also reported the transformation of $Mo_2C$ to $M_6C$ at higher temperatures and introduced the mechanism of phase transformation as follows:

$$Fe_3C \text{ ----> zones ----> } Mo_2C \text{ ----> } M_6C$$

Raynor, Whiteman and Honeycombe [39], concluded that the streaks noticed in the diffraction pattern indicated the presence of very thin needle precipitates of $Mo_2C$, possessing the same morphology and orientation relationship with the matrix as that determined for coarse $Mo_2C$ in ferrite and no direct evidence of solute zone clustering was found. They concluded that if coherent zones existed, they must co-existed with discrete fine scale precipitation. Such co-existence seems to be in agreement with Payson's conclusions with respect to the detection of expansion occurring with the rise in hardness over secondary hardening and the detection of fine $Mo_2C$ precipitation prior to peak hardness [27].

Finally the situation was clarified by Ustinovshchikov [40], who discovered the precipitation of cubic $Mo_2C$ carbide prior to the precipitation of the hexagonal $Mo_2C$ carbide. The precipitation of cubic $Mo_2C$ was associated with the secondary hardening of the steel. He found that the diffraction pattern of the cubic $Mo_2C$ was identical with that of $V_4C_3$ precipitated in vanadium steel, and the mechanism of carbide precipitation in molybdenum steels was found to be:

$$Fe_3C \text{ ----> cubic } Mo_2C \text{ ----> hex. } Mo_2C \text{ ----> } M_6C$$

In high speed steels, carbide precipitation in as-quenched and as-annealed steels have been intensively studied as

reviewed in the previous sections. However, the secondary carbide precipitation in high speed steels has never been satisfactorily clarified by following the precipitated phases in order to determine the exact mechanism of tempering high speed steels. Previous workers who investigated the precipitation of the secondary carbides, were simply interested in identifying the secondary carbide responsible for the secondary hardening of high speed steels. It is clear that the secondary hardening carbide would be either one of the carbides detected in the annealed state, or a metastable phase which transforms to one of those annealed steel carbides.

From the extensive review of the literature, three carbides have been reported as responsible for the secondary hardening in high speed steels. Those carbides are described below by refering to the original papers :

1- Kuo [7], used X-ray diffraction of extracted carbides to identify carbides present at different stages of tempering, and identified the secondary hardening carbide to be the hexagonal $Mo_2C$ carbide, which transformed to $M_6C$ in the annealed state. He also reported that no X-ray lines were observed at the peak hardness, however after peak hardness he detected hexagonal $Mo_2C$. He explained the disappearance of X-ray lines at peak hardness as a result of the very fine size of the needles of $Mo_2C$. The most interesting observation

reported in this paper is that in the X-ray photographs of the extracted carbides, in addition to the close-packed hexagonal structure, there was also some indication of the co-existence of close-packed cubic $W_2C$ (or $Mo_2C$). However he could not prove the presence of the cubic phase since he felt that it might be an example of a stacking disorder.

2- White and Honeycombe [41], using electron microscopy and selected area diffraction, identified the $M_{23}C_6$ as the secondary hardening carbide, which coarsened in the annealed state. However, they detected $M_{23}C_6$ after the peak hardness.

3. Mukherjee [42], using electron microscopy, introduced a single crystal diffraction pattern from the secondary hardening carbide and identified it as MC carbide, which coarsened in the annealed state. However he never introduced the photomicrograph of that precipitate and he did not consider the possibility of obtaining this pattern from a small primary MC carbide. He also ignored completely the fact that cubic $Mo_2C$ has the same crystal structure as that of $V_4C_3$ both have an fcc crystal structure and their lattice parameters are very close as shown in Table (1). This identification has been regarded by subsequent workers as the last word in the identification of the secondary hardening carbide in high speed steels.

The work described in the present thesis showed that the secondary hardening carbide in high speed steels was the cubic

$M_2C$ carbide.

Kupolova [43], identified the secondary hardening carbide as MC carbide and introduced a simple mechanism of phase transformation in high speed steels.

However, it is clear that the results of investigating high speed steels are dependent on the technique used in the investigation. In the present work, the sophisticated electron microscope Philips 400T fitted with an EDAX microanalysis machine was used to study the phase transformation in high speed steel and to identify each phase crystallographically and chemically.

## 2.3 Techniques Used In Investigating High Speed Steels

The metallurgical study of high speed steels is usually based on the following techniques :

### 2.3.1 Studies of the physical and mechanical properties

Phase transformations taking place during the heat treatment of steels are associated with changes in physical and mechanical properties of the steel. Changes in physical properties such as changes in size, magnetisation and electrical resistivity have been used to detect changes in microstructure of steels. A change in the hardness of steel is a well known simple test to follow the changes in steel microstructure.

The major disadvantage of such techniques is that they indicate the occurence of microstructural change without identifying the mechanism of such changes.

### 2.3.2 Microscopic observations

Earlier workers used optical microscopes, the resolution of which just enabled the observation of big primary carbides. The main useful outcome of optical microscopy is the determination of the volume fraction of the undissolved carbides. The volume fraction of each carbide specie in high speed steels is reported by using selective etching techniques [6,23].

Precipitation of secondary carbides is not observable by optical metallography. Higher magnifications are obtainable by scanning electron microscopy (SEM). The secondary carbides can be observed in their later stages of formation, but they are still not observable at the early stages of their formation. Some SEM's are fitted with energy dispersive X-ray analysers, which enable the chemical analysis of matrix and large carbides to be made.

### 2.3.3 Crystallography

The ability of crystals to diffract X-rays was employed in identifying crystals, since the diffracted waves will form a pattern dependent on the way the atoms are arranged within the crystal. However, the X-ray diffraction technique is based

on using extracted carbide powder which contains a mixture of different carbides of various particle size. The diffracted lines will be confused; because of the presence of different carbide species. Also the weak intensity lines of the smaller particles become non-identifiable compared with the stronger intensity lines of the larger particles. The principles of X-ray diffraction are explained in the literature, e.g. [44,45].

In transmission electron microscopes (TEM), electrons are travelling in the form of waves, and crystals have the same effect in diffracting the electron beam. Two main diffraction methods are used in electron microscopy :

1- selected area diffraction (SAD) : An aperture is used to limit the beam size and indicate the selected area from which diffraction is required.

2- convergent beam diffraction (CBD) : The design of electro-magnetic lenses in new electron microscopes enabled the beam to be focused down to a very small diameter which is then concentrated on the required individual particle to obtain the diffraction pattern.

The detail explanation of electron diffraction in TEM is well explained in the literature [45-47]. However, crystallography does not allow differentiation between carbides having similar crystal structure.

### 2.3.4 Chemical analysis

The technique of dissolving the ferritic matrix and extracting the residual carbides is not a reliable technique since it is impossible to separate the carbide species. It allows only a total analysis of all carbides present. The electron probe microanalyser (EPMA) was used to analyse the individual carbide particles. However, in high speed steels, this facility is only suitable to analyse big carbide particles and it is not possible to analyse fine secondary carbides by this method.

The most suitable technique for the chemical analysis of the tiny secondary carbides is the microanalysis carried out on a TEM fitted with an energy dispersive microanalysis system. The microanalysis with high spatial resolution is well explained in the literature [47-48]. The microanalysis technique used in the present work is explained in the experimental part of the present thesis (chapter four).

# CHAPTER THREE

# WEAR OF HIGH SPEED STEELS

## 3.1 General

The study of the wear of high speed steel cannot be separated from the general study of wear of materials, since wear is essentially a system property which includes tribological and metallurgical parameters [49], and wear occurs by several mechanisms acting at the same time [50]. Previous workers found it a necessity to study each parameter and each mechanism separately in order to determine the role of each on the wear resistance of materials.

Earlier workers were interested in studying the wear of surfaces under sliding contact taking into account the tribological parameters and simply the material hardness to represent the whole material parameters. However, it has often been shown that the hardness alone was inadequate for this purpose. In the last two decades, correlating wear resistance to the microstructure of materials has become of great interest.

## 3.2 Classical Models of Wear

Wear means removal of material from surfaces in relative motion by mechanical and/or chemical processes [51]. Thus, wear resistance may in the first instance be classed as a mechanical property [49].

Different mechanisms have been introduced to explain how wear occurs. Jahanmir, [52] reviewed ten different wear mechanisms. However, in practice, individual mechanisms of wear rarely occur alone, and material is often removed by the simultaneous action of more than one mechanism.

The wear properties of a certain material, thus, depend on how the different mechanisms occur and their relative significance [50].

Among the different wear mechanisms, adhesion and abrasion arise as the most important mechanisms causing failure of engineering materials [53].

Adhesive wear is the only type that is always observed whenever two solids slide over each other, whereas other forms of wear only arise in special circumstances [54]. It is often described as severe wear and is generally the starting point for a wear process developing between two conforming rubbing metal surfaces. Since engineering surfaces are rough and possess hills and valleys, the contact between two solids occurs only at a few isolated points resulting in a true area of contact which is a fraction of the apparent area. The

applied normal stress is therefore very high in the regions of contact and may exceed the yield point of one or both of the solids. The contact area will then weld together forming junctions, these must be broken to initiate and sustain relative motion and the force necessary to disrupt the junction is a measure of friction [55]. It has been shown [56] that the wear rate increases substantially when the applied load produces a compressive stress > 1/3 the hardness, being equivalent to the onset of plastic yield in the bulk material. Abrasive wear is responsible for 50% of wear in industry [57]. It can arise from the penetration and ploughing out of material from a surface by another body. If this body is free abrasive grit between two rubbing surfaces, either from an external source or internally generated abrasive wear particles, the situation is generally called three body abrasion. If the other body is a proud hard phase or a moving grit, the situation is termed two body abrasion. The latter accounts for the majority of industrial situations met in practice.

Adhesion and abrasion mechanisms of wear are well explained in the literature [55,58-60]. From this literature, it is clear that both mechanisms could be expressed by the following mathematical expression [52] :

$$W = K \cdot \frac{N \cdot S}{C \cdot H}$$

where:

W .... is the wear volume.

K .... wear coefficient.

N .... normal load.

S .... sliding distance.

C .... geometrical constant.

H .... material hardness.

The wear coefficient, K, in adhesive wear is the probability of an adhesion event leading to the formation of a wear particle [59], and in the case of abrasion, $K=\tan\theta$ , where $\theta$ is the angle between the abrasive and material surfaces [55,60]. A linear relation was reported [54] between the logarithm of wear coefficient and the coefficient of friction.

## 3.3 Wear and Material Hardness

As seen from the previous section, wear theories are based on a linear relation between wear rate and material hardness, and the hardness remains the term most commonly used to express the relation between material properties and wear rate, although it has often been shown to be inadequate for this purpose, particularly when dissimilar materials were under consideration [61].

The pioneering work of Kruschov in 1957 [62] introduced a

detailed study of the relation between the hardness of the metal and its resistance to sliding abrasion. For commercially pure metals and annealed steels, he found that the abrasion resistance was directly proportional to their bulk hardness. Lines of lower hardness were obtained for hardened and tempered steels. These lines intersected the main curve at the location of the data for the annealed conditon of the steel in question.

Moore [63], reported that bulk hardness was not a direct measure of the wear resistance of ferritic materials, but was related to the metallurgical structure in a similar way to the wear resistance. So that for materials of similar structure but of different composition, linear relationships existed. However, he suggested that material microstructure had a greater infuluence on wear resistance than the bulk hardness. Hurricks [49], found that the wear of tool steels followed a similar course to the variation of hardness with increasing tempering temperature.

For high speed steels, it is reported that wear rate depended linearly on hardness but with different sensitivity to hardness between one steel and another [25].

However, deviation from a linear correlation between wear rate and hardness is also reported. Saka [64], found that the minimum wear rate occured prior to the maximum hardness when tempered copper-chromium alloys were tested at different

hardness levels. For tempered steels, the linear relation between hardness and wear resistance reported by Kruschov [62] was described as oversimplified and the actual relation was reported to be nonlinear for a simple steel tempered at different hardness levels [65]. Also, when the vanadium content in M2 high speed steel was replaced by niobium, it was found that the performance of the niobium containing steel was better than ordinary vanadium containing steel despite the hardness of vanadium containing steel being higher than that of the niobium containing steel [66]. Gahr [67], has reported cases when wear resistance could increase while hardness decreased. In copper based solid solutions, with Si, Cr and Sn, it was found that an increase in solute content improved hardness linearly and decreased wear rate non-linearly [68]. Borik and Scholtz [69], reported a non-linear relationship between wear resistance and hardness for work-hardened surfaces, moreover they could not find an adequate relation between hardness and wear resistance for non work-hardened surfaces.

However, estimating the wear resistance on the basis of hardness alone may be reasonably safe within a certain alloy system but it cannot be applied if a significant change in microconstituents was involved [70].

## 3.4 Metallurgical Aspects of Wear

The inability of the simple models to exlpain the results for heat treated steels and the contradictory nature of some of the previous work suggested that metal removal was strongly affected by factors other than hardness [65]. The classical theories of wear have been criticised, since they completely ignored the physics and physical metallurgy of metal deformation, and the linear wear law did not provide any insight into the wear of metals under different sliding conditions [71]. It is becoming increasingly obvious that it is no longer sufficient to specify a reliable wear resistant material in terms of type , composition or mechanical properties alone, but in addition it is necessary to specify the metallographic microstructure [49]. The influence of the metallurgical factors on mechanical properties of metals has become fairly well investigated and established. Thus, with regard to wear, there is every reason to suppose that a relationship exists between wear resistance and metallurgical structure. An estimate of wear performance can usually be made when based on metallographic structure [49].

It is clear from the previous section that all the introduced mechanisms of wear postulated the occurence of plastic deformation in the wear process. Experimental observations confirmed the association of wear with plastic deformation even in the very hard heat treated high speed steels [72,73].

So, the factors affecting plastic deformation, would also affect the wear of steels.

The plastic deformation of crystalline materials is well explained by the dislocation theory [74]. There are three principle ways for strengthening the structure of steels; by alloying, by heat treating and by work-hardening [49]. However work hardening is of no interest in the present work concerned with high speed steels. The role of composition on wear and other mechanical properties has been reported [19,49,61,68,69, 75,76], and it has been shown that in steels, there was no convincing evidence that alloying elements other than the interstitial elements (carbon and nitrogen) had an appreciable effect on the mechanical properties of martensite in the quenched state [76]. However, Mills [77], has shown that in low carbon steels the ferrite microhardness increased as total residual elements increased.

Heat treating alloy and high speed steels results in what is known as secondary hardening which gives the steel the best possible combination of hardness and toughness. As has been shown in chapter two and also confirmed by the present experimental work, the secondary hardening of high speed steel is a precipitation hardening process during which very fine carbide precipitates give the steel improved mechanical properties.

## 3.5 Wear and Precipitated Carbides

A review of the literature showed two mechanisms in which the carbide phase contributed to the wear resistance of steels; either by a direct contribution to wear resistance by taking actual part in the wear process. Or indirectly by dispersion strengthening the matrix which finally resulted in reducing plastic deformation and reducing the wear rate.

With large differences in the abrasive wear resistance of different microconstituents, the overall wear resistance of the material may be low due to selective wear of the less wear resistant components, and the wear resistance could be expressed as the summation of the contribution of different phases. It has been reported that the increase in volume fraction of carbide phases enhanced the wear resistance of steels [61,69,78,79]. However, measurement of the volume fraction was usually carried out by optical methods, which counted only coarse carbide particles. This was applied to the primary carbides in hardened and tempered high speed steels. The importance of carbide volume fraction on wear resistance was based on the assumption that carbides were the hardest phases in steels, so, their wear rate should be much lower than that of the matrix. The hardness of the carbides, thus, would be the important factor in the microstructure in influencing wear resistance [70]. It has been shown that harder carbides gave better wear resistance to steels than

softer carbides. The work of Popov and Nagorny [78], has shown that MC carbide gave better wear resistance than $M_7C_3$ and $M_6C$ carbides, all having the same austenitic matrix. Apart from the carbide hardness, they explained that as MC gave the maximum probability of obtaining stable bonding across the boundaries, since MC had the least difference in lattice constant with the matrix. Also, it has been reported that harder cementite gave steel better wear resistance than a softer intermetallic compound $Fe_2Mo$ [70].

The increased volume fraction of the primary MC carbide was reported as the decisive factor in increasing the wear resistance of M2 high speed steel despite the associated decrease in the volume fraction of $M_6C$ carbide [80].

It was found that abrasives penetrated $M_3C$ and $M_6C$ fairly easily and these carbides had offered practically no resistance to the destructive effect of the abrasives, while vanadium and niobium carbides (MC type) held up the abrasive grains but underwent considerable damage in the process, in the form of cracks and chips which reduced their ability to withstand the abrasive in the next collision during the following cycle of work. The experimental results proved that the carbide resistance to wear depended on the energy needed to rupture the carbide atomic binding forces which depended on the nature of the carbide [81].

Alloyed carbides have been reported to have better strength

than pure carbides; when boron diffused into $Ti_{0.84}C$ or $V_{0.84}C$ carbides, it improved their strength remarkably [82]. It was found that M2 high speed steel, containing 1% vanadium + 1% niobium had the very best performance and secondary hardness compared with standard M2 high speed steel containing 2% vanadium or with M2 having the vanadium content replaced totally by 2% or 3% niobium [66]. This fact has also been confirmed when molybdenum steels were prepared as pure alloys and with some addition of Ta, Nb and Cr. It was found that the hardness of alloyed steels was higher than that of the pure steels despite the fact that the precipitated carbides were the same in all steels [83], from which it could be concluded that the carbides in alloyed Mo steels were alloyed carbides which gave the better properties to the steel.

It has also been reported that binary alloy carbides of TiC and VC had higher strength than any of the carbides alone [82].

The importance of the carbide size has been pointed out by previous workers during the wear testing of two M2 high speed steel samples, both of the same hardness (66.5 Rc) but having different primary carbide sizes. They showed that the steel containing the larger primary carbides had a greater wear rate [70]. Honeycombe [84] reported that one of the objectives of heat treating steels in order to achieve strength and toughness was to minimize the number of coarse particles of

the second phase, both within the grains and at the grain boundaries.

However, it has been reported that the very big carbide particles had no decisive influence on the wear resistance and a carbide free material was the most wear resistant [50]. Also, it has been reported that carbides below a certain volume fraction did not affect the wear of steels [78], and above a certain maximum limit of carbide content, there was no increase in wear resistance by increasing carbide volume fraction [50]. For alloys having $M_6C$ carbide, such a maximum value was reported as 30% volume fraction of $M_6C$ [78], and for MC carbide in M2 high speed steel, a 12% volume fraction was the maximum carbide content over which no improvement in wear resistance was observed [80]. However, Jahanmir [85] reported an optimum value of 5-7% carbide volume fraction to give his steel the maximum wear resistance, below or above that optimum value of volume fraction, the wear rate increased. In his review, Hurricks [49], reported that highly alloyed materials with large amounts of carbides were not necessarily the most wear resistant.

Despite the traditional assumption that primary carbides contribute significantly to wear resistance of high speed steels, the tool life data for both highly alloyed powder metallurgy and commercially produced M1 and M57 high speed steels contradicted that belief [86]. Despite the difference

in residual carbide content, the performance of drills made from highly alloyed powder metallurgy high speed steel was found to be the same as that of drills made from conventional M7 high speed steel, and the performance of drills made from M52 was better than both M7 and powder metallurgy produced high speed steel drills [87]. The same results were obtained from M1, M7 and high alloy powder metallurgy produced high speed steels [86], and from M50 (containing 2.6% volume fraction of carbides) and T1 (containing 15.2% volume fraction of carbides), [88].

However, despite the fact that carbides are very hard at room temperature, it has been reported that above 800°C, the hardness of carbides decreased drastically and carbides became soft and ductile [82,89]. The hardness of WC carbide dropped to about 7-10% of its room temperature value when the temperature was increased to 650°C and the hardness of the carbide had the same value as that of pure tungsten both measured at temperatures above 1000°C. Also, the hardness of TiC carbide dropped to about 25% of its room temperature value as the temperature was increased to 600°C [90]. The bulk hot hardness of tool steels at 650°C was found to equal about 70% of its value at room temperature [91]. It can be concluded from such data that both martensite and other carbide phases reach about the same level of hardness at high temperatures. The actual wear process takes place at such high temperatures

(>800-900 °C) [92], and this may explain how both matrix and primary carbides wore at the same rate in high speed steel tempered to its maximum secondary hardness [70].

The failure of high speed steels could be differentiated into two broad categories : a toughness-related (fracture) failure and a wear-related (continuous wear) failure [86]. Both mechanisms are controlled by the yield strength of the steel, therefore they are matrix dependent [86,87].

Suh [71,93], established his delamination theory of wear which explained the wear process as a sort of fracture resulting from subsurface crack nucleation and propagation, and he believed that fracture properties were the most significant which was mainly matrix dependent.

The work of Henderer [86,94-96], has shown that the strength of hardened and tempered high speed steels was derived mainly from the precipitation of the very fine secondary alloy carbides, and the contribution from the martensitic strength, and coarse primary carbides did not contribute to strength. The role of the second phase particles in strengthening steels is reported [97] and it could be attributed only to the precipitation of the very fine secondary carbides which caused the martensitic strengthening, secondary hardening and better wear resistance [33].

Although as yet not explicitly proved, the suggestion is that the wear resistance of high speed steel may be attributed

primarily to the precipitation of alloy carbides and that resistance to localised plastic deformation, such as that which occurs with many modes of continuous wear, depends on the same strengthening mechanisms as resistance to edge fracture. It is sufficient to alloy only to the point which upon austenitising results in a saturation of the matrix of elements which will precipitate as carbides upon tempering [95]. This was the idea behind the matrix steel, which with heat treatment could reach the strength of high speed steels [98].

However, Henderer [95], reported that he could not find in the literature any experimental data about the size and interparticle spacing of the fine secondary hardening carbides in high speed steels. He found that by assuming the volume fraction of secondary carbides in M1 high speed steel to be 5% with a particle size of 200 X 50 Å (needle shape) and an interparticle spacing of 322 Å, reasonable values of the strength of the steels could be calculated [95].

The difficulty of imaging the fine secondary hardening carbides in thin foils by the electron microscope and the unsuccessful extraction of those carbides by replica techniques has recently been reported [4].

However, the fine secondary hardening carbides in high speed steels have been successfully extracted in the present work and the particle size was found to be of the same order of the

size assumed by Henderer [95], but of platelet shape rather than the assumed needle shape.

The harmful role of the large primary carbides is also reported. More cracks were detected around large second phase particles [72]. Also due to the non-coherency of the large carbides, they facilitated the nucleation and propagation of cracks [67,71,72]. Primary carbides may be torn out from their initial positions and these loose carbides can act as abrasives and contribute to the wear process [50].

However, the factors affecting wear resistance could be sequenced according to their importance as follows :

-matrix properties.

-carbide properties.

-carbide quantity.

The amount of carbides would affect the wear resistance only in the case of the same matrix and the same carbide nature [78].

Finally, it is still a necessity to establish a more suitable material property term for use in the wear life prediction of a wide range of steels [61].

# CHAPTER FOUR

# EXPERIMENTAL WORK

## 4.1 General

The aim of the present work was to study the microstructure of high speed steel as it changed with tempering, and to study the wear rate of the steels after tempering at different tempering temperatures in order to correlate the changes in hardness and wear rate to the microstructure of high speed steels.

Cylindrical samples were heat treated and tempered at different tempering temperatures. A slice from each sample was pressed in bakelite for metallurgical investigations, and the rest of the cylinder was used for the crossed-cylinder wear test.

Metallurgical investigations included : optical microscopy, electron probe microanalysis, electron microscopy and microanalysis. All metallurgical investigations were carried out on the same sample for each tempered steel which gave confidence and consistency of the results.

## 4.2 Metallurgical Investigations

As can be seen from chapter two, the kinetics of the secondary carbide precipitation and the exact identification of the secondary carbide responsible for the secondary hardening in high speed steels are not clear from the literature. None of the previous workers has reported the chemical analysis of the fine secondary carbides, after extracting them out of the matrix and all identification of such carbides has been made using crystallographic techniques which could not differentiate between different carbides having the same or even close lattice parameters. Despite the reported difficulties and the previous unsuccessful extraction of such very fine carbides by replica techniques [4], the extraction of these carbides in order to determine their chemical composition, sizes and the range of stability of each secondary carbide are of considerable interest.

The main purpose of the present work was to define different secondary carbide phases, their crystal structure, chemical composition, range of stability and the sequence of carbide precipitation during tempering high speed steels. Special attention was given to the study of the secondary hardening carbides.

It was of interest to study changes in quantity, particle size crystallography and chemical composition of the primary carbides during the secondary hardening region.

### 4.2.1 Sample preparation

Commercial M42, M1 and M15 high speed steels were supplied by Aurora Steel Ltd. in the form of bars, of chemical composition as shown in Table (3).

Bars were machined down to cylinders 12.5 mm diameter and 25 mm in length to fit in the crossed-cylinder wear test rig. Each sample was marked by stamping a digit and a letter; the digit refered to the steel type and the letter to the tempering temperature.

Samples were commercially hardened in a vacuum furnace at Nemo Heat Treatment Company. The typical austenitising temperatures are shown in Table (4). One of the typical hardening cycles is shown in Fig.(5).

After hardening, each group of samples having the same letter were tempered at the temperature corresponding to that letter. Tempering temperatures were choosen in the range from 380°C up to 800 °C, while the tempering time was kept constant for two plus two hours with air cooling in between tempers in all cases. Tempering temperature increments were choosen to be 10°C in the range of secondary hardening (500-580°C) and gradually increased up to 50°C prior to and beyond that range.

Because the secondary MC carbide was not detected on tempering for two plus two hours at temperatures up to 700°C, more samples were double tempered for longer times at 700 and 800°C which allowed the detection of secondary MC carbide and the

study of the steel in the annealed state.

A slice about 3 mm thick was sliced off each sample and pressed in bakelite. The bakelite moulds were then marked with the same number and letter of their samples. The mounted samples were polished down to 1 μm diamond paste, thoroughly rinsed by methanol and etched. Several etchants have been tried and it was found that the successful replica extraction of the fine secondary carbides was achieved when samples were etched by diluted Vilella's reagent. The Vilella's reagent was diluted to 0.2-0.25 of its standard strength (i.e 1 gram picric acid + 5 ml hydrochloric acid were dissolved in 400-500 ml methanol instead of 100 ml as in the standard formula). This etchant was found not to attack the fine secondary carbides which made it possible to extract them by both carbon and non-carbon replica methods. However, the etching time was a critical factor in etching the steels and was dependent on the microstructure of the steel. Typical etching times varied from about 30 seconds for annealed steel to about two minutes for steels tempered to their peak hardness.

4.2.2 Hardness measurements

The hardness of the polished unetched samples was measured on a Vickers hardness testing machine using a load of 30 kg. The hardness in $MN/m^2$ was plotted against the tempering temperatures.

### 4.2.3 Optical observations

Optical microscopy was used to study the primary carbides, however coarsened secondary carbides in the annealed state were also observable. The optical technique was used together with the selective etching method described in the literature to determine the volume fraction and size distribution of the primary carbides over the tempering range automatically by using the Quantimet 720.

#### 4.2.3.1 Volume fraction and size distribution of the primary carbides

Polished samples were etched selectivly by the method explained by Kayser and Cohen [6]. To detect $M_6C$ carbides, samples were etched in 4% sodium hydroxide in water, concentrated with potassium permanganate. To reveal MC carbides samples were etched electrolytically in a freshly prepared 1% chromic acid solution at a voltage of 5 volts. This etching technique showed carbides dark in a white background. It was found that after etching, rinsing and drying, followed by slight polishing of the specimens on a smooth cloth, the carbide particles were better defined and the halo around them was removed.

The volume fraction of the carbide phase was determined by using the Quantimet 720 of UMIST. This facility gave automatically the volume fraction of the carbide phase, its particle size distribution and the average particle size. The

Quantimet measured the size in picture points (p.p.) which depended on the magnification used to determine the size in microns. In the present work one picture point (p.p.) equalled 0.28 microns. It was of great importance to well grind and to re-polish the surface in between the two selective etchings. The volume fraction, size distribution and average particle size of $M_6C$ and MC primary carbides were determined over the secondary hardening region. Each measurement was the average of 60 readings in order to overcome the non homogeneity in carbide shape, size and distribution and to achieve a statistically meaningful result .

4.2.4 Electron probe microanalysis

Electron probe microanalysis (EPMA) was used to analyse the primary carbides , such analysis was confirmed by the analysis obtained from the EDAX machine. EPMA was used to analyse the standard Fe-Mo binary alloy specimen used to calibrate the L line detection of Mo by the EDAX detector. It was also used to scan the microstructure in order to determine the distribution of each element.

The EPMA used in the present work was the Jeol JXA-50A electron probe microanalyser.

4.2.5 Electron microscopy

Electron microscopy was found to be the most suitable technique for studying the microstructure of high speed

steels. The scanning electron microscope (SEM) and the conventional and analytical electron microscopes (TEM and AEM) were employed in the present work.

The SEM was used in observing the precipitation of carbides of large particle size (primary carbides and coarsened secondary carbides), and to study the worn surfaces of high speed steel samples used in wear testing. The Cambridge stereoscan 600 was used in the present work.

TEM and AEM were the most successful techniques used in studying the microstructural changes in tempering high speed steels. Morphology, crystallography and chemical composition of precipitates could be determined, even for the very fine secondary carbides in their early stages of precipitation. The analytical electron microscope was used to study each precipitated phase crystallographically and to determine the chemical composition of the metallic part of the carbide. It was possible to detect carbon qualitatively by a window-less detector.

In the present work a Philips 400T electron microscope fitted with an EDAX 9100 X-ray detector and computer software SW9100 version 2.2, of UMIST, was used. Carbon was detected qualitatively in secondary hardening carbides by using the Philips 400T electron microscope fitted with a ZL-5 Link window-less detector of the University of Surrey. Carbon was detected after extracting the carbides on a non-carbon replica

(aluminium and silicon). However, it was not possible to detect carbon quantitatively since the software did not contain the carbon K factor and trials made to determine such a factor by using standard carbides prepared to their stoichiometric composition were not successful.

A coventional AE1 electron microscope was also used mainly to check the replica extraction, to obtain selected area diffraction patterns (SAD) from larger particles and in photomicrography.

The main difficulty in using transmission electron microscopy was the preparation of the special thin samples in the form of thin foils and extraction replicas.

4.2.5.1 Thin foil preparation

Rods 3 mm diameter were extracted from the 12.5 mm diameter cylindrical specimens by the electro-errosion technique, Fig.(5). Discs of about 1 mm thickness were sliced off the rods by a small slicer. The discs were held in a special holder and they were ground from both sides on abrasive papers down to 0.2-0.3 mm thickness. The specimens were dish shaped in a "Strues" electrolytic thinner at a voltage of 50 volts in a solution of 10% perchloric acid in sodium acetate. Discs were removed before perforation and finished to perforation in an Edwards ion beam thinner.

4.2.5.2 Carbon extraction replica

A carbon single stage replica was used in the present work. Carbon was evaporated in a vacuum of less than $10^{-4}$ torr by a direct spark between two graphite electrodes to precipitate a carbon film on the bakelite pressed etched sample. The carbon film thickness was determined by observing the colour of a porcelain chip fixed on the bakelite mount of the specimen.

The carbon film was separated off the sample surface electrolytically in a solution of 10% nital at a voltage of 100 volts. The carbon film was collected on copper grids out of the nital solution, rinsed in methanol, then transfered to a beaker filled with tap water to spread the creased carbon film on top of the surface of the water as a result of surface tension. Segments of the carbon replica were collected on copper grids and were allowed to dry in air on a filter paper. Thin foils and extraction replicas were kept in special boxes with a marked place for each sample.

4.2.5.3 Other replicas

In order to detect the carbon in the carbide particles, a carbon film could not be used, since the carbon film would contribute to the level of carbon detected. Therefore, a non-carbon replica was used for this purpose. A silicon replica was prepared by evaporating silicon monoxide in special evaporating baskets. No way was found to judge the

film thickness since the silicon monoxide layer was transparent and different thicknesses were obtained by varying evaporating times. However, the silicon monoxide replica showed a high oxygen peak which overlapped the carbon peak. An aluminium replica was therefore used instead of the silicon replica. It was easy to observe the aluminium film layer in the coating unit and it showed a smaller oxygen peak in the spectrum which allowed better detection of carbon. Both silicon and aluminium replicas were separated off the specimen in the same way employed in separating the carbon replica. However, attempts made to determine the carbon content quantitatively were not successful and it was possible to detect carbon in secondary hardening carbides qualitatively as will be discussed in chapter six of the present thesis.

### 4.2.6 Microanalysis

The chemical microanalysis was carried out using an EDAX 9100 detector, with a computer programme SW 9100 version 2.2, a Bryans type plotter and an A4 X-Y recorder . The idea of the analysis was based on detecting the characteristic X-rays emitted from any of the particles of interest as a result of electron-specimen interaction.

The interaction of a high energy electron beam with thin specimens results in a variety of signals for analysis as shown schematically in Fig.(6) [99]. The details of the physics of the process are well explained elsewhere [47,48].

However, the most important signal for energy dispersive X-ray (EDX) analysis is the emission of the characteristic X-rays which can be detected and processed to give a quantitative analysis of the specimen composition.

The primary (incident) electrons may interact with an electron in the sample, ejecting it from its orbit. If that electron was ejected from an inner atomic shell, the result would be an ion in an exited state. Through a relaxation, or de-exitation, process, this exited ion gives up some energy to return to normal state. The most likely process is that an electron from an outer shell "drops" into the vacancy in an inner shell, each drop results in the loss of a specific amount of energy which equals the difference in energy between the vacant shell and the shell contributing the electron. This energy is given up in the form of electromagnetic radiation (X-rays) in the case of high energy transitions involving inner shells.

The energy of the radiation uniquely indicates the element from which it came, hence they are called characteristic emission or characteristic X-rays.

The X-ray lines are usually named according to the shell in which the initial vacancy occurs and the shell from which an electron drops to fill that vacancy. For instance if the initial vacancy occurs in the K shell and the vacancy filling electron drops from the L shell, a $K_{\alpha}$ X-ray is emitted, if the electron drops from the M shell, the emitted X-ray is the

$K_\beta$ X-ray. Generally, the K, L and M indicate the shell where the vacancy occured and the greek letters $\alpha$, $\beta$ and $\gamma$ refer to the shell contributing the electron.

Each emitted X-ray produces a charge pulse in a semiconductor detector. This tiny and short-lived current is processed by complicated electronics, controlled by a high level computer programme in order to display the energy dispersed X-ray spectrum as peaks of different heights (or intensities), located at certain energy levels. The energy scale is given in K.ev and the intensity is in arbitrary units. Such a spectrum is quite useful in giving a qualitative indication of the chemical composition and could be used to identify different phases as well. A typical time needed to obtain a spectrum is 1-2 minutes. However, such spectrum could be processed by the computer programme to give the quantitative chemical composition either in weight percent or in atomic percent. The idea of quantitation is based on the ratio technique [100] such that, the characteristic X-ray intensity ratio $I_A/I_B$ of two elements A and B measured simultaneously in the analysed volume is directly related to the mass concentration ratio $C_A/C_B$ in the form,

$$C_A/ C_B = K_{AB} \cdot I_A / I_B$$

where $K_{AB}$ is a factor constant for each pair of elements. Cliff and Lorimer [101], were the first to introduce a series of K factors for elements relative to Si and $K_{AB}$ for elements

A and B relative to each other could be determined such that;

$$K_{AB} = K_{ASi} / K_{BSi}$$

The K factor is often termed the Cliff- Lorimer factor. The values of the K factor are usually reported for each separate line (K or L) [47].

In the present work all elements were detected from their K lines except Mo and W because their K line intensities were small enough not to be statistically satisfactory when distinguished from the background, hence measurements were made using the L lines.

It was recommended that the computer program was checked in quantitation when measuring from mixed shells [102]. Therefore a standard Fe-Mo binary alloy was supplied by MBH Analytical Ltd.( London). The standard alloy had a standard reference 13754D and was accompanied by a certificate of its composition containing 10.4% by weight Mo in Fe. The homogeneity of the Mo distribution in Fe was confirmed by analysing the bulk material in the EPMA, which showed a homogeneous solid solution of Mo in Fe, Fig.(7), and the Mo concentration equalled 9.53%. A thin foil was made from the bulk material in the same way used in making thin foils as described earlier. The foil was analysed by the EDAX machine. The analysis was satisfactory, giving the Mo content as 10.2±1%, Fig (8). Such calibration gave confidence in the computer programme which was used to carry out the analysis using different lines.

## 4.3 Wear Testing

The cylindrical specimens were tested on a crossed-cylinder testing configuration described by Mills and Redford [103]. The specimens were rubbed against a surface hardened steel workpiece. The bar was 76 mm diameter, of chemical composition as shown in Table (5) and of surface hardness 705 HV . The microstructure of the workpiece is shown in Fig (9). From the preliminary tests it was found that a speed of 40 m/min. (i.e 167 r.p.m.) and a normal load of 225 N gave reasonable figures for wear volume measurements. The wear volume was measured at intervals of four minutes (160 meters of sliding distance) by measuring the depth of the wear scar. However, interruption of the test to measure wear volume should not affect the test results [104].

The wear volume was calculated from the equation used by Halling [104];

$$V = \pi \sqrt{a \cdot b} \cdot d^2 - \frac{\pi}{8} \cdot \frac{a+b}{\sqrt{a \cdot b}} \cdot d^3$$

where,

a .... radius of specimen

b .... radius of workpiece

d .... depth of wear scar

V .... volume of wear scar

The depth of the wear scar was measured using a Talysurf and

the specimen was leveled to a horizontal position by a special adjusting screw. The Talysurf was calibrated to measure in the vertical direction (wear scar depth), while it scanned the scar horizontally by manual controls. The Talysurf plotted the wear scar profile, such that, the depth was represented on true scale, while the horizontal direction was not to scale. A typical wear scar profile is shown in Fig. (10).

For each specimen, the wear volume was plotted against the sliding distance and a straight line was fitted to the points using the departmental computer programme POLFT1. The slope of the line given by the computer was the wear rate in $m^2$. For each steel, the wear resistance (the inverse of the wear rate in $m^{-2}$) was plotted against the tempering temperature.

Worn surfaces of samples have been examined using scanning electron microscope (SEM). It was found that etching the worn surface with the diluted Vilella's reagent showed the worn surface of the primary carbides free from wear debris and other surface contamination, which facilitated the observation of the abrasion tracks on the worn surfaces of the carbides.

# CHAPTER FIVE

# RESULTS

## 5.1 Results of Metallurgical Investigations

The variation of hardness with tempering temperature for the three different high speed steels is shown in Fig.(11). It was found that the three steels had achieved their maximum secondary hardness after tempering for two plus two hours at 540°C.

It was found that secondary hardening of the three high speed steels examined was associated with the precipitation of the secondary hardening carbide. Before peak hardness, the secondary hardening carbide was found to precipitate heterogeneously as shown in Fig.(12). At peak hardness, colonies of the secondary hardening carbide could be extracted by replica methods as shown in Fig.(13). It is clear from this figure that the secondary hardening carbide particles were of platelet shape and had a maximum dimension of 200-400 Å. Attempts to measure their thickness stereoscopically and by convergent beam diffraction were unsuccessful. However, a reasonable estimate of the thickness could be made as will be discussed in the next chapter.

Thin foils made from steels tempered to peak hardness showed

the dense precipitation of the secondary hardening carbide, Fig.(14). Thin foil micrographs showed the secondary hardening carbide precipitated in colonies or groups which appeared as clouds of precipitates and it was not possible to determine the exact shape or size of the individual particles. It was not possible to carry out crystallographic and microanalysis investigations of these carbides using thin foils because of the high magnetisation of the foil, the fine size of the particles and the fact that the particles were completely embedded in the matrix. It is clear from thin foil micrographs that among the groups of the secondary hardening carbides, there were areas free from precipitates. This was confirmed by successful extraction of these carbides as shown in Fig.(15), where some areas appeared free from precipitates and they were surrounded by carbide colonies.

However, replica extraction of the secondary hardening carbides made it possible to obtain single crystal diffraction patterns as well as their microanalysis.

Single crystal diffraction patterns of the secondary hardening carbide, Fig.(16), revealed a face centred cubic crystal structure of lattice parameter equal to 4.17 A for M42 and M1 and a slightly smaller lattice parameter for the M15 secondary hardening carbide. The microanalysis of these tiny carbides precipitated in M42 and M1 high speed steels showed a carbide rich in molybdenum (about 55 at.%) and containing 20-30 at.%

vanadium. The secondary hardening carbides in M15 high speed steel contained higher amounts of vanadium. A typical chemical analysis of these carbides extracted from samples tempered to their peak hardness is shown in Table (6).

Carbon was detected qualitatively in the secondary hardening carbide. Fig.(17) shows the EDX spectrum of the secondary hardening carbide detected by a window-less detector, which confirmed the carbide nature of the precipitate. However, there was no way to determine quantitatively the amount of carbon in the carbide in order to determine if the carbide was an MC or $M_2C$ carbide.

The variation of chemical composition of the secondary hardening carbides in M42 and M1 high speed steels with tempering temperature, within their entire range of stability, is shown in Fig.(18). It is clear that after peak hardness, vanadium was partially replaced by chromium while the molybdenum content remained constant.

Cementite needles were still observable even after tempering the steel to peak hardness and beyond. However, at higher temperatures the cementite needles became smaller Fig.(19). Cementite was always distinguished from other carbides, especially from the hexagonal $M_2C$ which also had a needle shape, as it was the only iron rich carbide, Fig.(20). The typical composition of cementite precipitated in M42 high speed steel is shown in Table (7), and its composition

variation with temperature around the peak hardness region is shown in Fig.(21).

However, tempering steels for 2+2 hours at 650°C and above showed the disappearance of the secondary hardening carbide in the three steels examined and this was replaced by two other carbides; needle-like hexagonal $M_2C$ carbide rich in molybdenum (tungsten rich in the case of M15 high speed steel) and particles of $M_{23}C_6$ rich in chromium and iron as shown in Fig.(22). The chemical composition of these carbides is shown in Table (7).

After tempering the steels for 24 hours at 700 °C, the microstructure of the three steels examined was found to consist of coarse $M_{23}C_6$, some retained $M_2C$ needles, $M_6C$ particles and a new precipitated phase of tiny particles. This new precipitated phase had the same shape and morphology as the secondary hardening carbides, Fig.(23). The single crystal diffraction patterns obtained from this new phase were found to be identical with those obtained from the secondary hardening carbide. However, its chemical composition was quite different; it was a vanadium rich carbide of composition close to that of the primary MC carbide. The typical chemical composition of this new phase present in all three steels examined is shown in Table (8). In the annealed steels, after 24 hours at 800°C, the microstructure consisted of the three carbides; MC, $M_6C$ and $M_{23}C_6$ all in the coarse stable condition

Fig.(24). Single crystal patterns of MC, $M_6C$ and $M_{23}C_6$ are shown in Fig.(25). It was difficult to differentiate crystallographically between MC and the secondary hardening carbide or between $M_6C$ and $M_{23}C_6$. However, the EDX spectra of these carbides were quite different and could be differentiated one from the other as shown in Fig.(26) and Fig.(27) for cubic $M_2C$ and MC carbides and in Fig.(28) and Fig.(29) for $M_6C$ and $M_{23}C_6$ carbides respectively. The copper peaks appearing in the EDX spectra were an experimental artifact since the replicas were mounted on copper grids and such peaks occured in the background of the spectra as shown in Fig.(30) and Fig.(31) for carbon and aluminium replicas respectively. The sequence of carbide precipitation in the three high speed steels examined could be represented schematically as shown in Fig.(32).

The chemical composition of the primary carbides (MC and $M_6C$) did not vary with tempering temperature as shown in Fig.(33). They also maintained their crystal structure and no change was observed in their lattice parameters. The primary carbides were observable by optical microscopy and scanning electron microscopy as shown in Fig.(34) and Fig.(35) respectively. However, some small particles of the primary carbides were extracted by replica which enabled single crystal patterns to be obtained and microanalysis of these carbides to be carried out. Primary carbides were observable in thin foils, Fig.(36),

but chemical analysis of primary carbides from thin foils showed higher values of iron content than that obtained from analysing carbides extracted by replica, or when large particles were analysed by EPMA. Coarse primary carbide particles analysis made by EPMA was confirmed by the EDX analysis, Table (7). Also, specimens of M42 and M1 were scanned by EPMA for the detection of the distribution of different alloying elements as shown in Fig.(37) and Fig.(38) for M42 and M1 high speed steels respectively. It is clear that both $M_6C$ carbide precipitated in M42 and MC carbide precipitated in M15 high speed steels were deficient in cobalt. However, both carbides contained about the same amount of chromium as the matrix. $M_6C$ carbide was deficient in vanadium, rich in molybdenum and MC carbide was rich in vanadium, deficient in both molybdenum and tungsten.

Selective etching of steels showed the carbide of interest which appeared dark against a white background, Fig.(39), which facilitated the measurement of volume fraction, particle size distribution and average particle size of primary carbides by the Quantimet. It was found that the volume fraction of primary carbides did not vary with tempering temperature in the three steels examined , Fig.(40). Also, primary carbides maintained their average particle size, Fig.(41), and the particle size distribution remained unchanged and they maintained the distribution shown in

Fig.(42) for MC carbide and in Fig.(43) for $M_6C$ carbide. The relation between the volume fraction and the average particle size of the primary carbides is shown in Fig.(44). It is clear from this figure that the MC type carbide was more sensitive to particle coarsening with the increase of volume fraction than the $M_6C$ type carbide.

## 5.2 Wear Results

The wear volume was calculated as explained in the previous chapter and was plotted against sliding distance; a straight line using a least squares analysis was drawn through the results. Fig.(45) shows an example of the results obtained from samples of high speed steels tempered for 2+2 hours at 530 °C. The slope of each straight line given by the computer fitting programme was the wear rate in $m^2$. The wear resistance (the inverse of the wear rate in $m^{-2}$) was plotted against tempering temperature as shown in Fig.(46).

It was found that the wear resistance of specimens over-tempered beyond peak hardness was always lower than that of samples having the same hardness and tempered prior to peak hardness as shown in Fig.(47). Wear resistance was plotted against hardness for the three steels examined and the relation was found to be non-linear as shown in Fig.(48). Examination of the high speed steel wear surface showed that primary carbides in steels tempered to their peak hardness

were stable in their original places and were worn down to the same level as the martensitic matrix, Fig.(49). These carbides exhibited flat wear surfaces, Fig.(49) and Fig.(50). However, abrasion tracks, Fig(49) and Fig.(50) and cracks Fig.(51) were observed on the worn surfaces of these carbides.

In the case of annealed samples, it was found that carbides were loose and acted as abrasives which ploughed the surface of the high speed steels, Fig.(52).

# CHAPTER SIX

# DISCUSSION

## 6.1 Identification of Secondary Hardening Carbides in High Speed Steels

It is clear from chapter two that previous to the present work the secondary hardening carbides in high speed steels have been identified only by crystallographic methods. X-Ray diffraction identified hexagonal $M_2C$ carbide [7] to be the secondary hardening carbide. Electron diffraction identified $M_{23}C_6$ [41] and MC [42] to be the carbides responsible for the secondary hardening of high speed steels. The identification of MC carbide as the secondary hardening carbide has been confirmed by more recent work [4,43,105]. Apart from the replica extraction and the single crystal pattern introduced by Mukherjee [42], all the recent workers did not report the extraction of these carbides and the unsuccessful extraction of these carbides has been reported [4]. The study of these carbides from thin foils has shown this technique to be inadequate and the useful outcome from the thin foil technique was the ring pattern data [105].

Mukherjee [42], used selected area diffraction (SAD) in his

investigation since the convergent beam technique was not developed at that time. He introduced a ring pattern from the secondary hardening carbides extracted from sample tempered to its peak hardness. Then from an over-tempered sample, he introduced a single crystal pattern and claimed that this was from the secondary hardening carbide after it coarsened as he believed. He did not introduce the photomicrograph of the carbide from which he obtained the diffraction patterns, nither at peak hardness nor after coarsening of the over-tempered samples.

The present work has shown that the secondary hardening carbides did not coarsen after peak hardness but they dissolved in the matrix and disappeared. Also, it is clear from the present work that the primary MC carbide is always present in the microstructure. Some small particles of the primary MC carbide could be picked up by the replica and diffraction patterns were obtainable. However, Fig.(25) shows a single crystal pattern obtained from a primary MC carbide which is identical to that claimed by Mukherjee to be obtained from the secondary hardening carbide. However, this makes the single crystal pattern reported by Mukherjee questionable.

The present work introduced evidence of successful carbon and non-carbon replica extraction of these tiny carbides and for the first time introduced :

1. photomicrographs of the secondary hardening carbides

extracted from different high speed steels which enabled imaging and measuring of the size of such carbides, Fig.(13) and Fig.(15).

2. single crystal diffraction patterns obtained from the secondary hardening carbides, by using convergent beam diffraction, Fig.(16).

3. quantitative microanalysis of the metallic part of the secondary hardening carbides by EDX technique, Fig.(26) and Table (6).

4. qualitative detection of carbon present in these carbides which confirmed the carbide nature of the secondary hardening carbides, Fig.(17).

5. the mechanism of carbides precipitation in the tempering of high speed steels, Fig.(32).

In the present work, the diffraction patterns of the secondary hardening carbides revealed an fcc structure of lattice parameter 4.17 Å. The chemical composition of carbides extracted from M42 and M1 was rich in molybdenum and contained vanadium. It was concluded that the secondary hardening carbides were either MC carbides dissolving that amount of molybdenum or cubic $M_2C$ carbide containing vanadium. The cubic $M_2C$ carbide was recently discovered in molybdenum steels showing identical diffraction patterns to that of MC carbide and transforming at higher temperatures to hexagonal $M_2C$ carbide [40], in the same way as was observed in the present

work. However, following the variation in composition with tempering temperature for these carbides precipitated in M42 and M1 high speed steels,Fig.(18), it was found that secondary hardening carbides maintained constant molybdenum content. The vanadium content was partially replaced by chromium at higher tempering temperatures. Also, tempering steels after peak hardness at 650°C and above, no trace of these carbides could be detected in the three steels examined. The secondary hardening carbides were completely replaced by two other carbides; hexagonal $M_2C$ carbides of needle-like shape and particles of $M_{23}C_6$ carbide. This carbide replacement explains the confusion of the previous workers who identified either hexagonal $M_2C$ [7] or cubic $M_{23}C_6$ [41] as the secondary hardening carbide in high speed steels. This confusion was because those workers were interested in studying over-tempered specimens to allow the secondary hardening carbides to coarsen as they believed.

The metastable role of the secondary hardening carbide encouraged the belief that this carbide was the cubic $M_2C$ rather than being the MC carbide which is known as a stable carbide in steels. However, it was a necessity to detect the precipitation of the secondary MC carbide. In samples tempered up to 700°C for 2+2 hours, no trace of secondary MC carbide could be detected. More samples were tempered for longer times at 700°C instead of increasing the tempering temperature for

constant times in order not to be close to the austenite transformation temperature.

After tempering samples for 24 hours at 700°C, a new phase was found to precipitate, Fig.(23). This phase was rich in vanadium and its diffraction patterns were identical to those obtained from the secondary hardening carbides. This carbide was quite stable and had been detected in samples tempered for 24 hours at 800°C. This was the secondary MC carbide and the secondary hardening carbide was the cubic $M_2C$ carbide. Identifying the secondary hardening carbide as cubic $M_2C$ carbide was based on the following :

1. it had the same crystal structure as cubic $M_2C$ carbide.
2. it was rich in molybdenum.
3. it was a metastable phase in the three steels examined.
4. within its entire range of precipitation, it exhibited constant molybdenum content while the vanadium was partially replaced by chromium.
5. the precipitation of the secondary MC carbide was detected at higher tempering temperatures well beyond peak hardness.

The secondary hardening carbide in M15 high speed steel contained a higher vanadium content than the secondary hardening carbides in M42 and M1 high speed steels. However,

in M15, the secondary MC carbide showed a higher vanadium content than that determined in the secondary hardening carbide. However, further work is required to study the role of different alloying elements on the composition of the cubic $M_2C$ carbide.

It is clear that cubic $M_2C$ and MC carbides could be differentiated one from the other by determining the carbon content in the carbide. However, attempts have been made to determine quantitatively the carbon content in the secondary hardening carbide. Secondary hardening carbides were extracted on non-carbon replicas (silicon and aluminium) and it was possible to detect carbon qualitatively using a window-less EDX detector. However, the K factor of carbon to any other element was not available. Attempts were made to determine the K factor of carbon to chromium or molybdenum by using $Cr_3C_2$ and $Mo_2C$ carbides prepared to their stoichiometric compositions. The K factor would be determined by knowing the carbide chemical composition and comparing the X-ray intensities of carbon and the metal. Unfortunately, in both supplied carbides ($Cr_3C_2$ and $Mo_2C$), each carbide particle showed different X-ray intensity ratio between carbon and the metal. This showed the deviation of the carbides' composition from stoichiometry and they were no longer useful as standard carbides for the carbon K factor determination. Another method has been reported to determine the carbon K factor by

simultaneous analysis of the carbide by the EDX and EELS techniques [106]. However, due to lack of time, this attempt has not been made.

Determination of the carbon content in secondary hardening carbides is valuable in the study of the strengthening role of these carbides in high speed steels. It is reported that the carbon content affected the properties of carbides [89,107]. However, the quantitative analysis of carbon in the present work was not successful.

Although high speed steels could mainly be considered as high molybdenum or high tungsten steels containing other alloying elements, it is not clearly understood why all previous workers, using crystallographic data, identified the secondary hardening carbide as MC carbide and completely ignored the cubic $M_2C$ carbide which has the identical crystal structure as MC carbide [40], and has been known for four decades [108]. Also, the observation reported in 1953 by Kuo [7], about the possibility of the precipitation of cubic $M_2C$ carbide in high speed steels, did not receive consideration by other workers. However, studies of the crystallography, the chemical analysis and the kinetics of secondary carbide precipitation in the present work have introduced evidence that the cubic $M_2C$ carbide was the secondary hardening carbide in high speed steels.

The microanalysis technique played an important role in

identifying carbides whose crystallographic data were similar. The EDX spectrum of a carbide could be considered as its finger print which could not be confused with other spectra obtained from other carbides as shown in Fig.(26-29).

## 6.2 Shape, Size, Composition and Distribution of the Secondary Hardening Carbides

Henderer [95], assumed the secondary hardening carbides to be of needle-like shape, 200 Å long and 50 Å across. This estimation was made since the shape and size of these carbides have not been reported in the literature previous to the present work.

In the present work, the photomicrographs of thin foils tempered to peak hardness showed the secondary hardening carbides as clouds of precipitates. It was not possible to image the shape or measure the size of the carbide particles using thin foils. This was a result of the tiny size of the particles totally embedded in the strongly magnetic matrix. The difficulty of studying the secondary hardening carbides from thin foils has also been shown recently [4,105]. However, the replica extraction of these carbides has been carried out successfully in the present work. Secondary hardening carbides were of platelet shape, 200-400 Å across. Attempts made to measure the thickness of these platelets streoscopically and by convergent beam diffraction were unsuccessful due to the

small thickness of the plates. However, it has been reported from misfit calculations that VC carbide precipitated in α-iron matrix in a platelet shape having a thickness equaled to one sixteenth of the maximum dimension of the plate [109]. This allows the thickness of the secondary hardening carbides, which have an identical crystal structure to that of VC carbide, to be estimated as 15-30 Å. It is clear from Fig.(13) and Fig.(15) that carbides were different in thickness since they appeared different in darkness. The value of 25-50 Å would be a reasonable estimation of the thickness of these particles.

The chemical composition of the carbides could be studied in two ways. The first way would be to determine the metallic content, including all the substitutional atoms, of the carbide and the second way would be the determination of the carbon content and the role of the interstitial atoms. Both the content of the metallic elements and the carbon content in the carbides had a great effect on the properties of the carbide and on its role in strengthening the matrix [82,89,107].

In the present work, attempts to determine the carbon content of the secondary hardening carbides have been unsuccessful. However, studying the chemical composition of the metallic part of the secondary hardening carbide was interesting. The determination of the chemical composition of the secondary

hardening carbides provided a strong evidence to prove that these carbides were the cubic $M_2C$ carbide and not the MC carbide as thought before. The composition of the metallic part of the secondary hardening carbides in M42 and M1 high speed steels were close to each other over the entire range of their stability. They also showed a constant molybdenum and tungsten content over their range of stability. The vanadium content decreased in both carbides from about 30 at.% to about 20 at.%. Chromium replaced vanadium and its proportion increased from about 10 at.% to about 20 at.% as shown in Fig.(18). Up to the peak hardness, no vanadium-chromium replacement occured and the composition was constant. After peak hardness, changes in the vanadium and chromium contents occured. The vanadium-chromium replacement associated with constant high molybdenum content was more likely to occur in a molybdenum carbide rather than a vanadium carbide. This metal replacement provided additional evidence that these carbides were the cubic molybdenum carbide and not the vanadium carbide.

The vanadium-chromium replacement was associated with the dissolution of the secondary hardening carbides. However, more work is needed to show the exact role of chromium on the stability of the cubic $M_2C$ carbide precipitated in high speed steels.

Stiller and co-workers [4], using atom-probe field-ion

microscopy analysed the composition of the secondary hardening carbides precipitated in ASP60 powder metallurgy prepared high speed steel. They found that its metallic part contained about 30 at.% vanadium which was close to that determined in the present work. However, they identified the carbide as MC carbide and totally ignored the possibility of the carbide being the cubic $M_2C$ carbide. However, they did not study the variation of carbide chemical composition with tempering temperature.

It is clear from the micrographs of thin foils , Fig.(14) and the successfully extracted secondary hardening carbides, Fig.(15) that there were some regions which were free from carbide precipitation. This could be explained as a result of a non-homogeneous distribution of alloying elements in the steel. Such non-homogeneity is expected in the fabrication of high speed steel containing large amounts of primary carbides rich in these alloying elements. It has been reported that regions surrounding primary carbides were rich in carbon and alloying elements [110]. Molten high speed steel has the most homogeneous composition. However, as primary carbides precipitate by nucleation and growth, atoms of alloying elements migrate to form these carbides. This contributes to the non-homogeneity of the steel during solidification. Such non-homogeneity would lead to areas deficient in alloying elements where no precipitation could occur.

Apart from these areas free from precipitation, the secondary hardening carbides were well distributed in colonies of carbides (groups) all over the matrix.

## 6.3 Sequence of Carbide Precipitation in High Speed Steels

Cementite was detected well before peak hardness. It was also detectable even after peak hardness and up to tempering temperatures of about 600°C. The cementite needles at higher temperatures became smaller as shown in Fig.(19). However, the disappearance of cementite, beyond peak hardness, was associated with a change in its chemical composition, where iron was partially replaced by chromium as shown in Fig.(21). Cementite was always differentiated from other carbides, especially the hexagonal $M_2C$ carbide which showed the same needle shape, as it was the only iron-rich carbide precipitated in high speed steels, Fig.(20).

The fine needles appearing in (b) of Fig.(19) were at first thought to be the initial hexagonal $M_2C$ carbide precipitates, however, the EDX spectrum obtained from these needles confirmed their cementite identity.

At the beginning of secondary hardening, the hardness started to increase and secondary hardening carbides were found to precipitate heterogeneously, as shown in Fig.(12). At peak hardness, the secondary hardening carbide precipitates became

very dense as shown in foils, Fig.(14) and the extraction replica, Fig.(15). However, areas free from precipitation have been observed.

After peak hardness, the secondary hardening carbides dissolved into the matrix and did not coarsen as thought before. The dissolved secondary hardening carbides were replaced by the precipitation of two other carbides; hexagonal $M_2C$ carbide rich in Mo/W and cubic $M_{23}C_6$ rich in Cr and Fe. The in-situe transformation of the cubic $M_2C$ to hexagonal $M_2C$ reported earlier [40], was not observed in the present work.

After tempering the steel for 24 hours at 700 °C, the precipitated carbides were found to consist of some retained needle-like hexagonal $M_2C$ carbide, $M_{23}C_6$ particles, secondary $M_6C$ carbide and the new precipitated secondary MC carbide. This new phase was richer in vanadium than the secondary hardening carbide and had a chemical composition very close to that of the primary MC carbides, Table (8).

After tempering the steels for 24 hours at 800°C, The detected secondary carbides were of types MC, $M_6C$ and $M_{23}C_6$ carbides, all in the stable coarse state as shown in Fig.(24). These secondary carbides were the carbides dissolved during austenitising of the steels, since the volume fraction, particle size and particle size distribution of the primary MC and $M_6C$ carbides were found unchanged with heat treatment, and all the $M_{23}C_6$ carbide formed during tempering the steels as a

secondary carbide, Fig.(32).

It is clear that the four main alloying elements in high speed steels; molybdenum/tungsten, vanadium and chromium exhibited their own mechanisms of carbide precipitation in high speed steels as they do in pure ternary steels. The presence of vanadium resulted in the precipitation of MC carbide directly out of the matrix which coarsened at high temperatures. Chromium showed direct precipitation of $M_{23}C_6$ carbide without the precipitation of the metastable $M_7C_3$ carbide in the same way reported earlier for steels rich in Mo/W and Fe. The mechanism of precipitation of molybdenum carbide was of interest. Molybdenum behaved in high speed steels in the same way as it did in pure molybdenum steels. Fig.(32) shows the sequence of carbide precipitation in high speed steels. It is clear that the precipitation of molybdenum carbides in high speed steels occured in the same sequence as reported recently for molybdenum steels [40]. However, due to the presence of other alloying elements, the high speed steel carbides were alloyed carbides and not pure carbides as in the case of pure ternary alloy steels. It is clear from the present work that molybdenum was the predominant alloying element in molybdenum high speed steels. The secondary hardening was a direct result of the precipitation of a molybdenum carbide ($M_2C$ type). The predominance of molybdenum in steels containing vanadium in solution is contradictory to the early work of Payson [27] who

reported that vanadium carbide would precipitate in steels containing vanadium and molybdenum if the vanadium content exceeded 0.9 % by weight.

## 6.4 Primary Carbides in High Speed Steels

Primary carbides could be identified as those carbides formed during solidification and secondary carbides as those precipitated on tempering high speed steels. Primary carbides are of the types MC and $M_6C$. The $M_{23}C_6$ carbide was a secondary carbide which precipitated on tempering the steel and completely dissolved during austenitising. Secondary MC and $M_6C$ carbides also precipitated during the tempering of high speed steels. The secondary carbides MC, $M_6C$ and $M_{23}C_6$ are those which dissolve in the matrix during the hardening process and precipitate during tempering the steel. However, they are the final form of the sequence of carbide precipitation in tempered high speed steels, Fig.(32). The present work has shown that the primary MC and $M_6C$ carbides were not affected by heat treatment of high speed steels. These carbides maintained their volume fraction, average particle size, particle size distribution, chemical composition and constant lattice parameter over the whole tempering range, being unchanged from the as quenched state. As the volume fraction of primary carbides increased from one

steel to another, the average particle size of the carbide increased. However, the particle size of MC carbide showed a greater sensitivity to volume fraction than $M_6C$, Fig. (44). This underestimated the role of the increased volume fraction of MC carbides in high speed steels, since this would result in an increase in particle size, which is not recommended from a strengthening view point for steels [84].

It is clear that there was no reason to correlate the phenomena of secondary hardening to the presence of primary carbides. In previous work [95], the strength of M1 high speed steel was attributed to the precipitation of the fine secondary hardening carbides (72%) and the martensite strength (28%), while the contribution of primary carbides to the strength of M1 high speed steel was found to be insignificant (0.1%). Also, the intensity of the secondary hardening and the associated increase in wear resistance could not be attributed to the quantity of primary carbides. This is in contradiction to the work of Roberts [80], who correlated the higher intensity of wear resistance of M2 high speed steel to the increased quantity of MC carbide despite the decrease in the amount of $M_6C$ carbide. It has been shown that M42 high speed steel containing 5% MC exhibited a higher hardness and wear resistance than M15 high speed steel containing 10% MC. The 10% volume fraction of MC carbide is close enough to the 12% volume fraction of MC carbide reported earlier as the value

above which no increase in wear resistance, by a further increase in volume fraction, occured [80]. As for the total primary carbide content (MC + $M_6C$), it was found that M1 high speed steel containing a higher amount of primary carbides than M15 high speed steel showed a lower hardness and wear resistance than M15 high speed steel. This agreed with the previous work which attributed no role to the primary carbides in contributing to the strength and wear resistance of high speed steels [70,86,87,94-96].

The chemical composition of primary carbides determined in the present work was found to agree with that reported by previous workers as shown in Table (9) and Table (10). It is clear from these tables that primary carbides in high speed steels are alloyed carbides. The composition of the metallic part of the MC carbide formed in different high speed steels contained 58-73 at.% vanadium, 15-29 at.% molybdenum + tungsten, 6-11 at.% chromium, 1-6 at.% iron and very little cobalt even when the steel contained cobalt. The MC carbide formed in M42 high speed steel was found to contain less than 1 at.% cobalt, despite the steel having a cobalt content of 8 % by weight. The composition of the metallic part of $M_6C$ carbides formed in different high speed steels usually contained 34-57 at.% molybdenum + tungsten with the remainder of the elements being iron, cobalt, vanadium and chromium. This confirmed the $\eta_1$ nature of this double carbide as shown previously in chapter

two. It was observed that both MC and $M_6C$ carbides contained about the same chromium content (5-10 at.%). The variation in the chemical composition of the carbides was mainly a result of the variation of the composition of the steels.

## 6.5 Wear of High Speed Steels

The wear of high speed steel tools could be a result of either continuous wear (classical wear process), or a result of edge chipping (a fracture procss). In the present work, the continuous wear of high speed steel has been considered. A crossed-cylinder wear test was used for wear testing, in which a stationary cylindrical sample rubbed against a surface hardened steel bar.

From the wear data, it is clear that the secondary hardening peak was associated with another peak in the wear resistance. The relation between wear resistance and hardness was found to deviate from the linear relation reported by Roberts [25]. A lower wear resistance was found for the samples tempered above peak hardness than that for samples tempered below peak hardness for samples having the same hardness, Fig.(47). This strongly supports the conclusion that the microstructure of high speed steel affects both hardness and wear resistance, but with different sensitivity to microstructure.

It is clear from the metallurgical study in the present work

that over the temperature range of the secondary hardening region, many changes took place in the microstructure of high speed steels. Cubic $M_2C$, hexagonal $M_2C$, $M_{23}C_6$, MC and $M_6C$ carbides were replacing cementite in the sequence shown in Fig.(32). At the same time the composition of the matrix was obviously dependent on the type and quantity of the precipitated second phase. The non-linear relation between wear resistance and bulk hardness may be explained as a result of the significant changes occuring in the microstructure of high speed steels.

Below peak hardness, the microstructure consisted of a martensitic matrix with a dispersion of secondary hardening carbide precipitates. As the tempering temperature increased up to the peak hardness, the amount of secondary hardening carbide increased to its maximum volume fraction. This was associated with an increase in secondary hardness and wear resistance. Up to peak hardness, the only second phase detected was the secondary hardening carbide as well as some cementite needles. As the tempering temperature increased, the amount of the secondary hardening carbide increased and the amount of cementite decreased.

However, after peak hardness, the secondary carbide dissolved. The dissolution of this carbide was associated with a change in its composition which would be expected to affect its properties and its strengthening effect on the matrix.

The dissolution of the secondary carbide was followed by the precipitation of different carbide species, Fig.(32). The precipitation of these phases as well as the continuous decomposition of martensite would give the steel a lower wear resistance at the same level of hardness compared with samples tempered before peak hardness. This finding is in agreement with that of Moore [63], who reported different roles of microstructure on wear and hardness.

A review of the literature in chapter three showed that primary carbides had no significant role in contributing to the strength and wear resistance of high speed steels. The present work has shown that the wear resistance and hardness could not be correlated to the presence of primary carbides. The volume fraction, particle size, crystal structure and chemical composition of the primary carbides did not change during the secondary hardening of the steels. The previously held view that increased amount of primary carbides result in better wear resistance has not been confirmed in the present work.

The matrix of samples tempered to peak hardness was strong enough not to ploughed by the primary carbides. The primary carbides were held in their initial places and wore down to the same level as the matrix. This provided evidence that the wear rate of primary carbides was the same as that of the martensitic matrix, hence they provide no contribution to wear

resistance of the steel. This has also been shown in the previous work of Kasak and Neumeyer [70].

The worn surface of the primary carbides exhibited abrasion tracks. Abrasion tracks, as a result of plastic deformation, were hardly expected to appear on surfaces of hard carbides. However, hard carbides are known to be brittle materials at room temperature, but it has been reported that at high temperatures, the hardness of carbides fell drastically and that they deformed plastically on slip systems analogous to fcc metals as explained by Toth [107].

The exact interfacial temperature between two mating surfaces rubbing against each other is not yet known nor has been determined experimentally in the present work. However, Trent [92], reported that such temperatures might reach 1000°C in the case of cutting tools. Such high temperatures are high enough to cause drastic softening to the carbides allowing them to deform plastically, which may explain the abrasion tracks which appeared on the worn surface of the carbides. Some carbides exhibited cracks and chipping as shown in Fig.(51). This may be explained as a result of the random shape of the carbides. The wear process may result in thin weak sections within the carbide particles which may crack under the effect of the normal load and the friction forces. Also, as explained by previous workers [81], such chipping and cracking would appear in the early cycles of rubbing when the

carbide surfaces were at a low temperature and carbides were still in a brittle state.

In annealed high speed steels, the matrix was soft enough to be ploughed by the primary carbides. Examination of the wear surface of such steels by SEM showed the harmful role of the primary carbides. Primary carbides appeared loose on the worn high speed steel surface and they acted as abrasives, forming a three body abrasion system, Fig.(52). This harmful role of the primary carbides contributed to the drastic fall in wear resistance of over-tempered high speed steels.

Primary carbides did not contribute to the wear resistance of high speed steels at any stage of tempering, however, these carbides contributed to the wear rate of the over-tempered steels. Thus, the presence of the primary carbides in high speed steels did not appear to contribute to improved mechanical or wear resistant properties. This agreed with the previous work which also showed that primary carbides made no contribution to increasing the hardness and wear resistance of high speed steels [70,86,87,94-96].

Despite the clear relation between microstructure and wear resistance, it is still difficult to express this relation mathematically.

However, more work should be carried out to contiue the work of Roberts and Hamaker [98], to develop matrix steels of improved properties. The idea behind the matrix steel was to

produce a primary carbide-free steel. Roberts and Hamaker limited the composition of their steel to be similar to that of the quenched matrix. On austenitising such steel, the grain size coarsened. Consequently, they austenitised the steel at lower temperatures to allow some undissolved carbides to remain in order to restrict grain coarsening. It is clear that the quenched matrix produced by this method was deficient in carbon and alloying elements. Consequently, such matrix steel showed slightly lower secondary hardening than conventional high speed steels [80]. These quantities of undissolved carbides required to stop grain coarsening would be allowed to form by increasing the alloying elements to a level sufficient to form this limited quantity of undissolved carbides. In this case, the steel can be austenitised at the normal high austenitising temperature without excessive grain growth. The quenched matrix will be as rich in carbon and alloying elements as the matrix of the normal high speed steel . This matrix should display a secondary hardness of the same magnitude as that of normal hiqh speed steels. Such steels will contain a limited quantity of primary carbides which should limit their harmful effect in the over-tempered steels. At the same time, such steel would be cheaper owing to the reduced quantities of expensive alloying elements normally present in the form of primary carbides, which are not realy required.

# CHAPTER SEVEN

## CONCLUSIONS

1. The secondary hardening carbide in high speed steels was found to be the cubic $M_2C$ carbide and not the MC carbide as was previously thought.

2. The secondary hardening carbide did not coarsen beyond peak hardness, but dissolved in the matrix and other carbide species precipitated.

3. The secondary vanadium carbide (MC type) was found to precipitate in the over-tempered state well beyond the peak hardness.

4. High speed steels exhibited the same sequence of carbide precipitation as those reported in simple ternary steel systems.

5. The microanalysis technique was found to be a reliable technique in identifying high speed steel carbides.

6. Primary carbides remained unaffected during the tempering of high speed steels and did not contribute to the secondary hardening of high speed steels.

7. The precipitation of secondary hardening carbides in high speed steels was found to be associated with an increase in hardness and an increase in wear resistance.

8. In samples tempered to peak hardness, primary carbides wore down to the same level as the matrix giving no contribution to wear resistance. In over-tempered steels primary carbides were observed to abrade the matrix of high speed steel, thus contributing to an increase in the wear rate.

9. The wear resistance of over-tempered high speed steels was found to be lower than that of steels of the same hardness tempered below peak hardness.

10. The relation between wear resistance and hardness of high speed steels was found to be non-linear, with different sensitivity to hardness from steel to another.

## RECOMMENDATIONS FOR FUTURE WORK

1- In the present work, the cubic $M_2C$ carbide has been discovered to precipitate in high speed steels as the secondary hardening carbide. The data available on this carbide is very limited. The effect of various elements on the stability and mechanical properties of this carbide should be studied. This may then lead to high speed steels of improved composition having more stable secondary hardening carbides of better properties, which would lead to improved mechanical and wear resistance properties of such steels.

2- The presence of the primary carbides has been shown to be of no benefit and to be even harmful to the wear resistance of high speed steels beyond peak hardness. The idea of manufacturing matrix steel free from primary carbides needs to be reconsidered. Matrix steel normally contains a limited quantity of undissolved carbides to restrict grain growth during austenitising of the steel at high temperature. This quantity of carbides should be allowed to form by the addition of the necessary amounts of alloying elements instead of by lowering the austenitising temperature as was done in the early trials on matrix steels. This would allow the steel to be austenitised at the usual high temperatures in order to produce a matrix rich in carbon and alloying elements. The secondary hardening of such steel may have the same intensity as that of the original high speed steel.

3- The development of high speed steel in the past has been by trial and error. However, by the addition of the alloying elements which give the optimum composition of the secondary hardening carbide and limiting the quantity of primary carbide, it may be possible to design improved high speed steels.

REFERENCES:

[1] PAYSON P. ;"The Metallurgy of Tool Steels"; 1966; London; John Wiley and sons.

[2] Taylor F. ; Trans. A.S.M.E.; 28; 1907; p. 38-58 .

[3] Westgren A. and Phragmen G. ; Trans. Am. Soc. for Steel Making; 13(4); 1928; p. 539-554.

[4] Stiller K., Sevevson L-E, Howel P., Wang Rong H-O and Dunlop G. ; Acta. Metall.; 32(9); 1984; p. 1457-1467.

[5] Kim C., Biss V. and Hosford W.F. ; Metall. Trans.; 13 A; 1982; p. 185-191.

[6] Kayser F. and Cohen M. ; Metall. Progress; 61; 1952; p. 79-85.

[7] Kuo K. ; J.I.S.I.; 174; 1953; p. 223-228.

[8] Westgren A. ; Jernokontorets Annaler; 117; 1; 1933; p. 1-14 (in German).

[9] Goldschmidt H.S. ;"Interstitial Alloys"; 1967; London; Butterworth.

[10] Kuo K. ; Acta Metall.; 1; 1953; p. 301-304.

[11] Fraker A.C. and Stadelmaier H.H. ; Trans. of the Metall. Soc. of A.I.M.E.; 245; 1969; p. 847-850.

[12] Powder Diffraction File Index ; 1983; International Centre for Diffraction Data; USA; index no. 14-407.

[13] Goldschmidt H.J. ; Metallurgia; 40; 1949; p. 103-104.

[14] Inoue A. and Masumoto T. ; Metall. Trans.; 11 A; 1980; p. 739-747.

[15] Cescon T. ; 37th. Annual congress of the ABM; Rio de Janeiro; July 1982; p. 1-22; B.I.S.I.T.S. translation no. BISI 21728-T; May 1983.

[16] Goldschmidt H.J. ; J.I.S.I.; 186 ;1957; p. 68-85.

[17] Goldschmidt H.J. ; J.I.S.I.; 160; 1948; p. 345-362.

[18] Kuo K. ; J.I.S.I.; 184; 1956; p. 258-268.

[19] Honeycombe R.W.K. ; "Structure and Strengthening of Alloy Steels"; 1974; London; Climax Molybdenum Co. .

[20] Andrews K.W., Dyson D.I. and Keown S.R. ; "Interpretation of Electron Diffraction Patterns"; 2nd. edition; 1971; London; Adam Hilger.

[21] Blickwede D.J., Cohen M. and Roberts G.A. ; Trans. A.S.M.; 42; 1950; p. 1161-1191 .

[22] Pacyna J. ; Archiv Fur Eisenhuttenwesen; 55(6); 1984; p. 291-298 (in English).

[23] Kim K., Johnson A.R. and Hosford W.F. ; in "Processing and Properties of High Speed Steels"; edited by : Wells M.G.H. and Lherbier L.W.; 1980; Las-Vegas; The Metallurgical Society of A.I.M.E.; p.32-74.

[24] Scott H. ; Scientific papers, Bureau of Standards; 16; 1920; p. 521-536.

[25] Roberts G.A., Hamaker J. and Johnson A. ;"Tool Steels"; 3rd. edition; 1962; A.S.M. .

[26] Cohen M. ; Trans. A.S.M.; 41; 1949; p. 35-94.

[27] Payson P. ; Trans. A.S.M.; 51; 1959; p. 60-93.

[28] Bain E.C. and Jeffries Z. ; The Iron Age; 112 (13); 1923; p. 805-810.

[29] Cohen M. and Koh P.K. ; Trans. A.S.M.; 27; 1939; p. 1015-1051.

[30] Gordon P. and Cohen M. ; Trans. A.S.M.; 30; 1942; p. 569-591.

[31] Seal A.K. and Honeycombe R.W.K. ; J.I.S.I.; 188; 1958; p. 9-15.

[32] Tekin E. and Kelly P.M. ; J.I.S.I.; 203; 1965; p. 715-720.

[33] Smith E. ; Acta Metall.; 14; 1966; p. 583-593.

[34] Davenport A.T. ; Ph.D. Thesis; 1968; University of Sheffield.

[35] Kuo K. ; J.I.S.I.; 173; 1953; p. 363-375.

[36] Kuo K. ; Jern. Annlr.; 140 (1); 1956; p. 24-46. (in English)

[37] Irani J.J. and Honeycombe R.W.K. ; J.I.S.I.; 203; 1965; p. 826-833.

[38] Preston G.D. ; Proc. Roy. Soc.; 167 A; 1938; p.526-583.

[39] Raynor D., Whitemen J.A. and Honeycombe R.W.K. ; J.I.S.I.; 204; 1966; p. 349-354.

[40] Ustinovshchikov Yu. I. ; Metal Science; 18; 1984; p. 337-344.

[41] White C.H. and Honeycombe R.W.K. ; J.I.S.I.; 197; 1961; p. 21-28.

[42] Mukherjee T. ; in "Materials for Metal Cutting"; 1970; I.S.I. report no. 126; p.80-96.

[43] Kupolova I.K. ; Metal Science and Heat Treating of Metals; 22 (7-8); 1980; p. 522-527.

[44] Woolform M.M. ; "X-ray Crystallography"; 1979; Cambridge; Cambridge University Press.

[45] Barrett C. and Massalski T.B. ; "Structure of Metals"; 3rd. edition; 1982; Oxford; Pergamon Press.

[46] Hirsch P., Howie A., Nicholson R.B., Pashley D.W. and Whelan M.J. ; "Electron Microscopy of Thin Crystals"; 1977; Florida; Robert E. Krieger Publishing Co. .

[47] Williams D.B. ; "Practical Analytical Electron Microscopy in Material Science"; 1984; New-Jersey; Philips Electronic Instruments.

[48] Russ J.C. ; "Fundamentals of Energy Dispersive X-ray Analysis"; 1984; London; Butterworth.

[49] Hurricks P.L. ; Wear; 26; 1973; p. 285-304.

[50] Hogmark S. and Vingsbo O. ; Wear; 31; 1975; p. 39-61.

[51] Tabor D. ; Journal of Lubrication Technology; 99(4); 1977; p. 387-395.

[52] Jahanmir S. ; in "Iternational Conference of The Fundamentals of Tribology"; edited by Suh N.P. and Saka N. ; 1980; Mass. Inst. Technol.; p. 455-467.

[53] Eyre T.S. ; Tribology International; 11; 1978; p. 91-96.

[54] Rabinowicz E. ; Trans. A.S.M.E.; 103; 1981; p. 188-193.

[55] Sarkar A.D. ; "Wear of Metals"; 1976; Oxford; Pergamon Press.

[56] Burwell J.T. and Strang C.D. ; Journal of Applied Physics; 23(1); 1952; p. 18-28.

[57] Eyre T.S. ; Tribology International; 10; 1976; p. 203-212.

[58] Finkin E.F. ; Materials in Engineering Applications; 1; 1979; p. 154-161.

[59] Archard J.F. ; Journal of Applied Physics; 24(8); 1953; p. 981-988.

[60] Rabinowicz E. ; "Friction and Wear of Materials"; 1966; London; John Wiley and Sons.

[61] Clayton P. ; Wear; 60; 1980; p. 75-93.

[62] Khruschov M.M. ; in "Proc. Conf. on Lubrication and Wear"; 1957; London; Inst. Mech. Eng. p. 655-659.

[63] Moore M.A. ; Wear; 28; 1974; p. 59-68.

[64] Saka N., Pamies-Teixeira and Suh N.P. ; Wear; 44; 1977; p. 77-86.

[65] Mutton P.S. and Watson J.D. ; Wear; 48; 1978; p. 385-389.

[66] Keown S.R., Kudielka E. and Heisterkamp F. ; Metals Technology; 7 (2); 1980 p. 50-57.

[67] Gahr K.H.Z. ; Z. Metallkunde; 68 (12); 1977; p. 783-792. (in English).

[68] Pamies-Teixeira J.J., Saka N. and Suh N.P. ; Wear; 44; 1977; p. 65-75.

[69] Borik F. and Scholz W.G. ; Journal of Materials; 6 (3); 1971; p. 590-605.

[70] Kasak A. and Neumeyer T.A. ; Wear; 14; 1969; p. 445-454.

[71] Suh N.P. ; Wear; 25; 1973; p. 111-114.

[72] Suh N.P. ; in "Fundamental Aspects of Structural Alloy Design"; edited by Jaffee R.I. and Wilcox B.A.; New York; 1976; Plenum Press; p. 565-594.

[73] Doyle E.D. ; Wear; 27; 1974; p. 295-301.

[74] Cottrell A.H. ; "Theory of Crystal Dislocations"; 1956; New York; Gordon and Breach Science Publishers.

[75] Saka N. ; in "Fundamentals of Tribology"; edited by Suh N.P. and Saka N.; 1980; Mass. Inst. of Technology; p. 135-170.

[76] Honeycombe R.W.K. ; in "Metallurgical Developments in High Alloy Steels"; I.S.I. Report no. 86; 1964; London; I.S.I.; p. 1-24.

[77] Mills B. ; Phil. Trans. Roy. Soc. London; 295 A; 1980; p. 87-88.

[78] Popov V.S. and Nagorny P.L. ; Russian Casting Production; 8; 1969; p. 337-339. (in English)

[79] Larsen-Badse J. and Mathew K.G. ; Wear; 14; 1969; p. 199-206.

[80] Roberts G.A. ; Trans. of Metall. Soc. of A.I.M.E.; 236; 1966; p. 950-963.

[81] Popov V.S., Nagorny P.L. and Garbuzov A.S. ; Physics of Metals and Metallography; 28 (8); 1969; p. 150-154.

[82] Hollox G.E. ; Materials Sciences and Engineering; 3; 1968/1969; p. 121-137.

[83] Seal A.K. and Honeycombe R.W.K. ; J.I.S.I.; 188; 1958; p. 343-350.

[84] Honeycombe R.W.K. ; in "The Effect of Second Phase Particles on the Mechanical Properties of Steels"; I.S.I. Special Report No. 145; I.S.I.; p. 136-142.

[85] Jahanmir S., Abrahamson II E.P. and Suh N.P. ; in "3rd. North American Metalworking Research Conference"; edited by Shaw M.C.; 1975; Soc. of Manufacturing Engineering; p. 854-864

[86] Henderer W.E. ; in Proc. of Int. Conf. on Cutting Tool Materials; 15-17 Sept. 1980; Kentucky; 1981; A.S.M.; p. 854-864.

[87] Henderer W.E. ; The 1981 Fagresta High Speed Steel Symposium; 8-10 Sept. 1981; p. 38-43.

[88] Rescalvo J.A. and Averbach B.L. ; Metall. Trans.; 10 A; 1979; p. 1265-1271.

[89] Westbrook J.H. and Stover E.R. ; in "High Temperature Materials and Technology"; edited by Campell I.E. and Sherwood E.M.; 1976; New York; John Wiley and Sons; p. 312-348.

[90] Atkins A.G. and Tabor D. ; Proc. Roy. Soc.; 292 A; 1960; p. 441-459.

[91] Hirth J.P., Dulis E.J. and Chandhok V.K. ; in "Strength of Metals and Alloys"; edited by Gifkins R.C.; 1982; Pergamon Press; p. 185-191.

[92] Trent E.M. ; "Metal Cutting"; 2nd. edition; 1984; London; Butterworth .

[93] Suh N.P. ; Wear; 44; 1977; p. 1-16.

[94] Henderer W.E. ; Trans of A.I.M.E.; 101 B; 1979; p. 217-222.

[95] Henderer W.E. ; in "Processing and Properties of High Speed Tool Steels"; edited by Wells M.G.H. and Lherbier L.W.; 1980; Las Vegas; Metall. Soc. of A.I.M.E.; p. 19-31 .

[96] Henderer W.E. and Von-Turkovich B.F.; in "Influence of Metallurgy on Hole Making Operations"; 1978; A.S.M.; p. 17-37.

[97] Nicholson R.B. ; in "The Effect of Second Phase Particles on the Mechanical Properties of Steels"; I.S.I. report no. 145; 1971; p. 1-8.

[98] Roberts G.A. and Hamaker J.C. ; U.S.A. patent 3,117,864; Jan. 14, 1964.

[99] Williams, D.B. and Edington, J.W. ; Norelco Reporter; 28 (1); 1981; p. 2-25.

[100] Goldstein, J.I. ; in "Introduction to Analytical Electron Microscopy"; edited by Hern J.J.; 1979; New York; Plenum Press; p. 83-120.

[101] Cliff, G. and Lorimer, G.W. ; Journal of Microscopy; 103 (2); 1975; p. 203-207.

[102] Cliff, G. ; Department of Metallurgy and Material Science; University of Manchester; Private Communications.

[103] Mills, B. and Redford, A.H. ; Annals of the CIRP; 28

(1); 1979; p. 165-169.

[104] Halling, J. ; Wear; 4; 1961; p. 22-31.

[105] Wright, C.S. and Irani, R.S. ; Journal of Material Science; 19; 1984; p. 3389-3398.

[106] Thomas, L.E. ; in "Microbeam Analysis"; edited by Gooly, R.; 1983; San Fransisco Press; p. 70-78.

[107] Toth, L.E. ; "Transition Metal Carbides and Nitrides"; 1971; New York; Acadimic Press.

[108] Lander, J.J. and Germer, L.H. ; Tr. A.I.M.E.; 175; 1948; p. 648.

[109] Lapointe, A.J. and Baker, T.N. ; Metal Science; 16; 1982; p. 207-216.

[110] Irani, R.S. , Wright, C.S. and Wronski, A.S. ; Journal of Material Science Letters; 1; 1982; p. 318-320.

[111] Powder Diffraction File Index; index numbers 3-980, 5-0721 and 15-457; 1983; USA; International Centre for Diffraction Data.

[112] Sevenson L-E., Howell P.R., Andren H-O., Nordon H. and Dunlop G.L.; in "Quantitative Microanalysis With High Spatial Resolution"; The Metal Society; London; 1983; p.256-261.

[113] Brandis H., Haberling E. and Weigand H.H.; in "Processing and Properties of High Speed Tool Steels"; edited by M.G. Wells and L.W. Lherbeir; 1980; Las-Vegas; The Metallurgical Society of A.I.M.E.; p.1-18.

[114] Ghomashchi M.R. and Sellars C.M.; Metal Science; 18;

1984; p.44-48.

[115] Haberling E., Rose A. and Weigand H.H.; Stahl u. Eisen; 93(14); 1973; p.645-651. (in English)

[116] Fredreksson H. and Nica M.; Scandinavian Journal of Metallurgy; 8; 1979; p.243-253.

| $M_6C$ | $M_{23}C_6$ | MC | cubic $M_2C$ | reference |
|---|---|---|---|---|
| 11.08 | | | | 3 |
| 11.04 | | | | 3 |
| 11.04 | 10.64 | 4.131-4.1655 | | 9 |
| 11.26 | | | | 10 |
| 11.095-11.14 | | | | 11 |
| 11.04-11.08 | 10.638-10.51 | 4.3 | | 13 |
| | 10.618 | | | 14 |
| 11.04 | 10.51-10.638 | 4.3 | | 17 |
| 11.064-11.2 | | | | 16 |
| 11.0823 | 10.621 | 4.16 | | 20 |
| 11.05 | 10.59 | 4.175 | | 23 |
| 11.08 | 10.59 | 4.175 | | 23 |
| 11.08 | 10.64 | | | 35 |
| 11.04 | 10.659 | | 4.14 | 111 |

Table(1): Some reported values for lattice parameters of high speed steel carbides in the pure form and as precipitated in steels, in Angstrom units [Å].

| steel type | aust. temp. [°C] | carbide content % | |
|---|---|---|---|
| | | $M_6C$ | MC |
| T1 | 1288 | 97 | 3 |
| T4 | 1288 | 96 | 4 |
| T2 | 1288 | 92 | 8 |
| M1 | 1204 | 87 | 13 |
| M2 | 1218 | 85 | 15 |
| M10 | 1204 | 61 | 39 |
| M4 | 1280 | 44 | 56 |
| M15 | 1250 | 34 | 66 |

Table (2): Percentage of excess carbides existing as $M_6C$ and MC in hardened high speed steels [25].

| elements / wt.% / steel | C | Mo | W | V | Cr | Co |
|---|---|---|---|---|---|---|
| M 42 | 1.09 | 9.82 | 1.66 | 1.3 | 3.62 | 8.09 |
| M 15 | 1.56 | 3.06 | 6.02 | 4.82 | 4.75 | 4.76 |
| M 1 | 0.78 | 9.00 | 1.86 | 1.27 | 3.87 | 0.13 |

Table (3): Chemical composition of high speed steels .

| steels | M 42 | M 15 | M 1 |
|---|---|---|---|
| temp. [°C] | 1180 | 1225 | 1225 |

Table (4): Austenitising temperatures of different high speed steels .

| elements | C | Mn | Si | Ni | Cr | Cu | Mo |
|---|---|---|---|---|---|---|---|
| wt. % | 0.51 | 0.95 | 0.27 | 0.22 | 0.14 | 0.27 | 0.05 |

Table (5): Chemical composition of workpiece .

| elements / steels [%] | Mo | | V | | Cr | | Fe | | Co | | W | |
|---|---|---|---|---|---|---|---|---|---|---|---|---|
| | wt. | at. | wt. | at. | wt. | at. | wt. | at. | wt. | at. | wt. | at. |
| M 42 | 61.8 | 53 | 16 | 25 | 9.5 | 15 | 1.6 | 2.3 | 0.1 | --- | 10.8 | 4.7 |
| M 1 | 59.4 | 49 | 21.2 | 32.5 | 7.4 | 11 | 2.7 | 3.7 | 0.3 | --- | 8.8 | 3.7 |
| M 15 | 16.5 | 15 | 27.4 | 47 | 8.3 | 14 | 1.6 | 2.5 | 0.3 | --- | 45.7 | 22 |

Table (6): Chemical composition of secondary hardening carbides extracted from different steels tempered to their peak hardness .

| elements / carbides [%] | Mo | | V | | Cr | | Fe | | Co | | W | |
|---|---|---|---|---|---|---|---|---|---|---|---|---|
| | wt. | at. | wt. | at. | wt. | at. | wt. | at. | wt. | at. | wt. | at. |
| $M_3C$ * | 12.3 | 8 | 1.7 | 2 | 11.8 | 14 | 62.6 | 65 | 5.7 | 6 | 5.9 | 2 |
| $M_2C$ hex. | 67 | 59.5 | 5 | 8.3 | 16 | 26.2 | 1 | 1.5 | 3 | 4.5 | 9 | 4.2 |
| MC | 40 | 27 | 45 | 57.8 | 5.5 | 6.3 | 5.5 | 5.8 | 1 | 0.9 | 5.5 | 1.8 |
| $M_6C$ | 60 | 52.9 | 2 | 3.5 | 3 | 5 | 20 | 32 | 3 | 4.5 | 9 | 4.1 |
| $M_{23}C_6$ | 15 | 9 | 2.5 | 2.3 | 50 | 55 | 30 | 30.8 | 2 | 1.9 | 1.5 | 1.5 |

Table (7): Chemical composition of different carbides precipitated in - M42.

* composition after tempering for 2+2 h at 550 °C .

| element [%] / steel | Mo | | V | | Cr | | Fe | | Co | | W | |
|---|---|---|---|---|---|---|---|---|---|---|---|---|
| | wt% | at% | wt% | at% | wt% | at% | wt% | at% | wt% | at% | wt% | at% |
| M42 | 28.9 | 20 | 52.2 | 66 | 6.7 | 8.5 | 1.7 | 2 | .35 | .4 | 11.2 | 4 |
| M15 | 27 | 23 | 32.5 | 52.5 | 4.8 | 7.5 | 1.5 | 1.8 | .4 | .4 | 34 | 15 |
| M1 | 37.4 | 26 | 47 | 61 | 5.5 | 7 | 1.7 | 2 | -- | -- | 8.3 | 3 |

Table(8); Chemical composition of secondary MC carbide precipitated in the three steels examined.

| Mo [at%] | V [at%] | Cr [at%] | Fe [at%] | W [at%] | Co [at%] | reference |
|---|---|---|---|---|---|---|
| 19.4 | 59.9 | 7.6 | 4.2 | 8.8 | 0.7 | 4 |
| 13 | 69.3 | 6.6 | 3 | 8 | -- | 5 |
| 14.2 | 73 | 6.4 | 1.8 | 5.8 | -- | 23 |
| 12.9 | 69.4 | 6.6 | 3 | 8 | -- | 23 |
| 16.3 | 61 | 6.5 | 5.5 | 8.1 | 0.5 | 112 |
| 9.9 | 69.4 | 6 | 5.6 | 9 | -- | 113 |
| 9.9 | 59.6 | 6.4 | 1.3 | 11.8 | -- | 114 |
| 11.4 | 66.2 | 6.9 | 5.6 | 9.9 | -- | 115 |
| 11.3 | 64.7 | 10 | 4.9 | 9 | -- | 116 |

Table(9): Some reported chemical compositions for MC carbide precipitated in different high speed steels.

| Mo [at%] | V [at%] | Cr [at%] | Fe [at%] | W [at%] | Co [at%] | reference |
|---|---|---|---|---|---|---|
| 23.1 | 4.7 | 5.6 | 40.7 | 14 | 7.5 | 4 |
| 20.5 | 7 | 6.1 | 48.7 | 17.7 | -- | 5 |
| 1.7 | 6.93 | 5.66 | 39.4 | 46.2 | -- | 16 |
| 20.26 | 7 | 6.12 | 48.8 | 17.68 | -- | 23 |
| 24.04 | 5.99 | 5.5 | 48.9 | 15.5 | -- | 23 |
| 23.4 | 5.8 | 5.8 | 39.3 | 15.9 | 5.8 | 112 |
| 17.9 | 5 | 6.5 | 54.7 | 16.1 | -- | 113 |
| 18.04 | 7.2 | 4.9 | 52 | 17.8 | -- | 114 |
| 17 | 5.58 | 6.29 | 54.5 | 16.5 | -- | 115 |
| 20.2 | 6.58 | 7.4 | 48.9 | 16.8 | -- | 116 |

Table(10): Some reported chemical compositions for $M_6C$ carbide precipitated in different high speed steels.

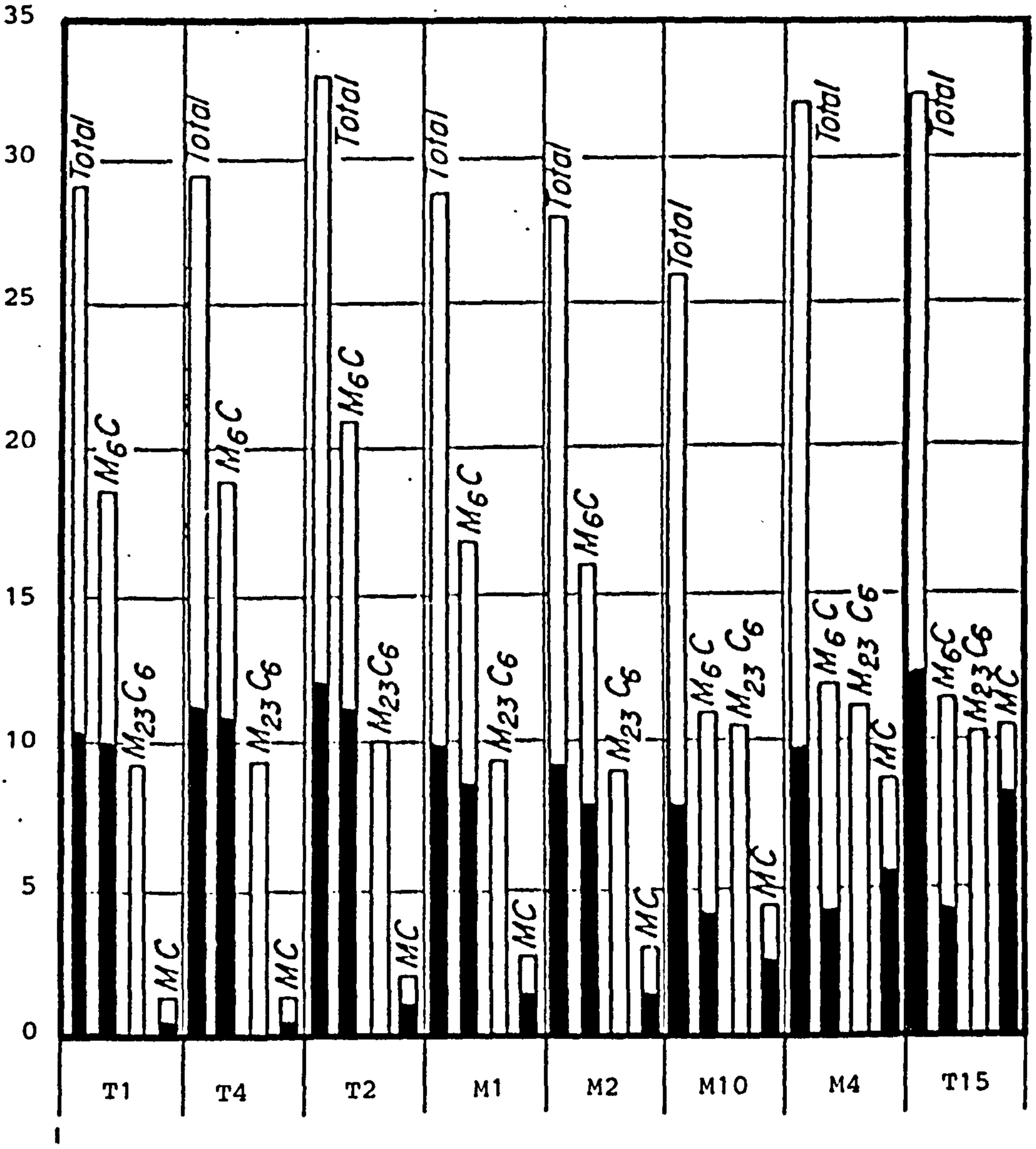


Fig.(1) Volume percent of carbides in some quenched and annealed high speed steels [ 6 ] .

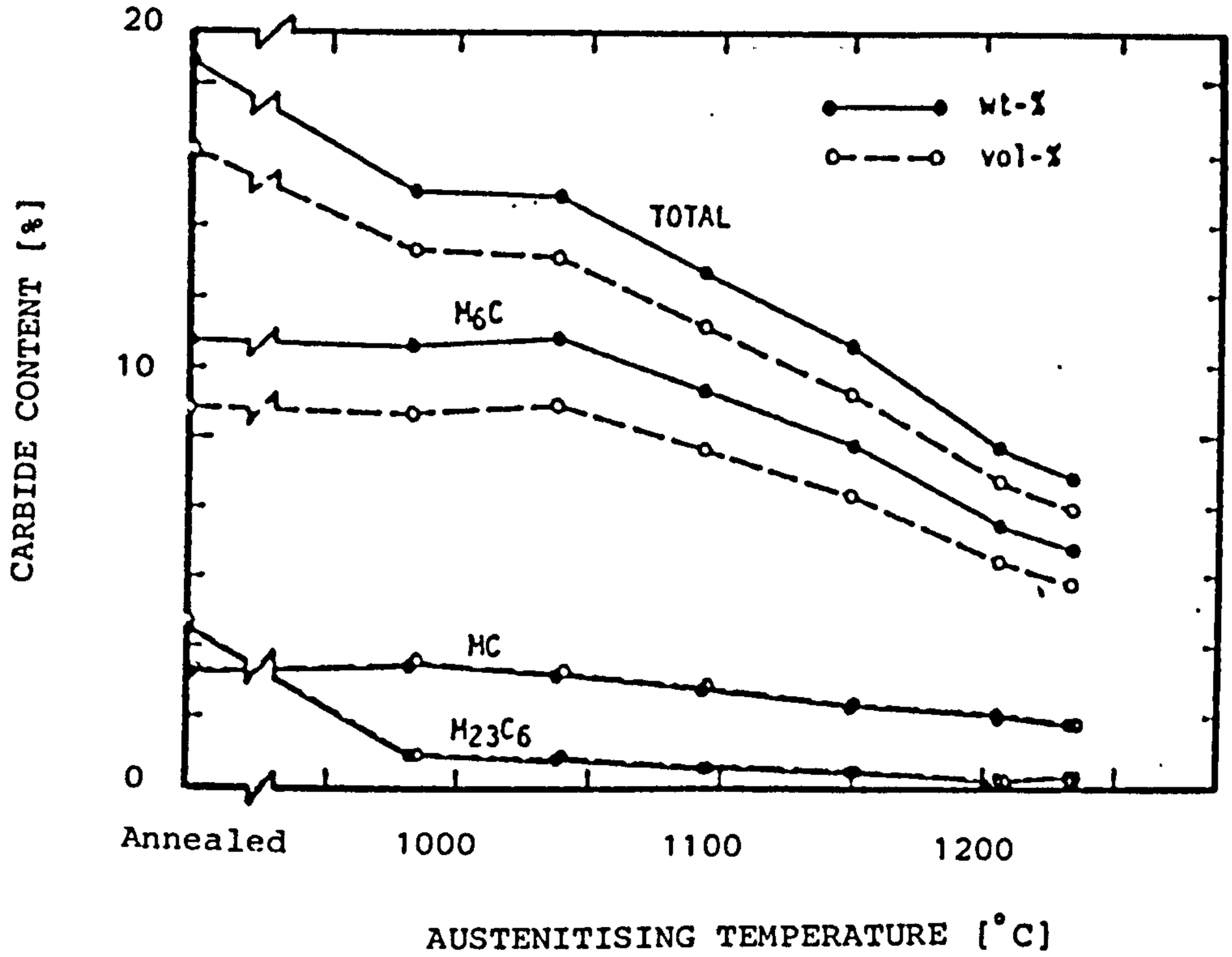


Fig. (2): Amount of undissolved carbides against austenitising temperature for M2 high speed steel [5,23] .

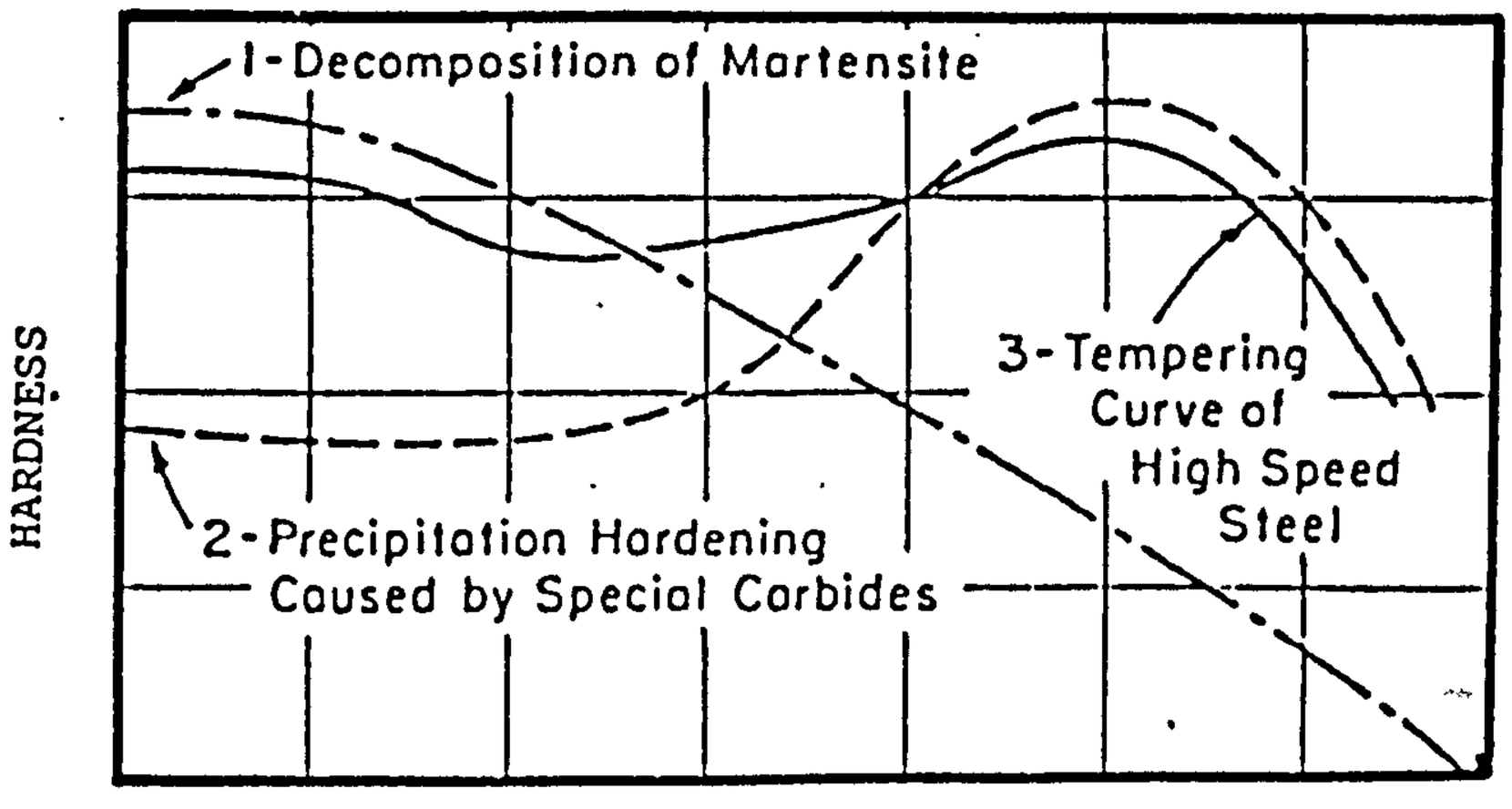


Fig.(3): Schematic diagram for tempering high speed steels [27].

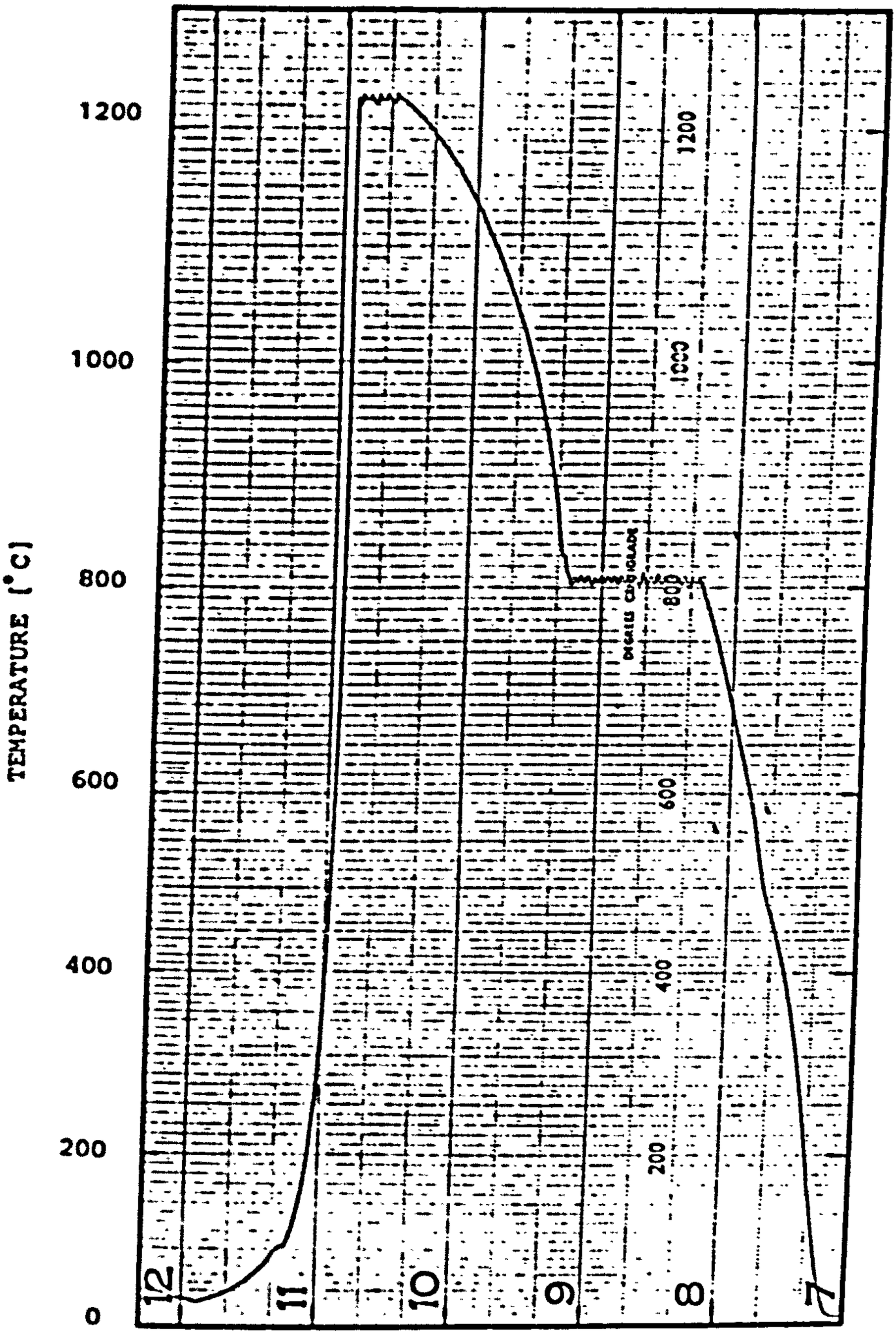


Fig.(4): Chart of hardening cycle for M1 and M15.

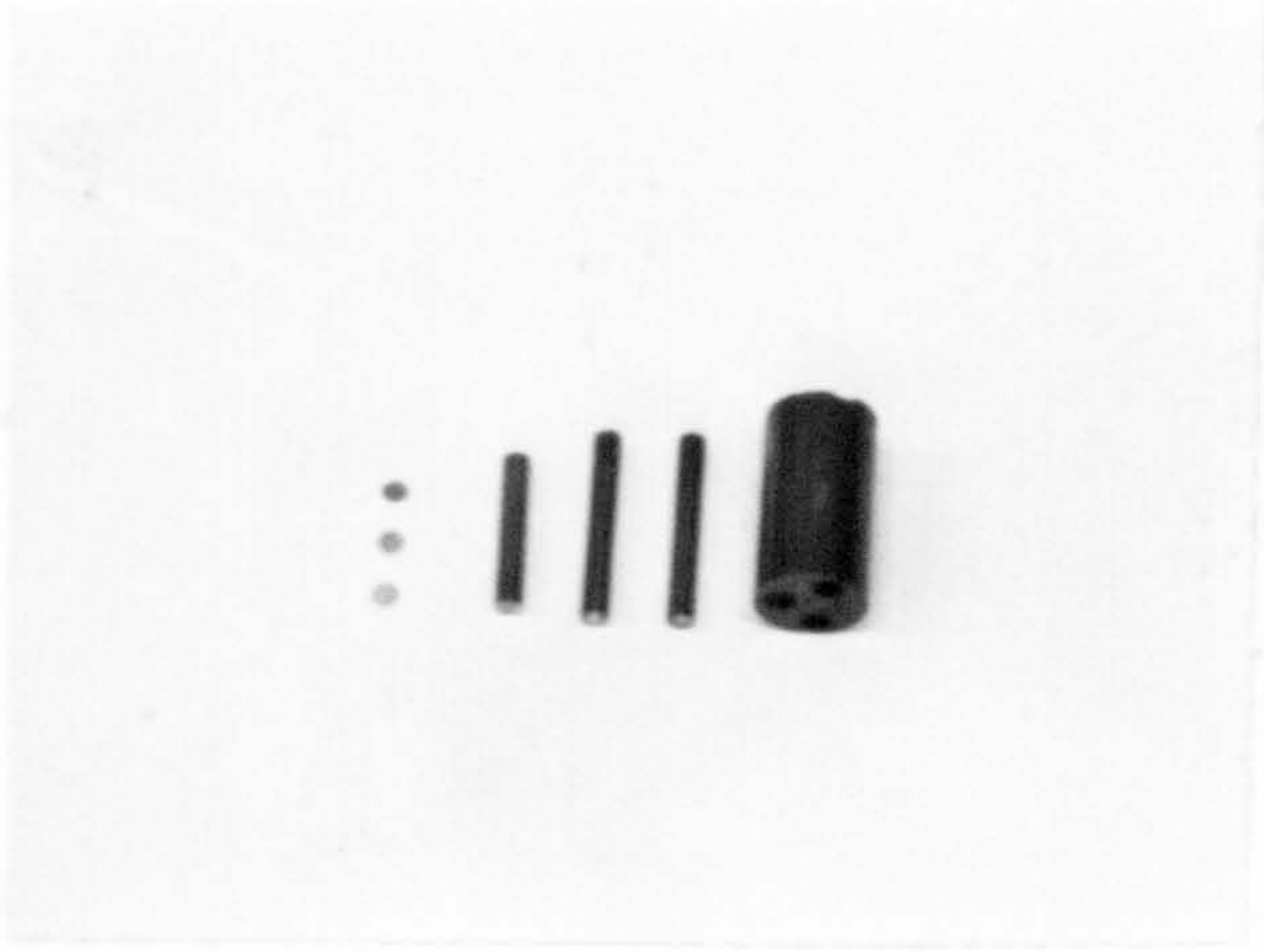

Fig.(5): Rods extracted from round specimens by electro-errosion technique and discs sliced from the rods.

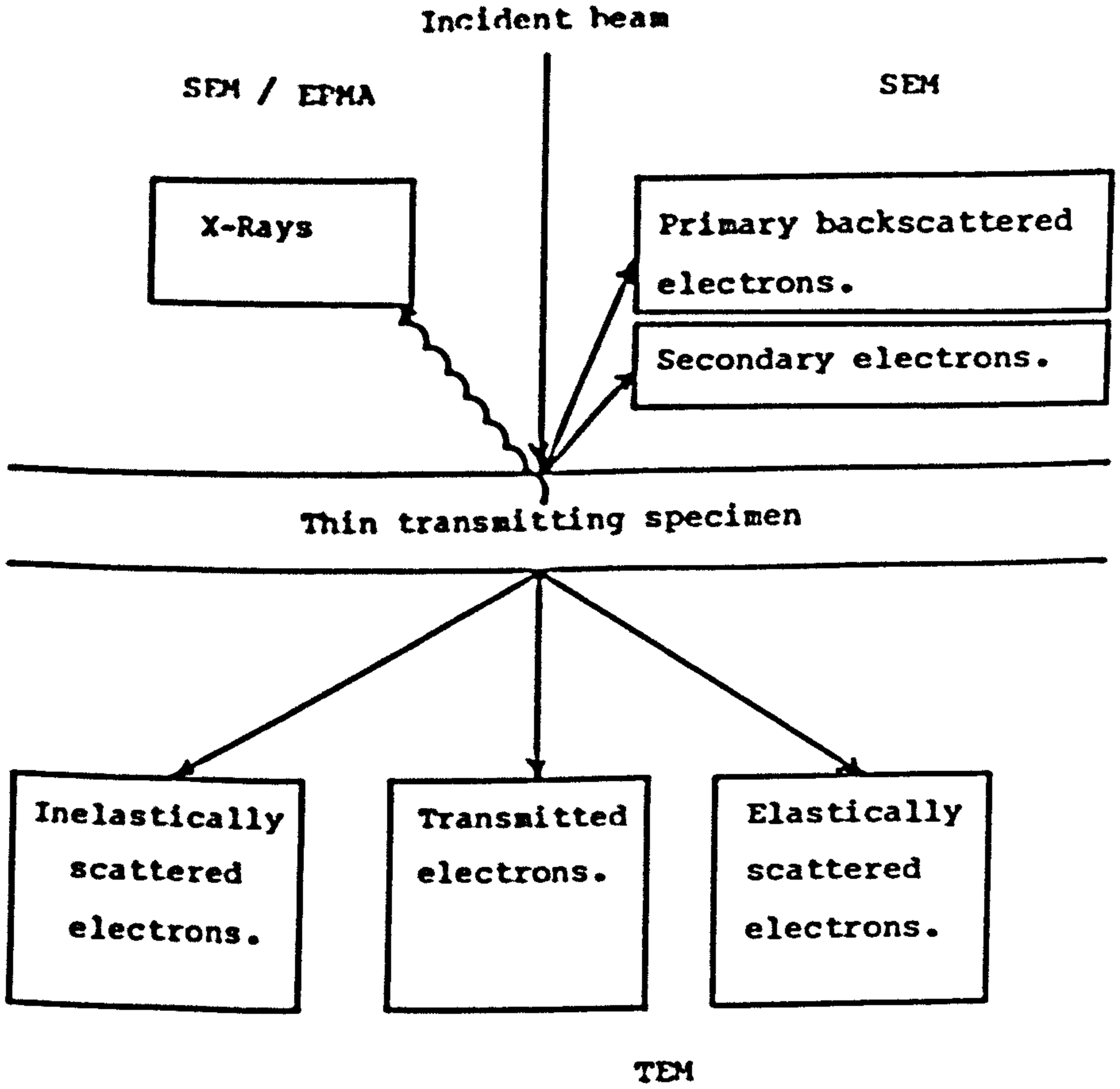


Fig.(6): Signals resulting from the interaction of a high energy electron beam with a crystalline material [99].

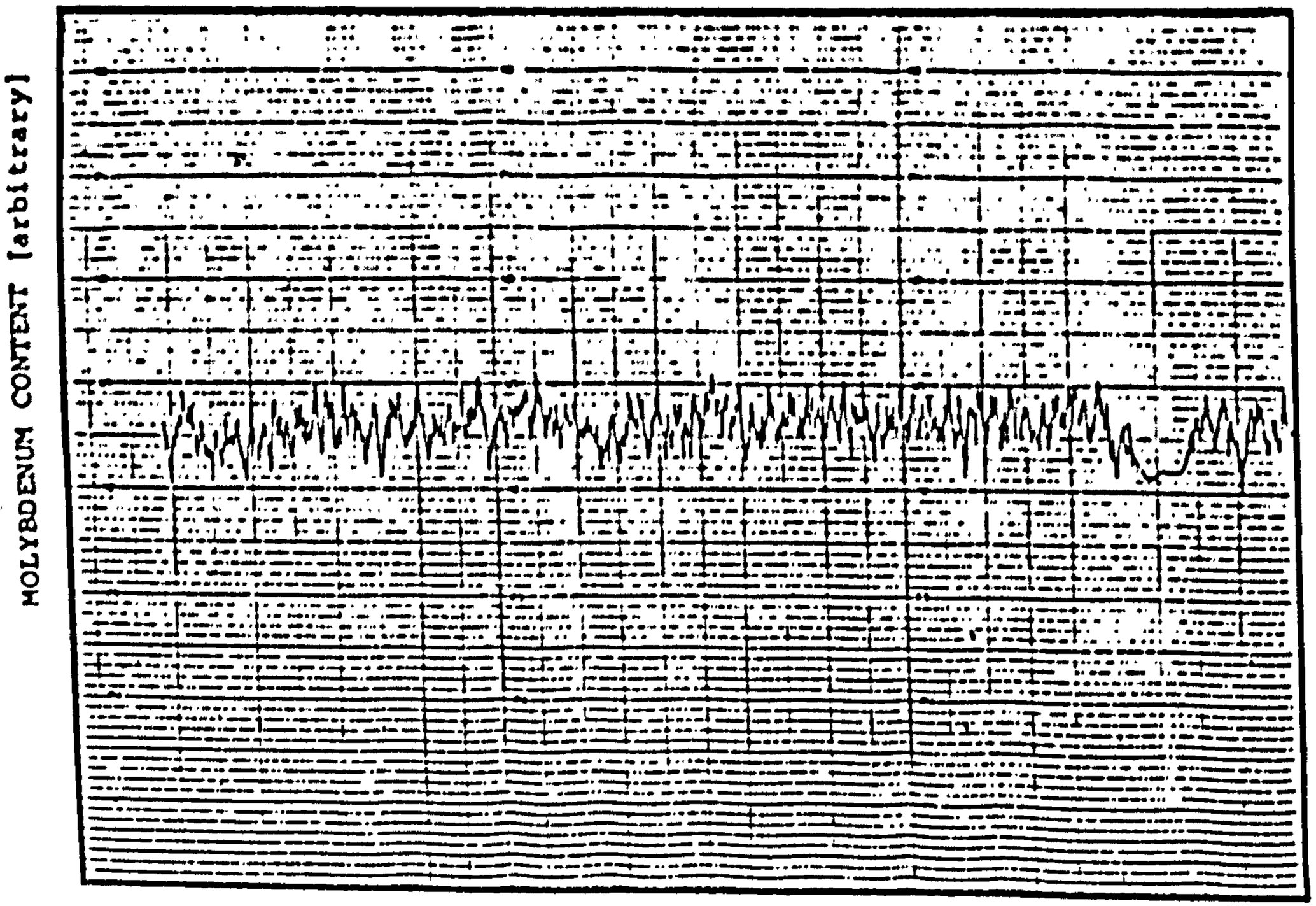


Fig.(7): EPMA chart showing constant molybdenum content across the standard Fe-Mo binary alloy specimen.

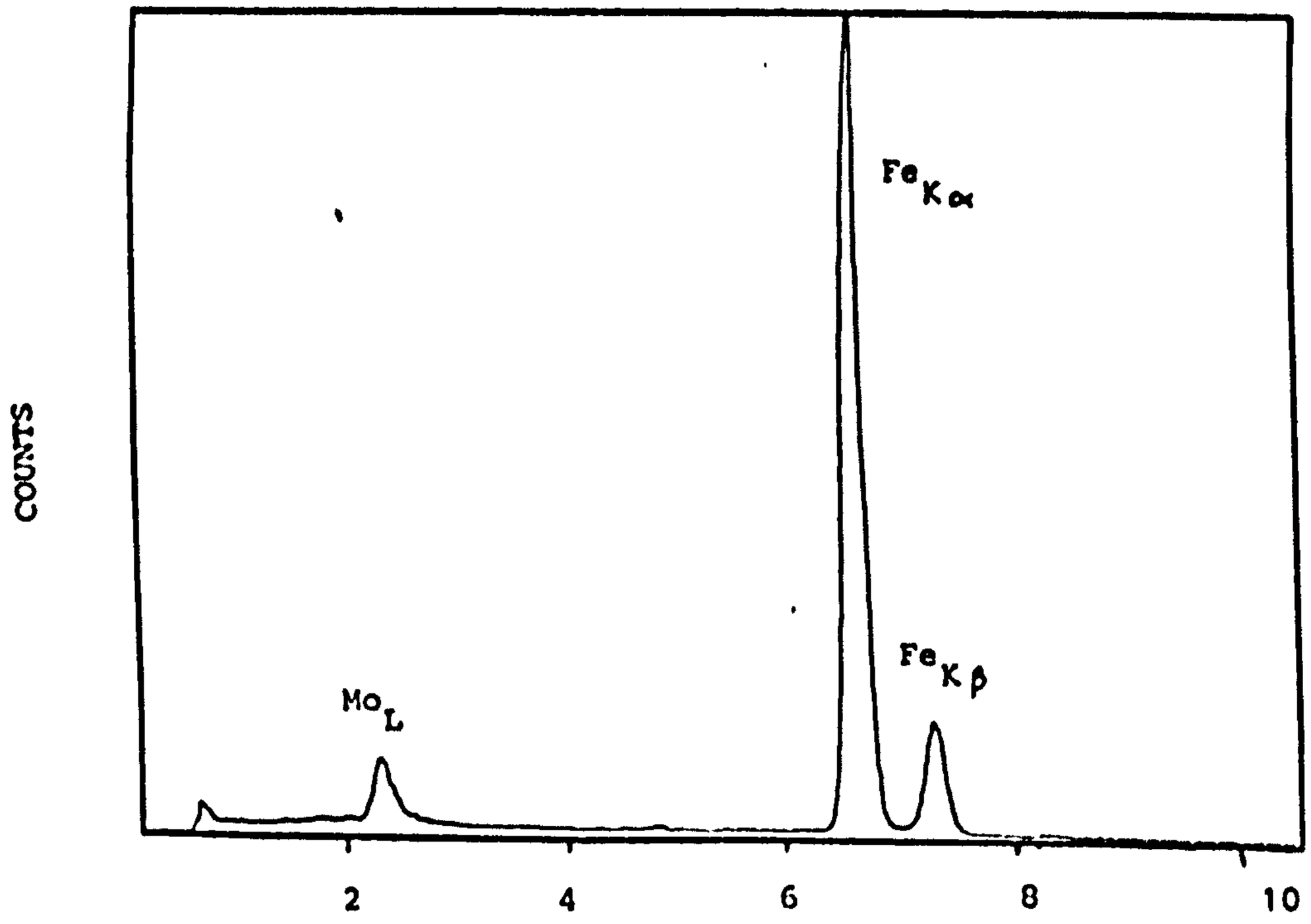


Fig.(8): Characteristic EDX spectrum obtained from the standard Fe-Mo binary alloy.

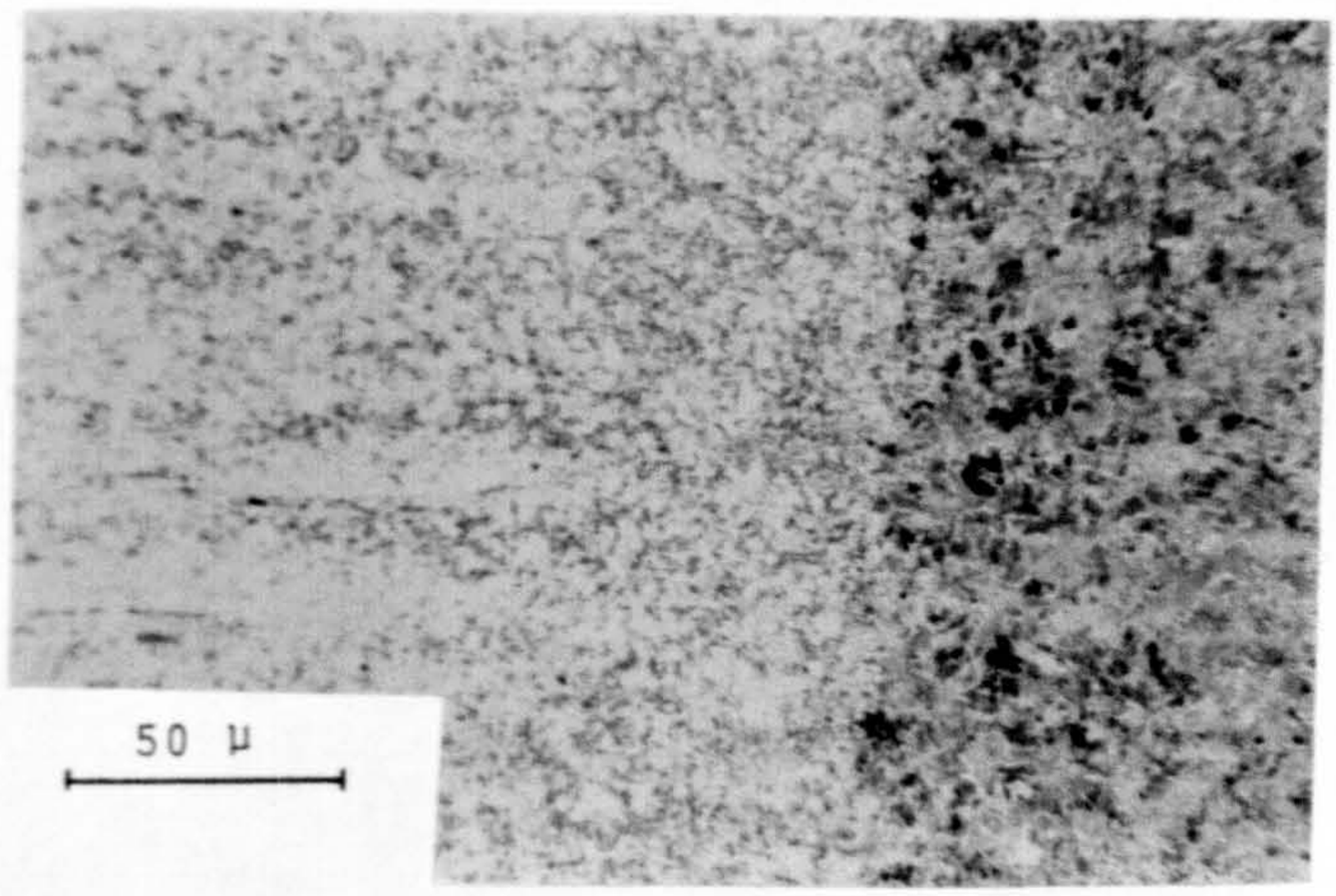


(a)

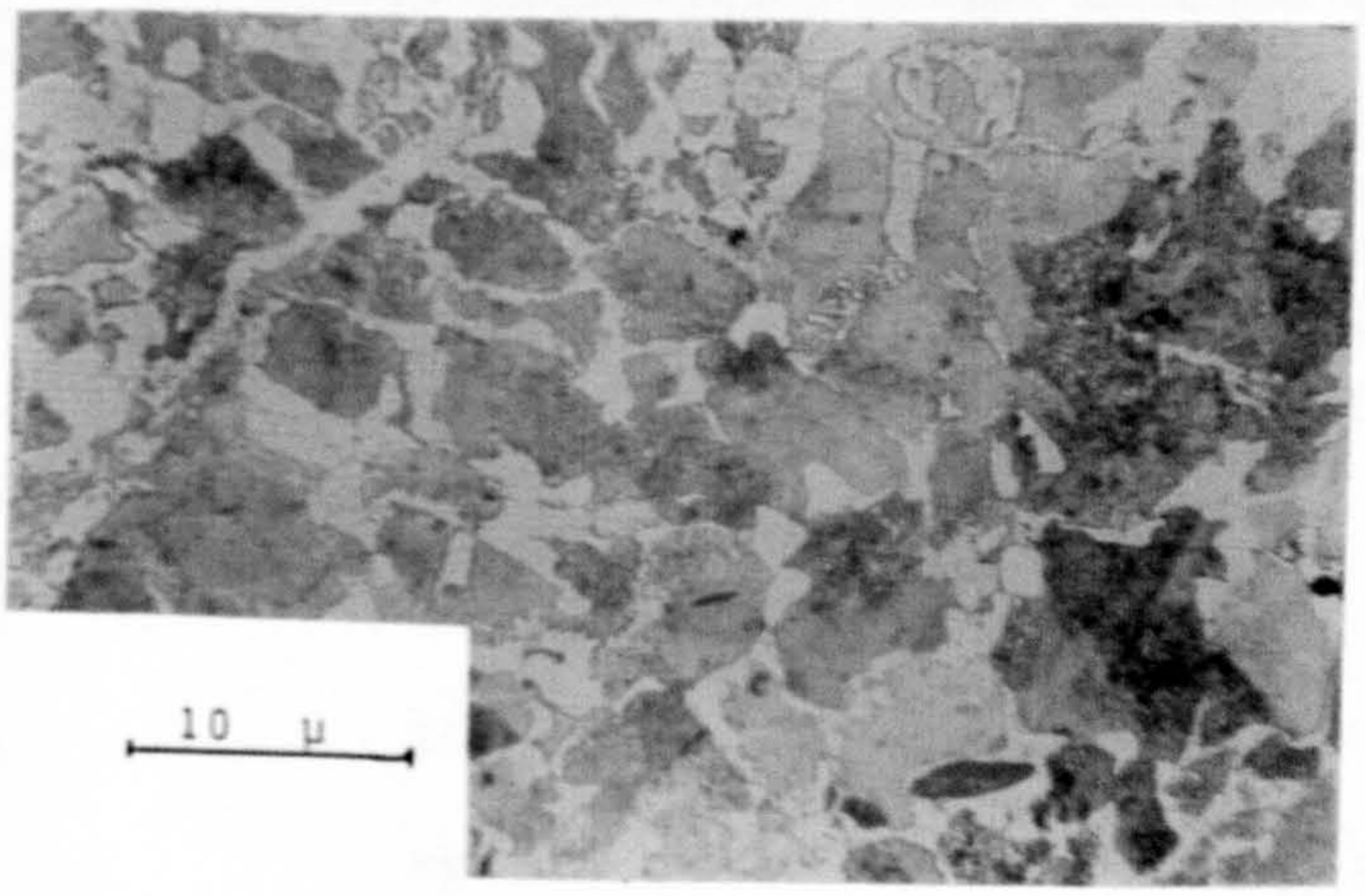


(b)

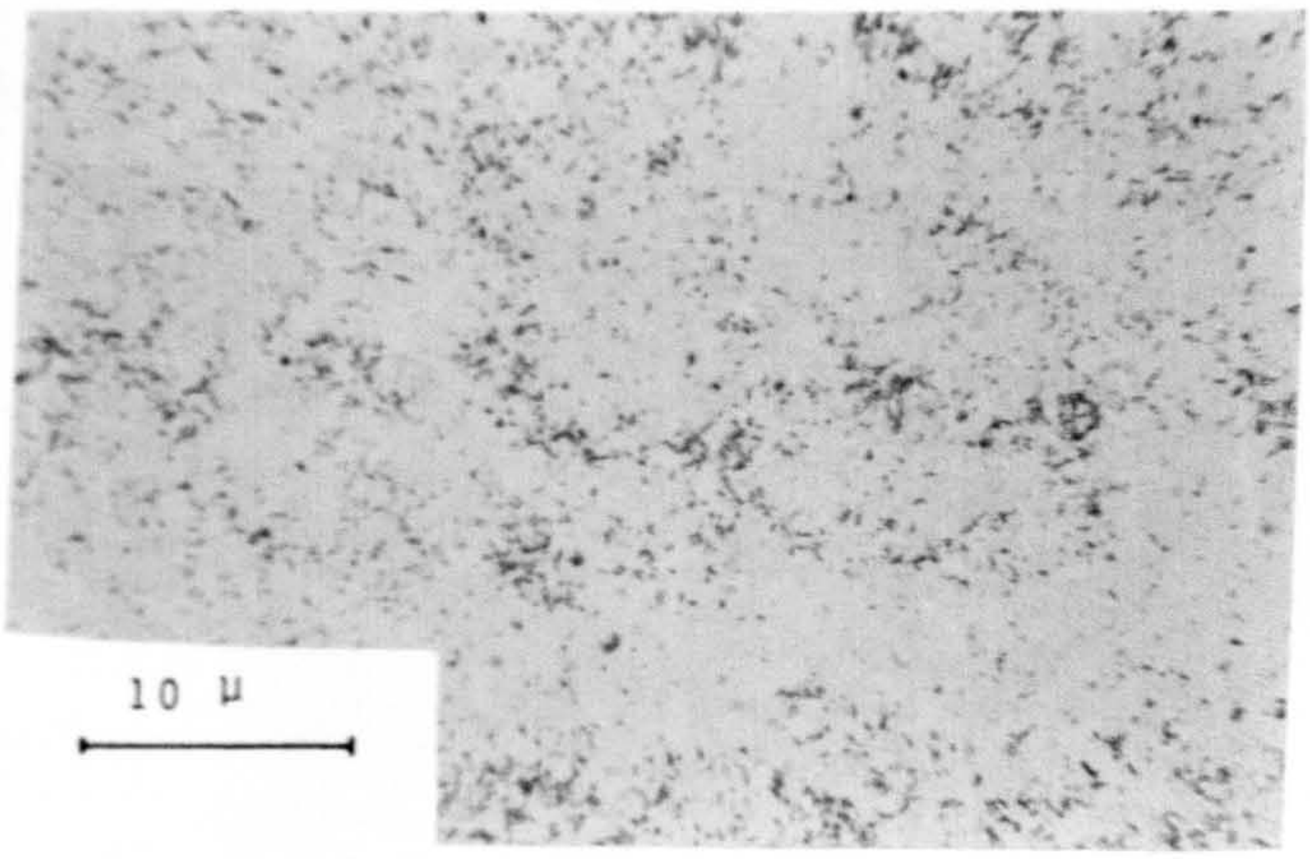


(c)

Fig.(9): Optical micrographs of workpiece microstructure.

(a) core and hardened surface.

(b) non-hardened core.

(c) hardened surface.

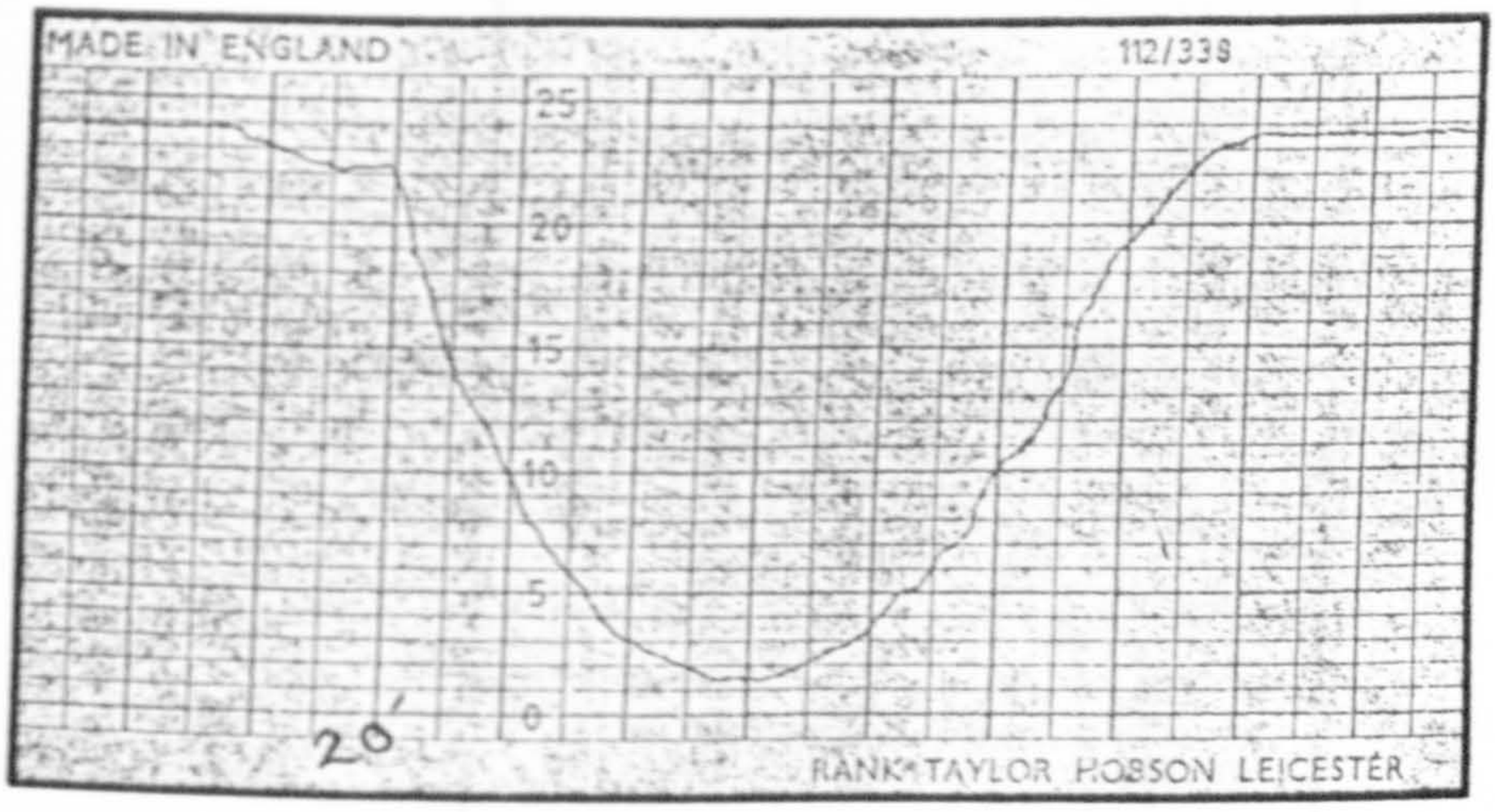


Fig.(10): Chart of Talysurf measurement of wear scar depth.

This particular chart shows wear scar in M1 high speed steel tempered for 2+2 h at 600 °C, after sliding for 800 meters (20 minutes).

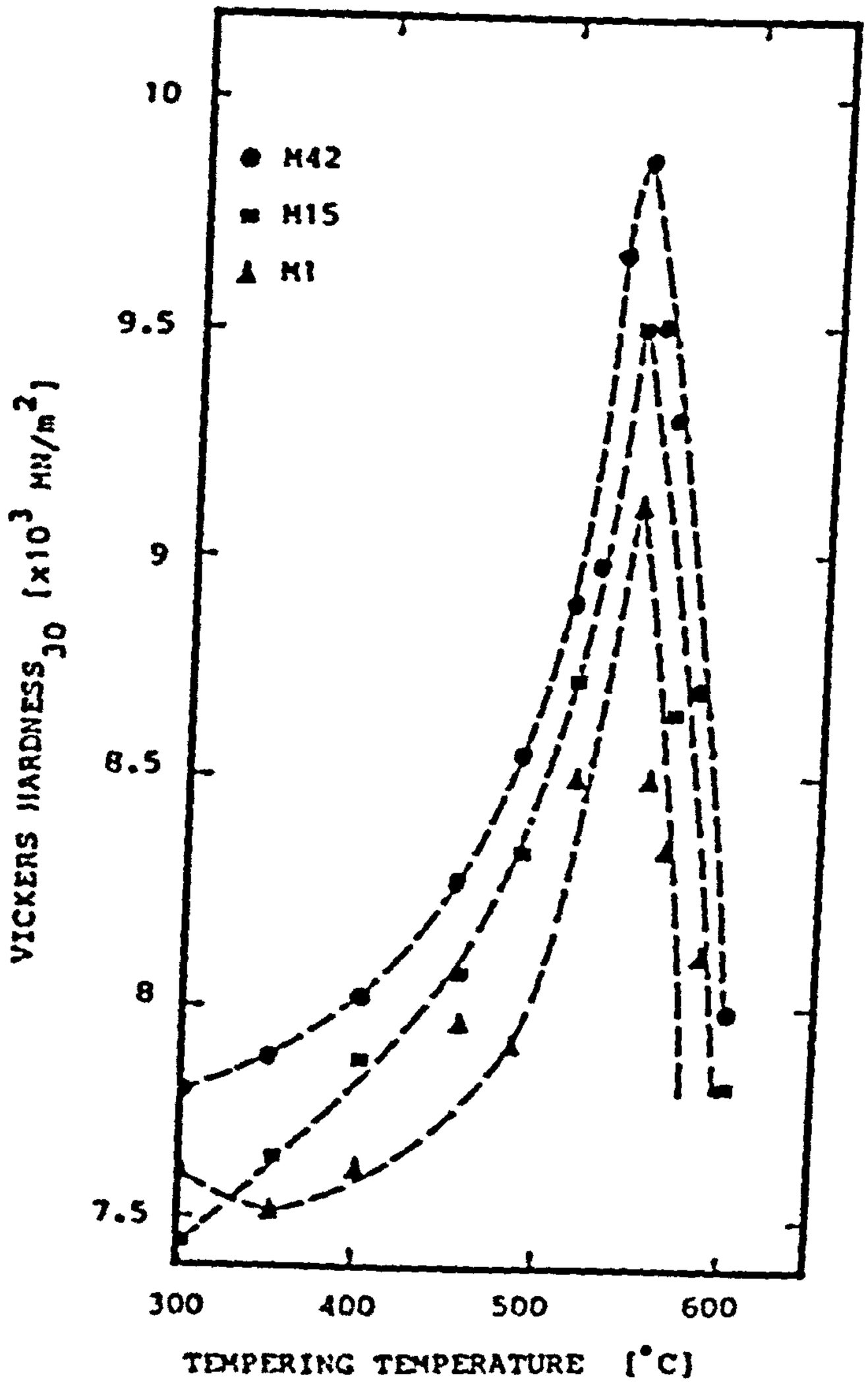


Fig.(11): Variation of hardness with tempering temperature.

(a)

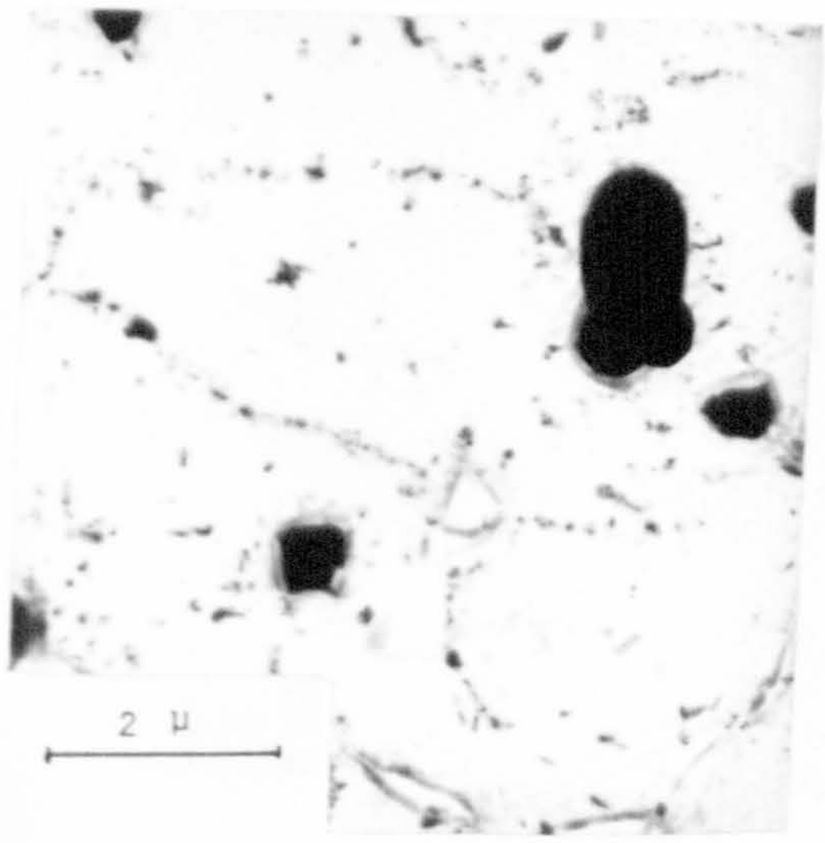


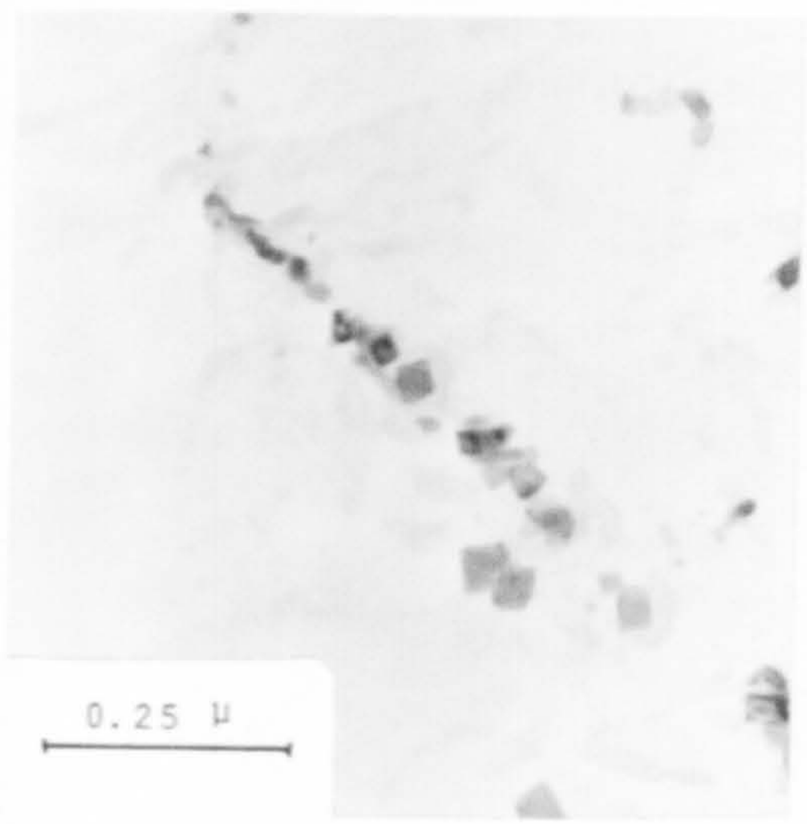


(b)

(c)

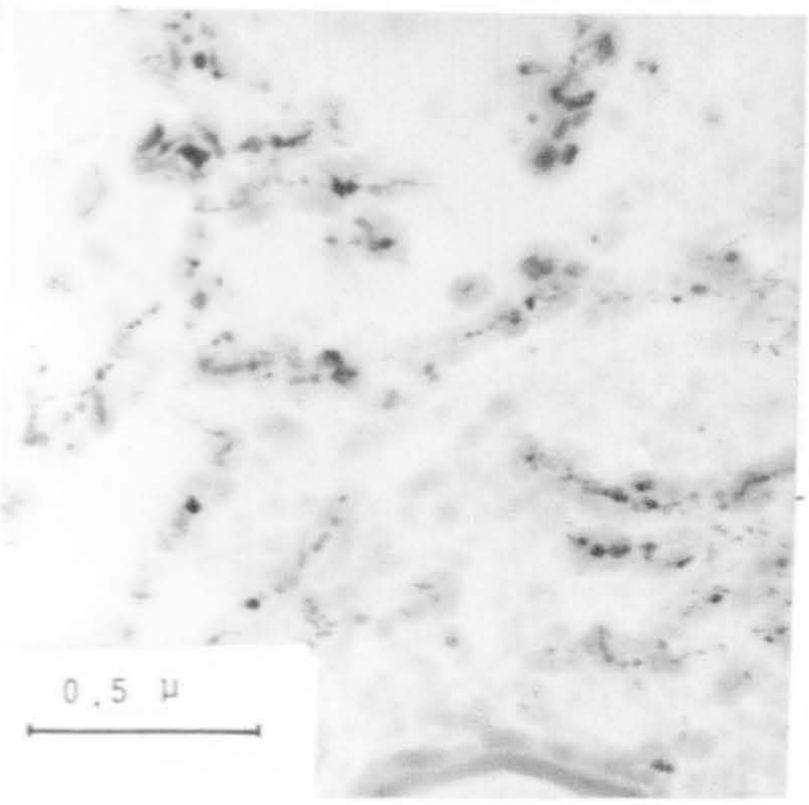


Fig.(12): Carbon replica micrographs showing heterogeneous precipitation of secondary hardening carbides after tempering,

(a),(b) M42 for 2+2 h at 430°C.

(c) M1 for 2+2 h at 480°C.

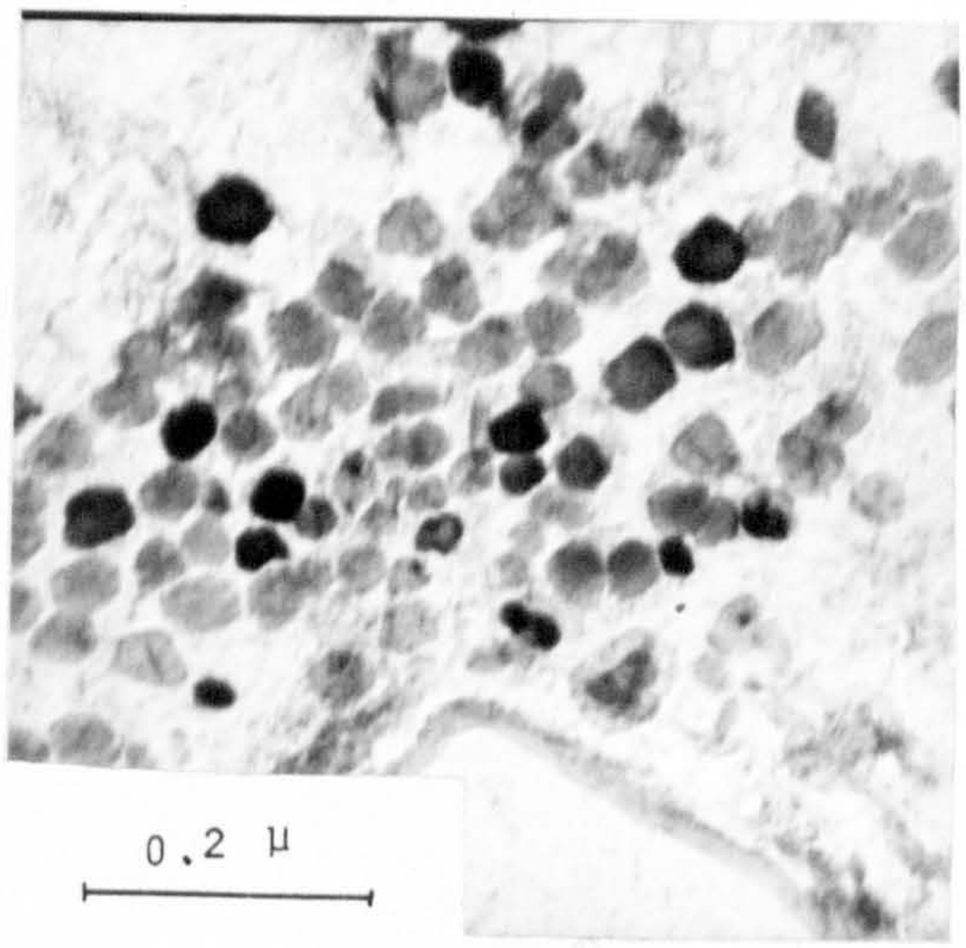


(a)

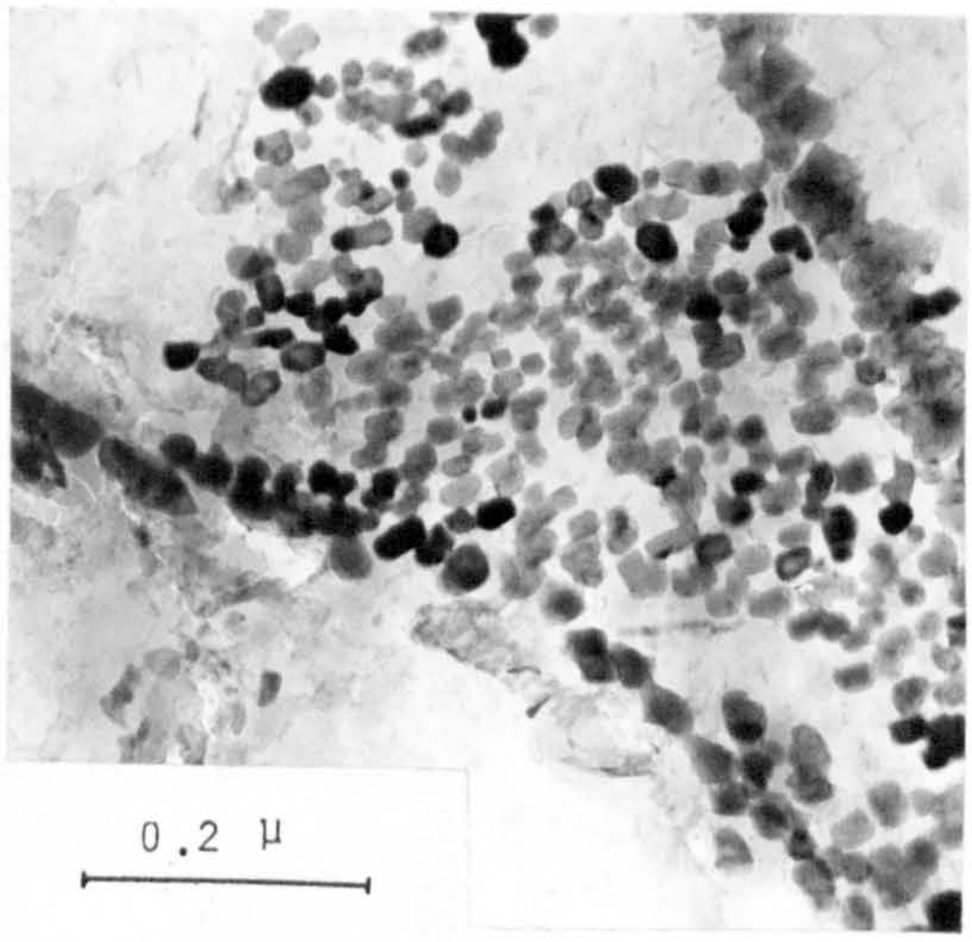


(b)

(c)

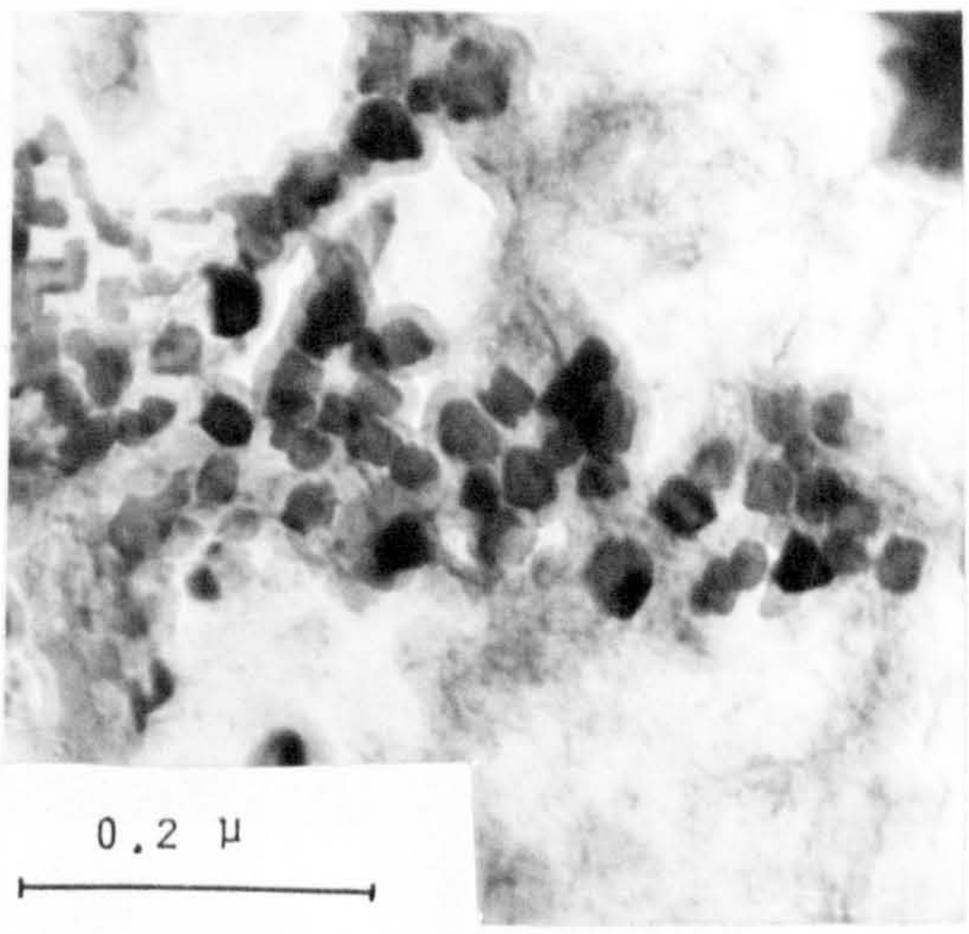


Fig.(13): Carbon replica micrographs showing secondary hardening carbides precipitation after tempering to peak hardness.

(a),(b) M42.

(c) M15.

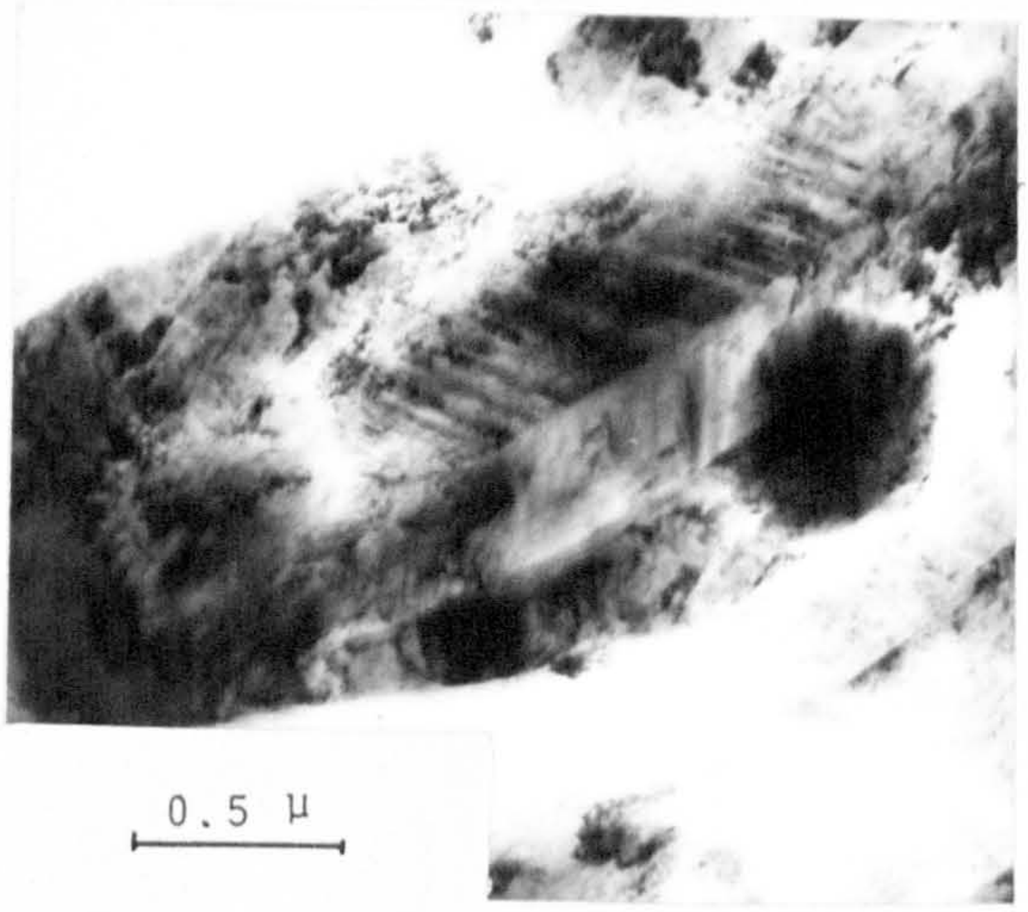


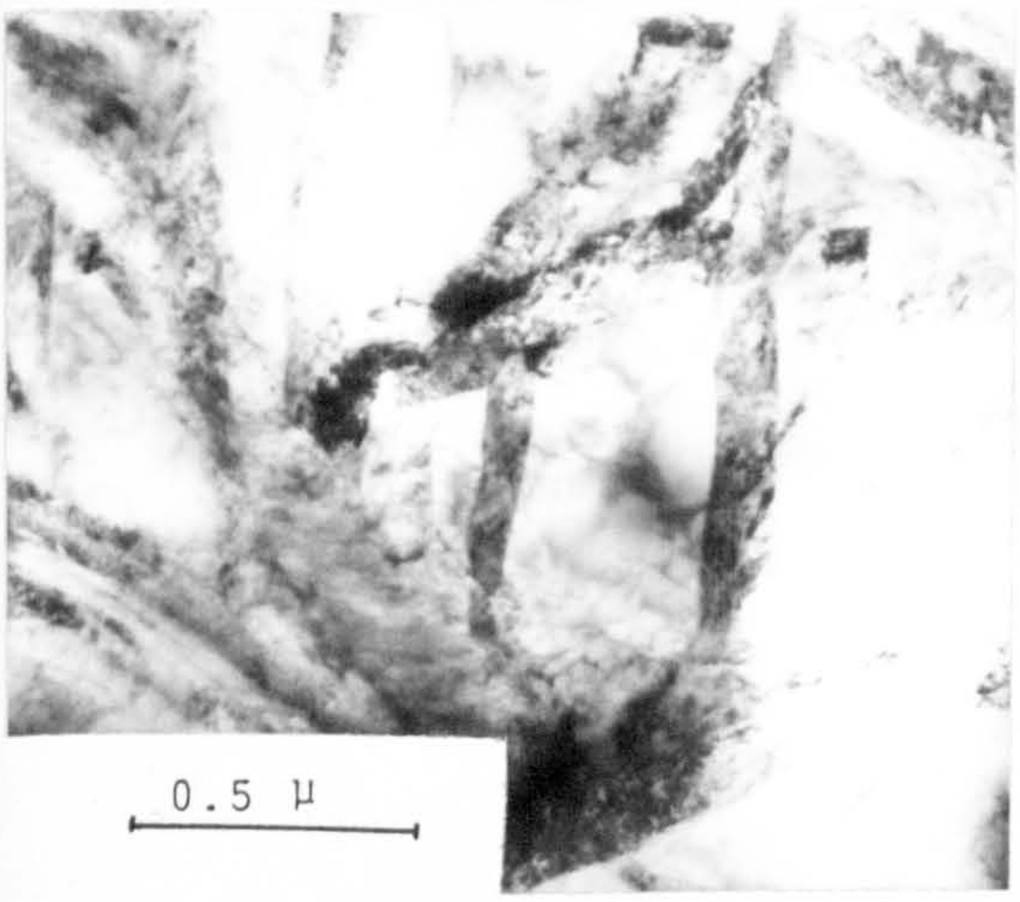


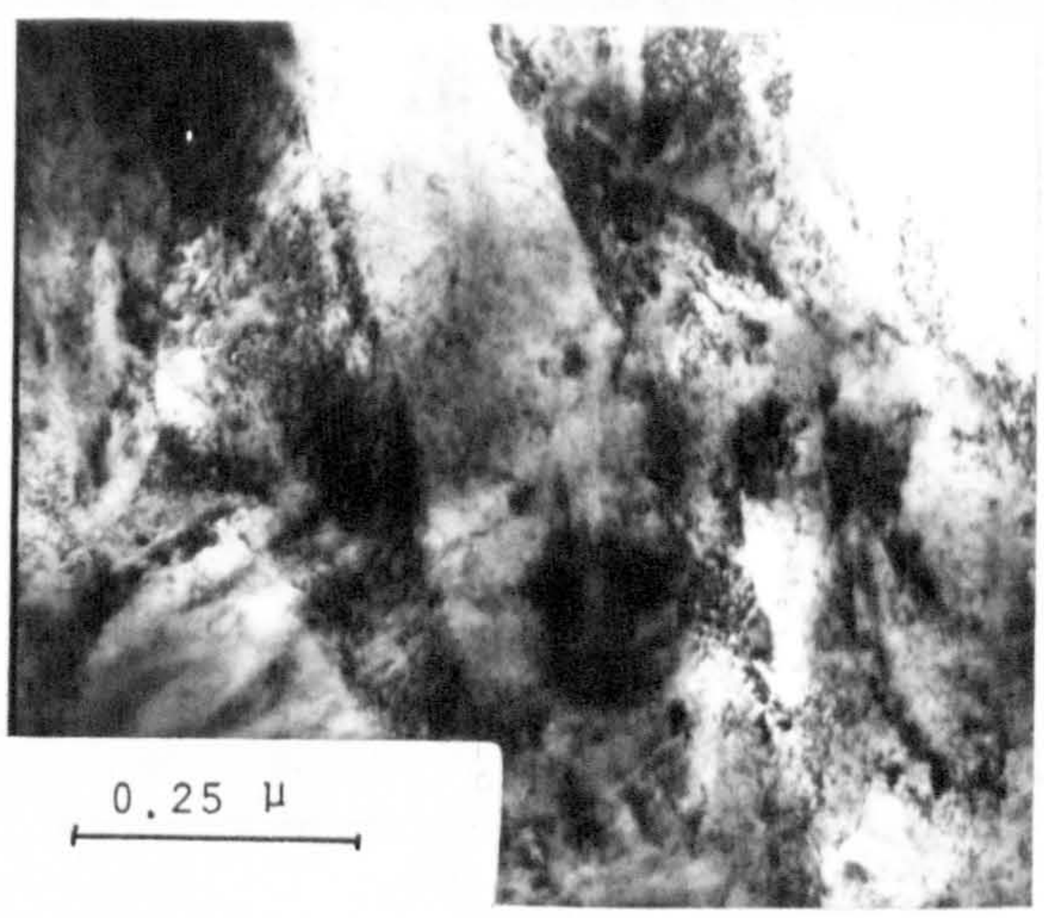


Fig.(14): Thin foil micrographs showing secondary hardening carbide precipitated in M42 tempered to peak hardness.

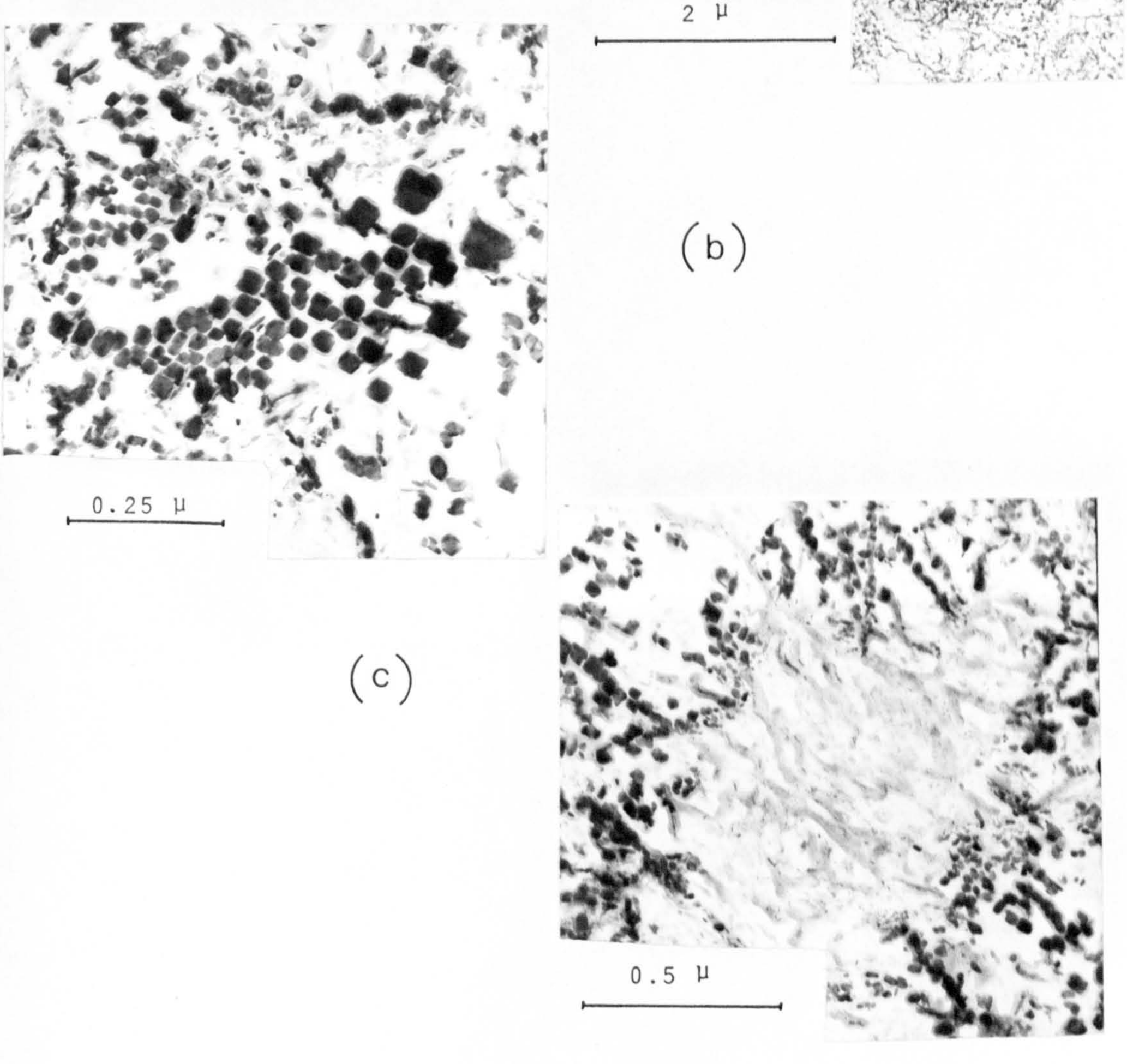


Fig.(15): Carbon replica micrographs showing successful extraction of secondary hardening carbides from M42 tempered to its peak hardness.

(a) low magnification (b) high magnification

(c) area free from carbide precipitation.

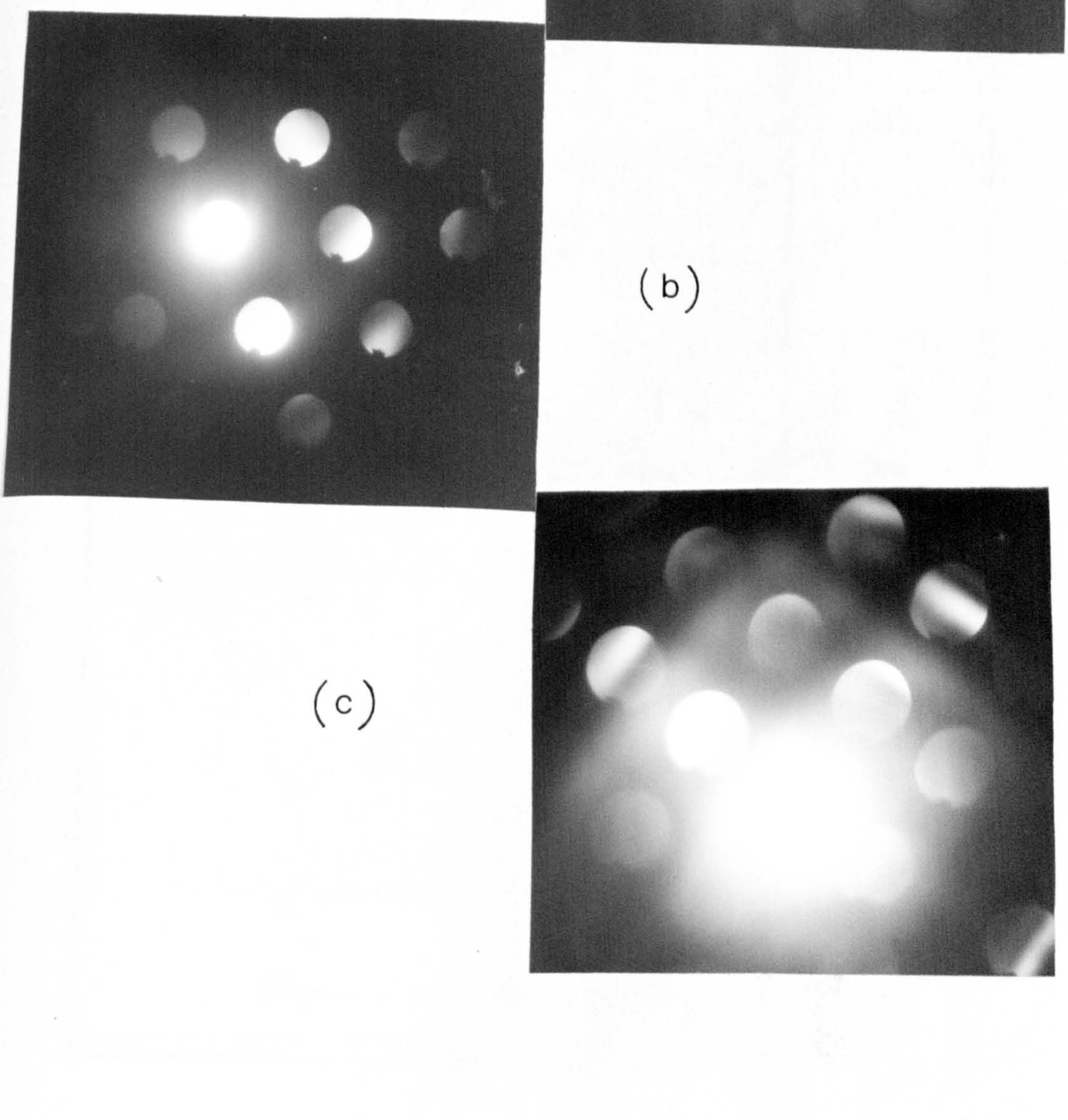

(a)

(b)

(c)

Fig.(16): Convergent beam single crystal diffraction patterns of secondary hardening carbides extracted from :

(a) M42, zone axis [011]  (b) M42, zone axis [$\bar{1}$14]

(c) M15, zone axis [$\bar{2}$33]

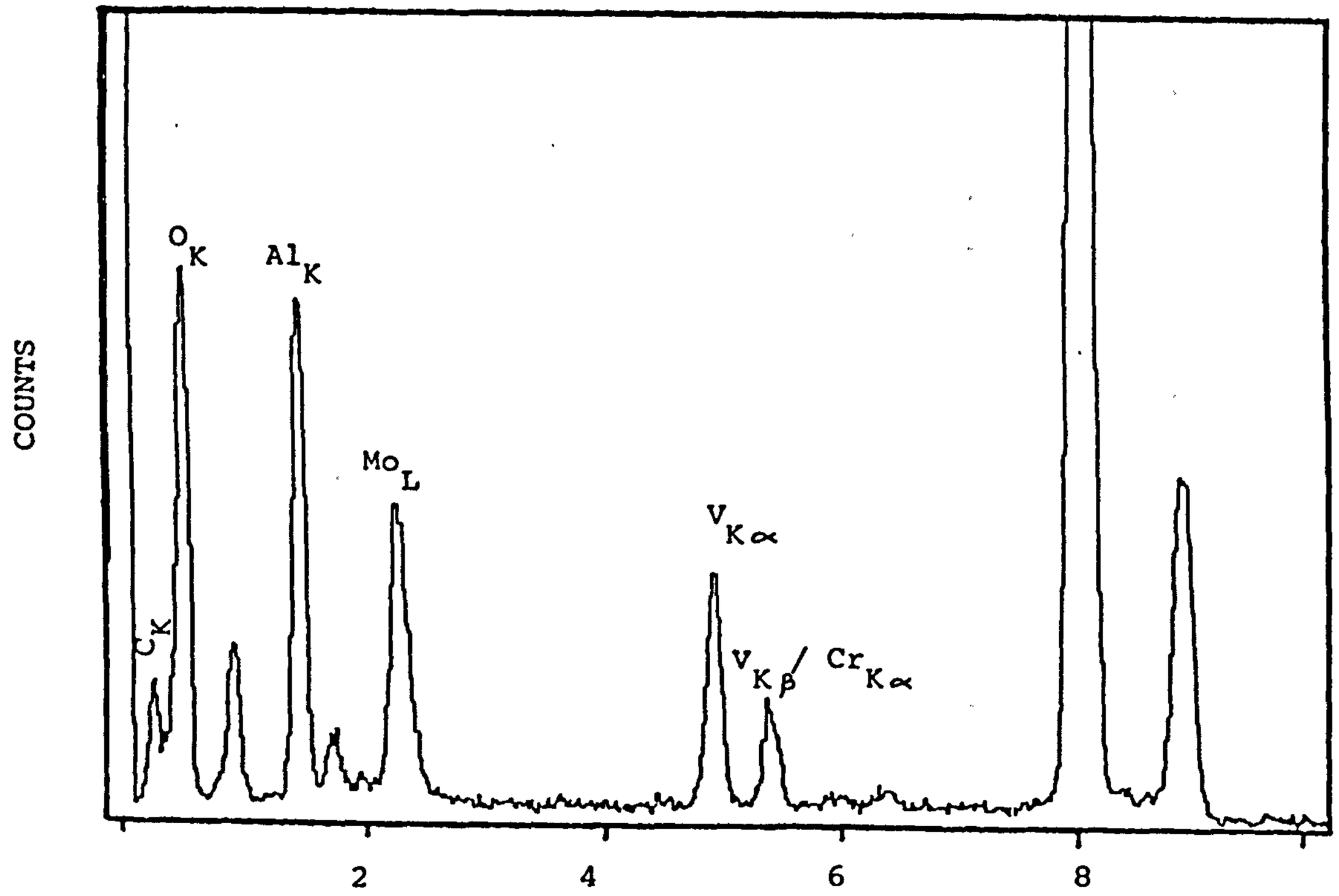


Fig.(17): Characteristic EDX spectrum obtained from secondary hardening carbide of M42 using window-less detector.

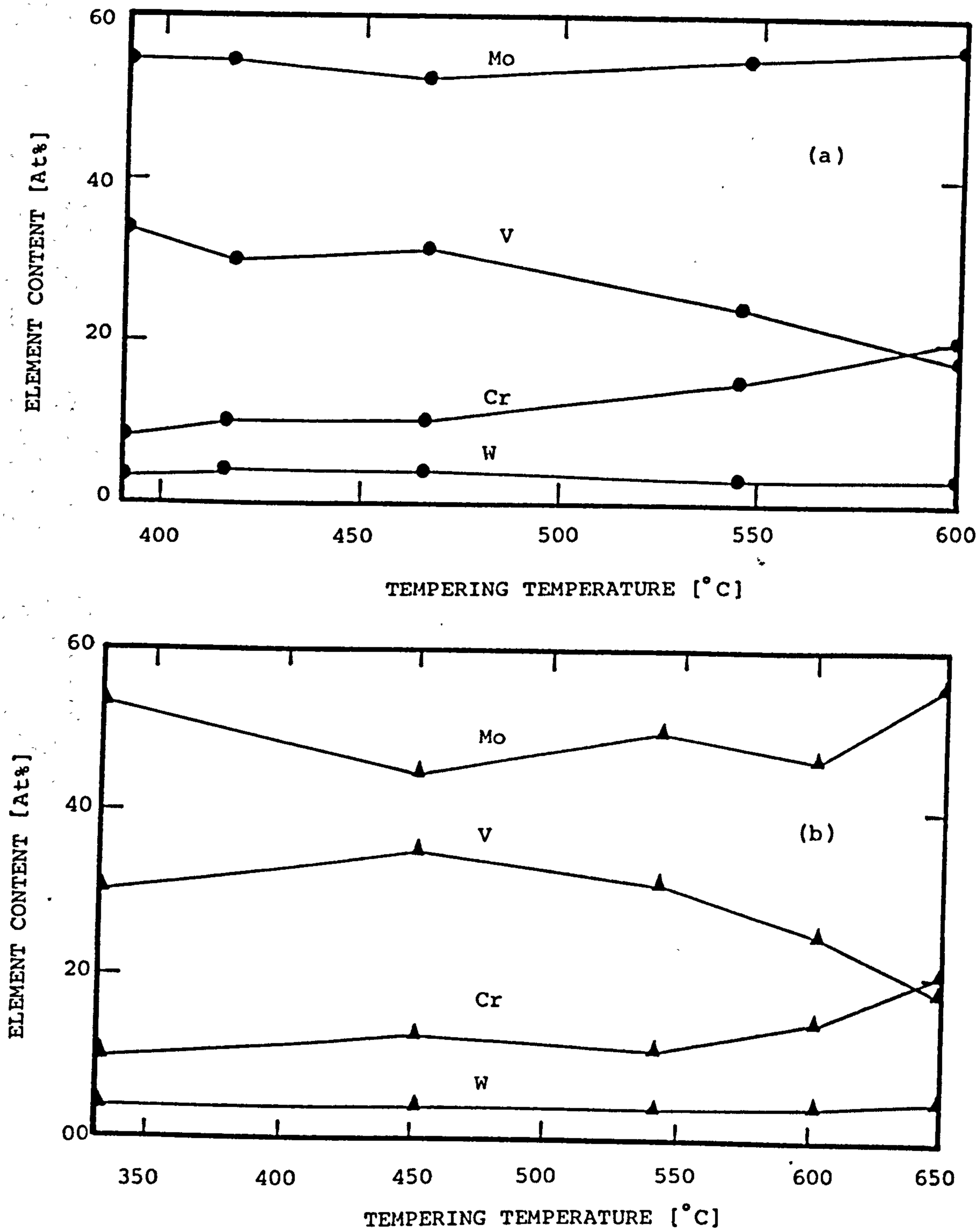


Fig.(18): Variation of chemical composition of secondary hardening carbide with tempering temperature;

(a) M42 .

(b) M1 .

(a)

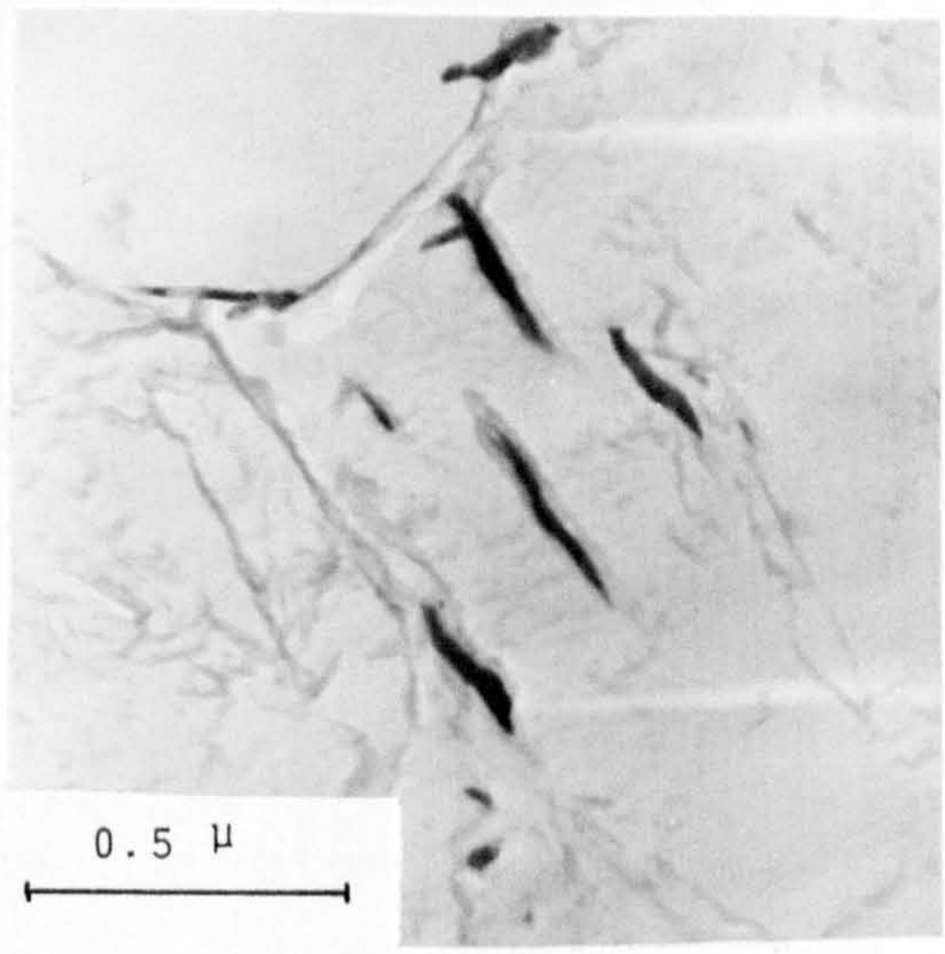

0.5 μ

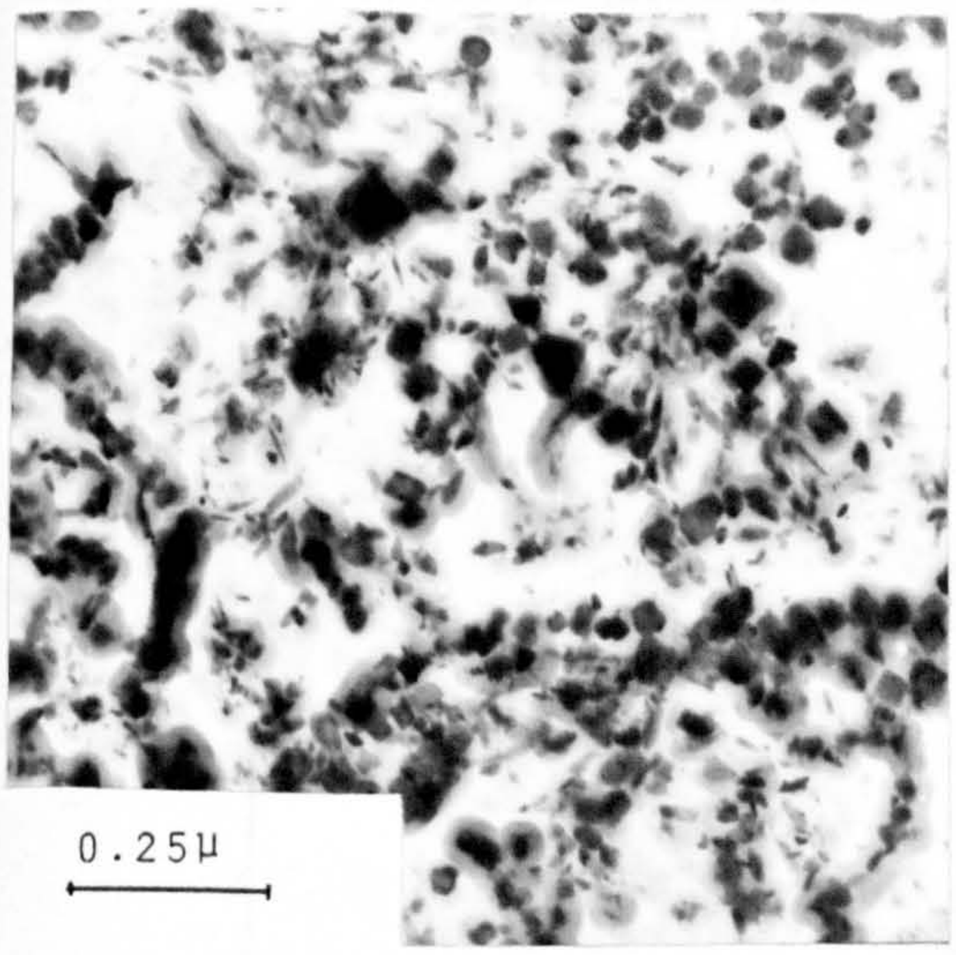

0.25μ

(b)

(c)

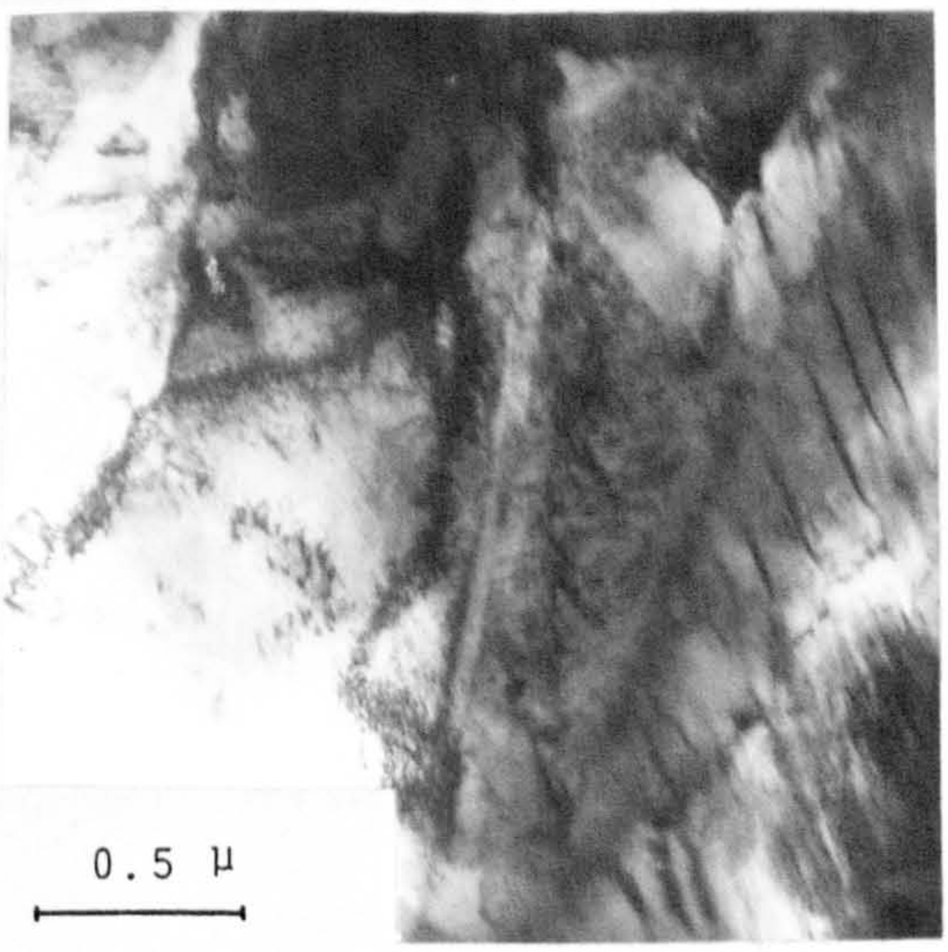

0.5 μ

Fig.(19) : Electron micrographs showing cementite needles precipitated in M42.

(a) carbon replica from specimen tempered at 480°C

(b) carbon replica from specimen tempered to peak hardness

(c) thin foil tempered to peak hardness.

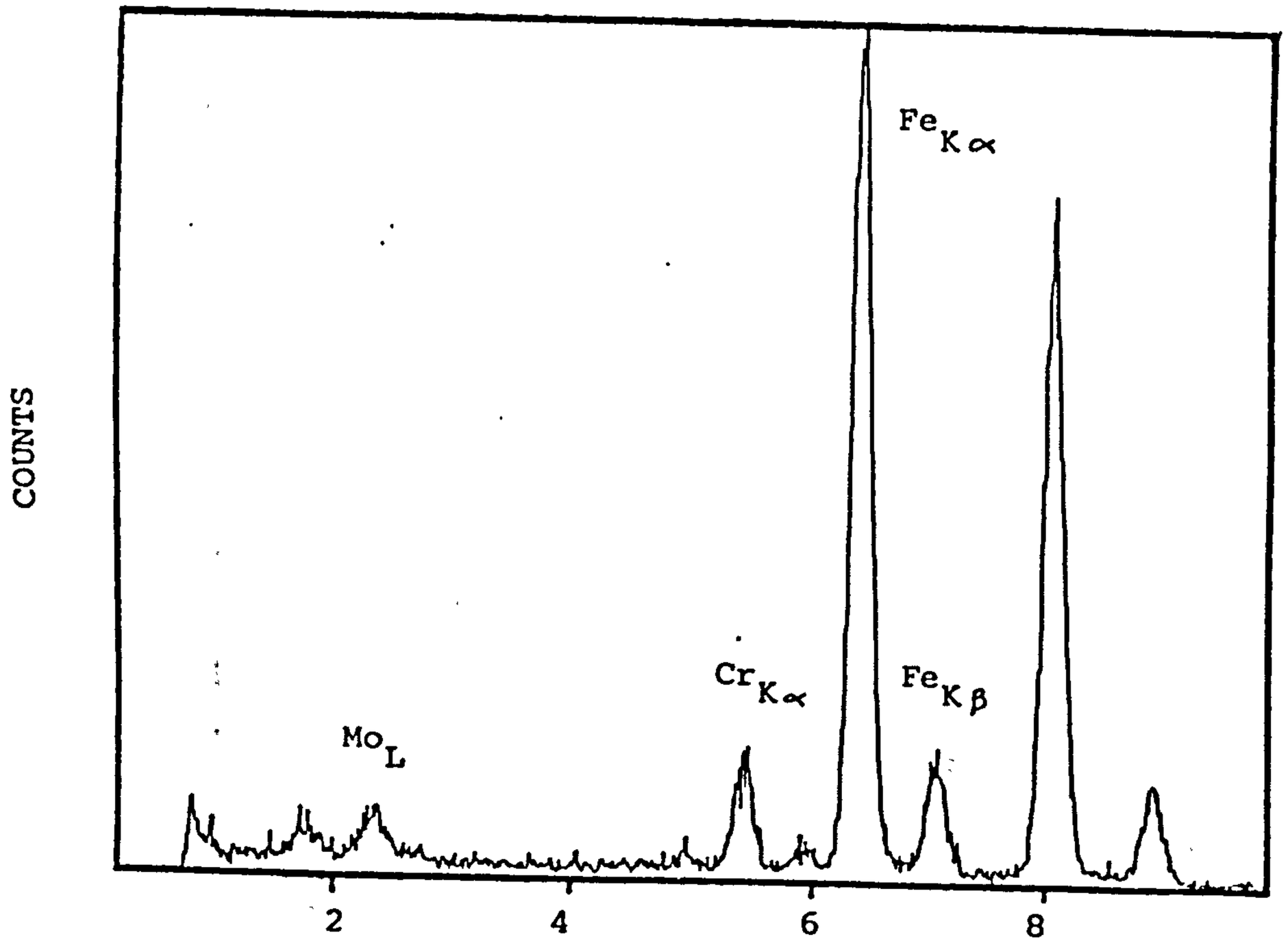


Fig.(20): Characteristic EDX spectrum of cementite extracted from M42.

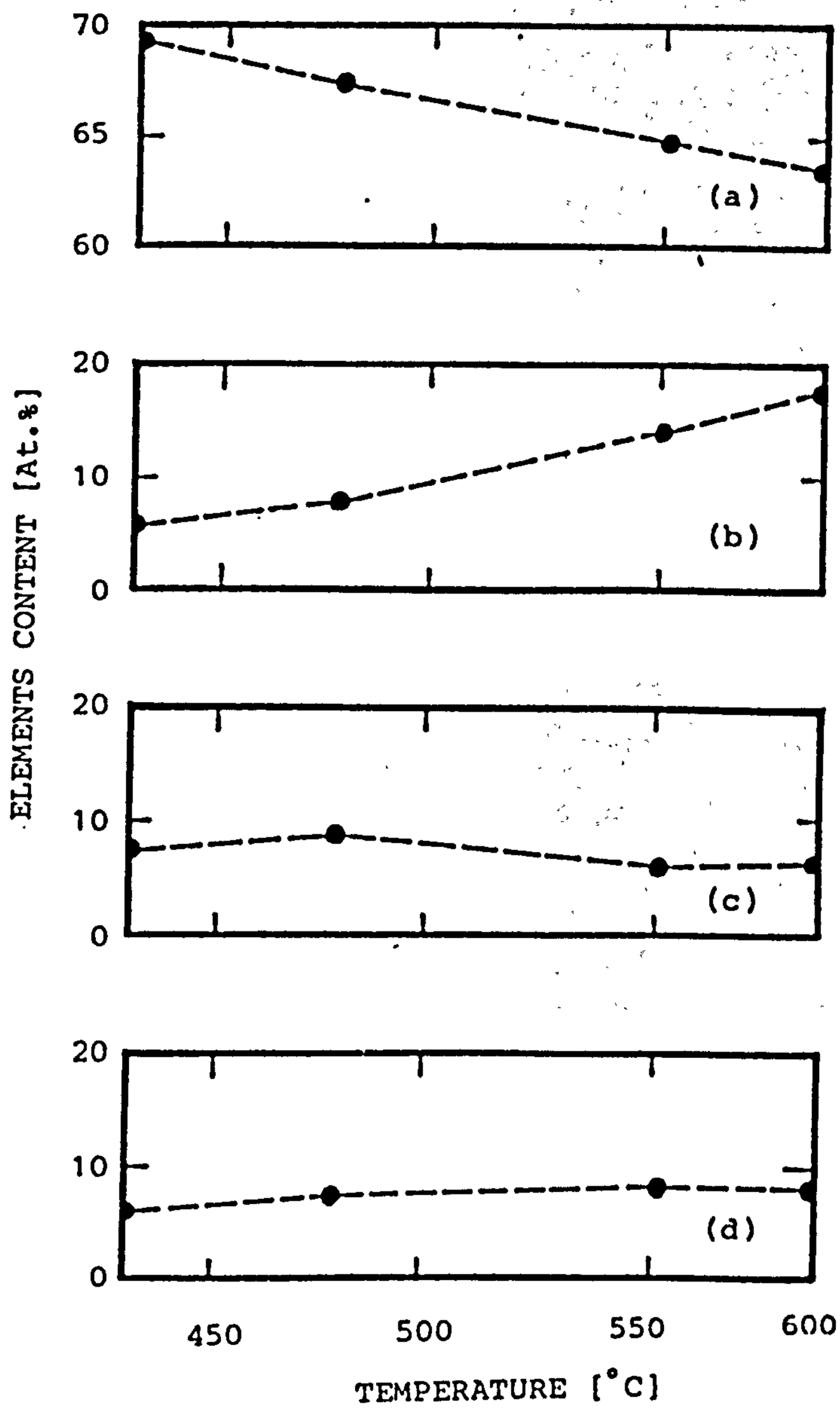


Fig.(21): Variation of chemical composition of cementite with temperature.

(a) Fe, (b) Cr, (c) Co and (d) Mo.

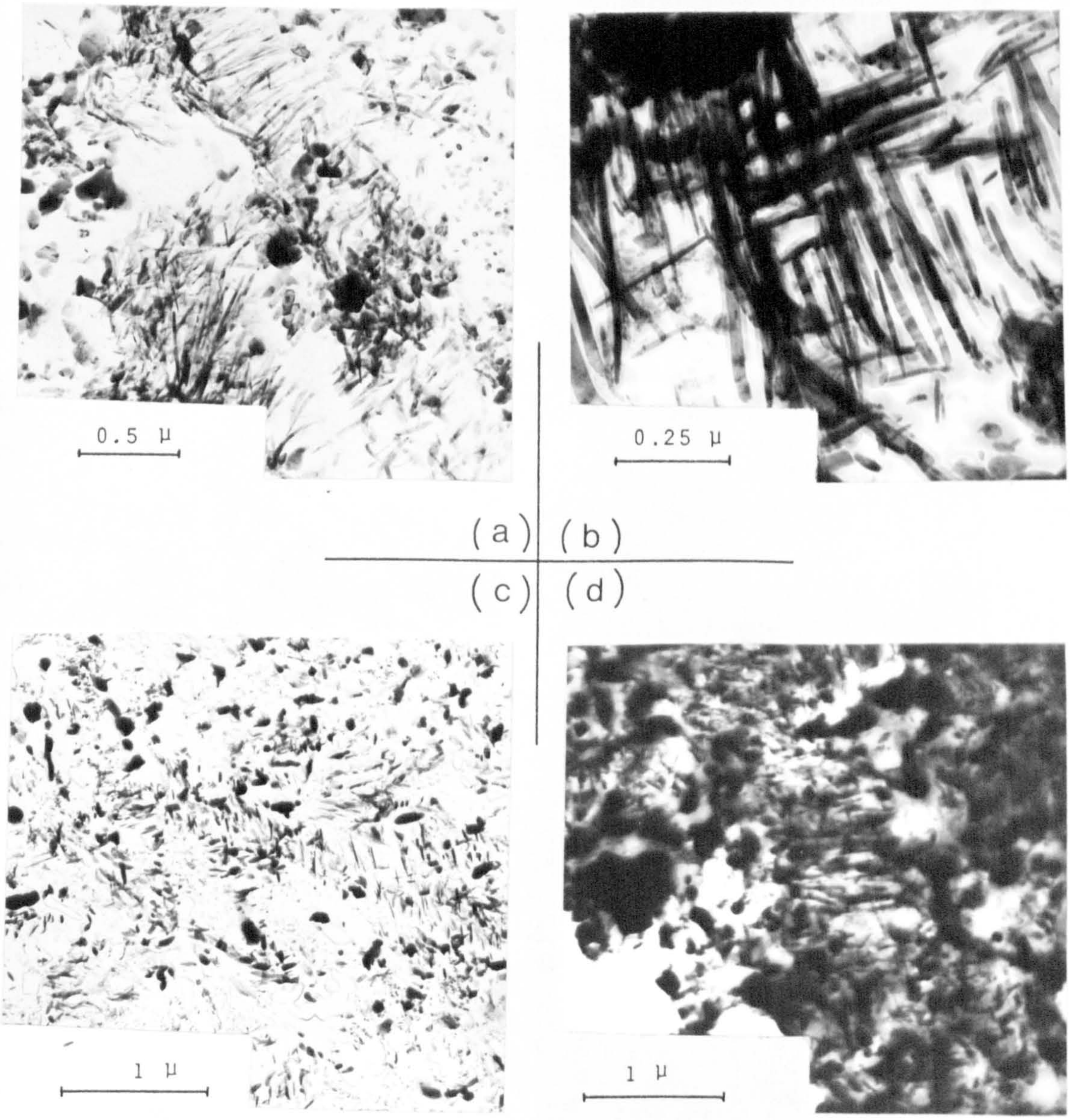


Fig.(22): Electron micrographs showing hexagonal $M_2C$ needles and $M_{23}C_6$ particles precipitated after tempering for 2+2 h at 700°C.

(a),(b) carbon replica from M42

(b) carbon replica from M15.

(c) thin foil from M1.

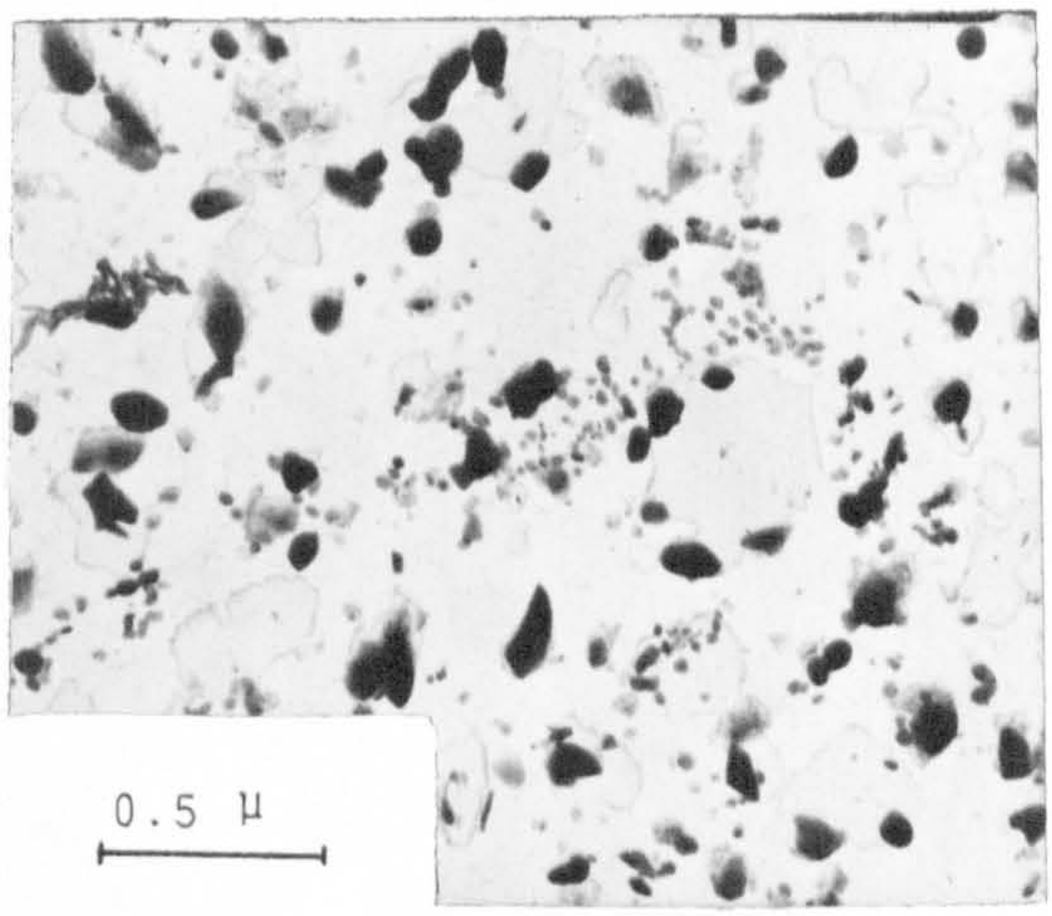


(a)

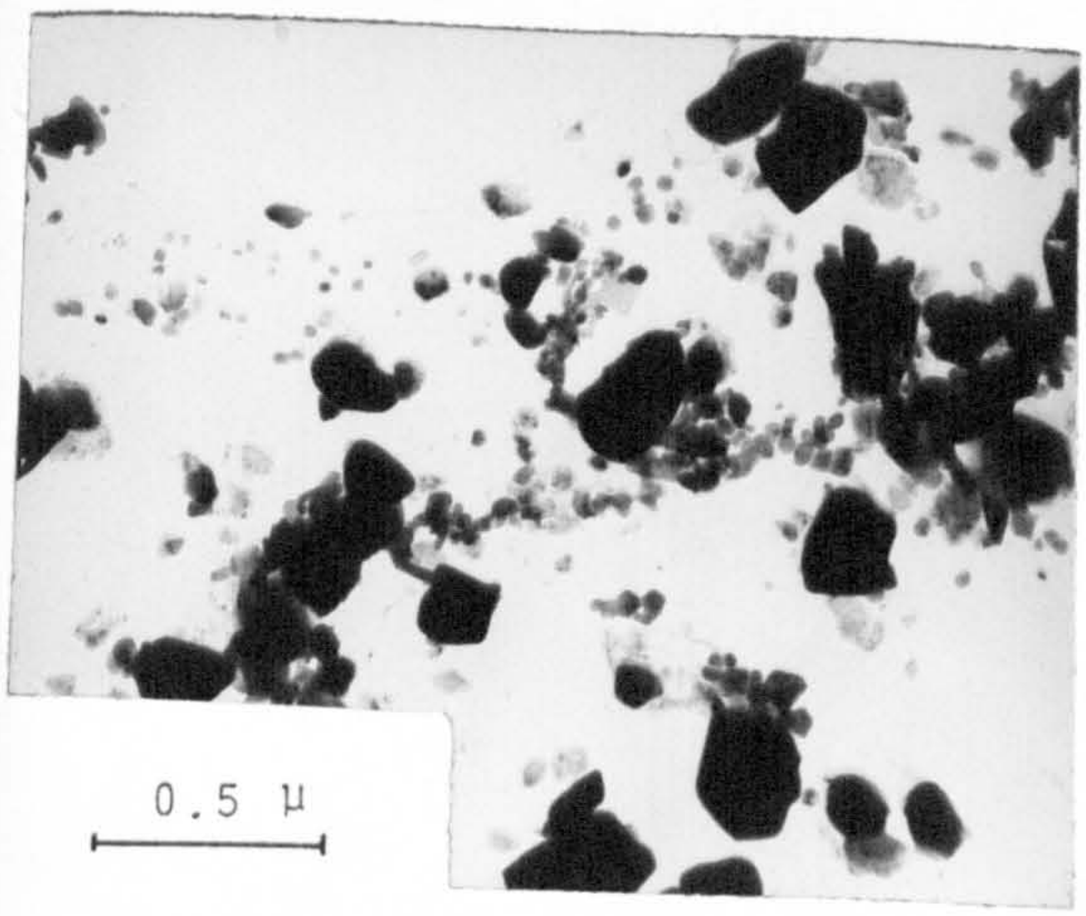


(b)

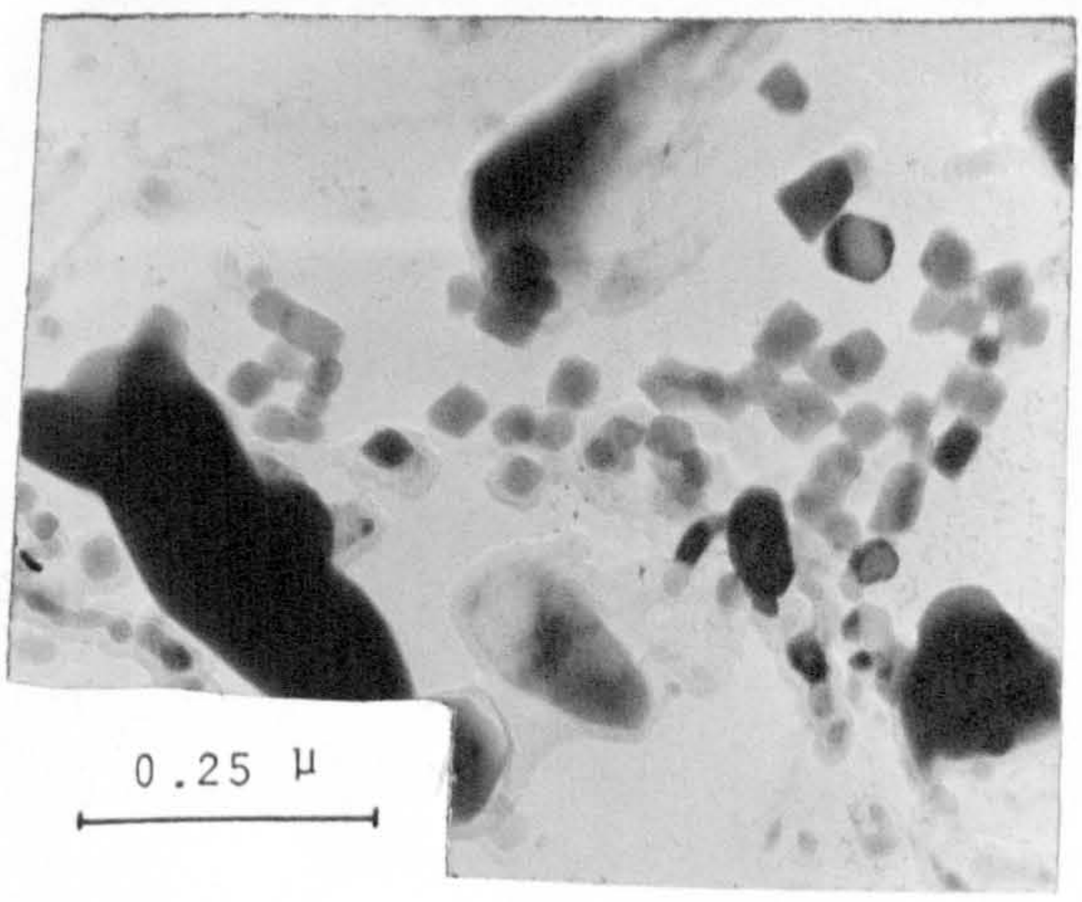


(c)

Fig.(23): Carbon replica micrographs showing the precipitation of secondary vanadium carbide after tempering for 24 h at 700°C.

(a) M42 (b) M1 (c) M15.

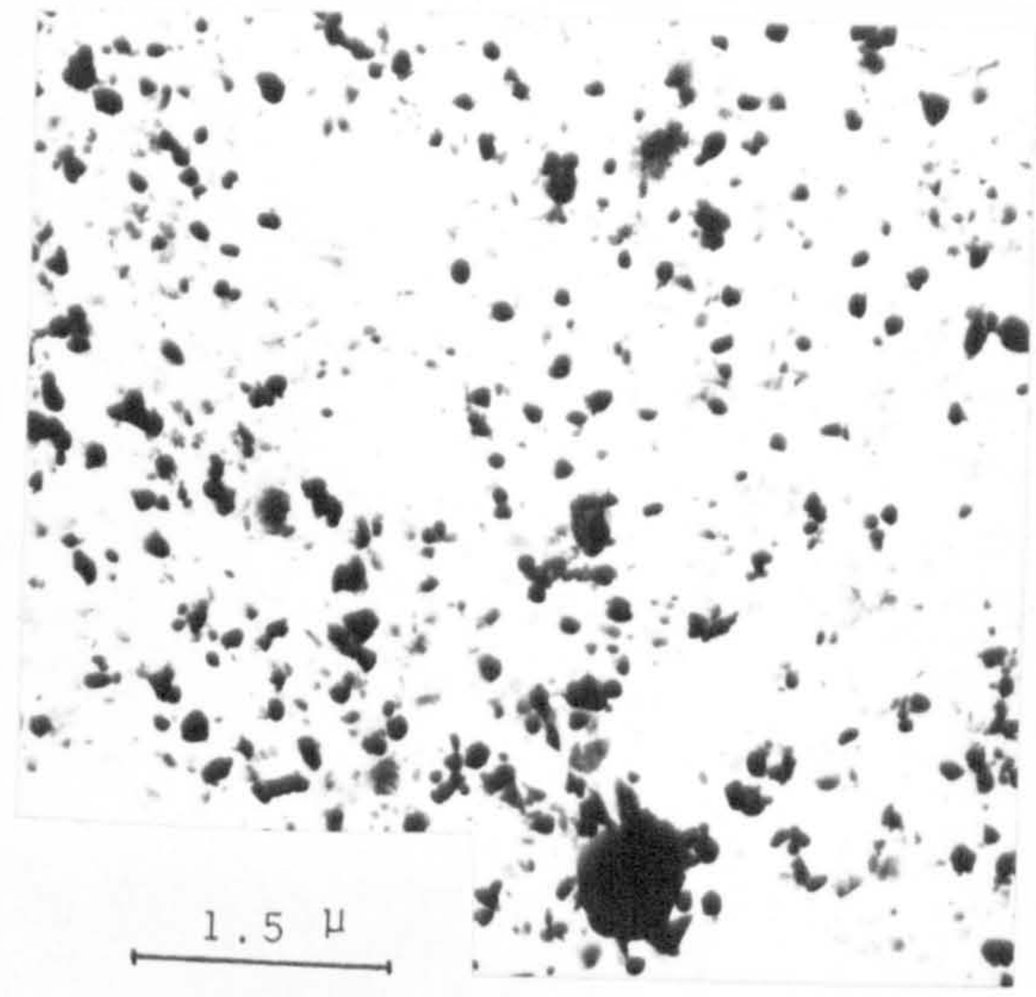


(a)

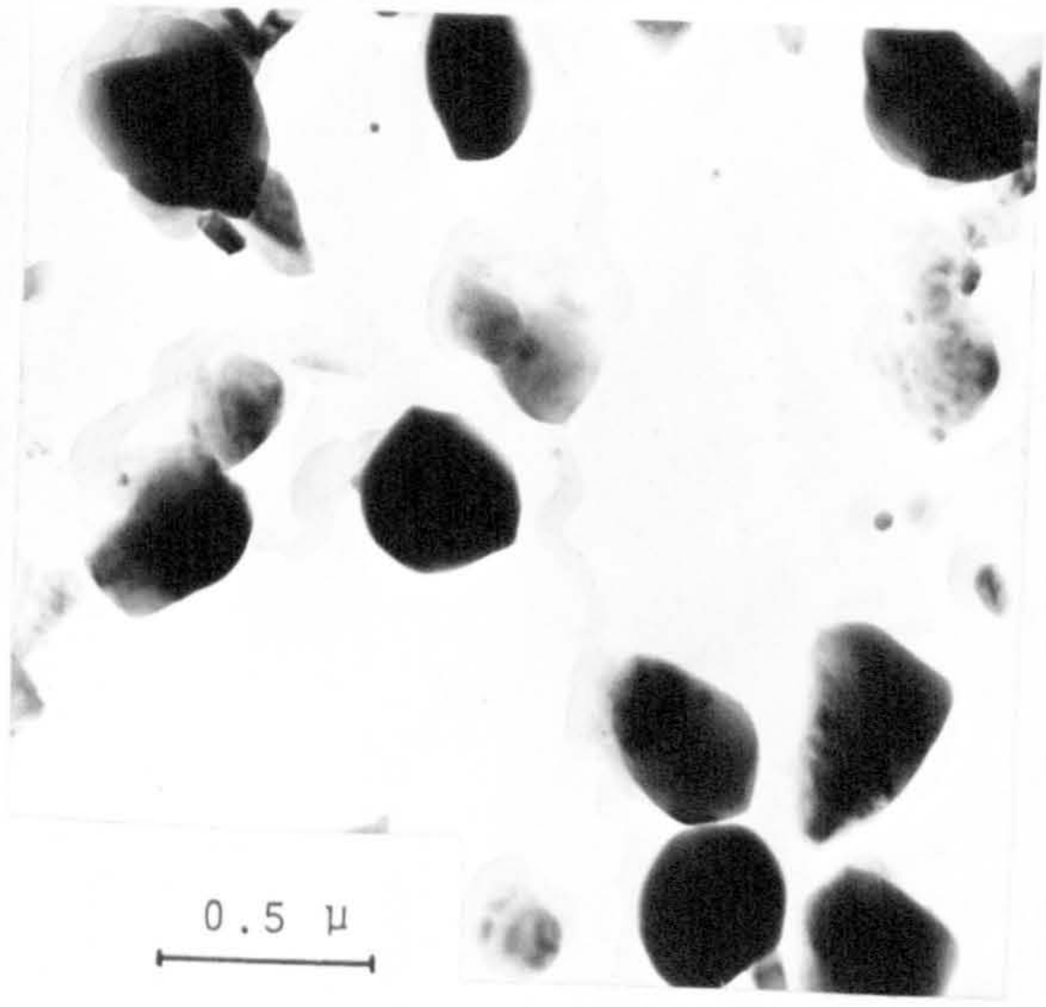


(b)

Fig.(24): Carbon replica micrographs showing the microstructure of M42 after tempering for 24 h at 800 °C, which is similar to that of other steels examined.

(a) low magnification (b) high magnification .

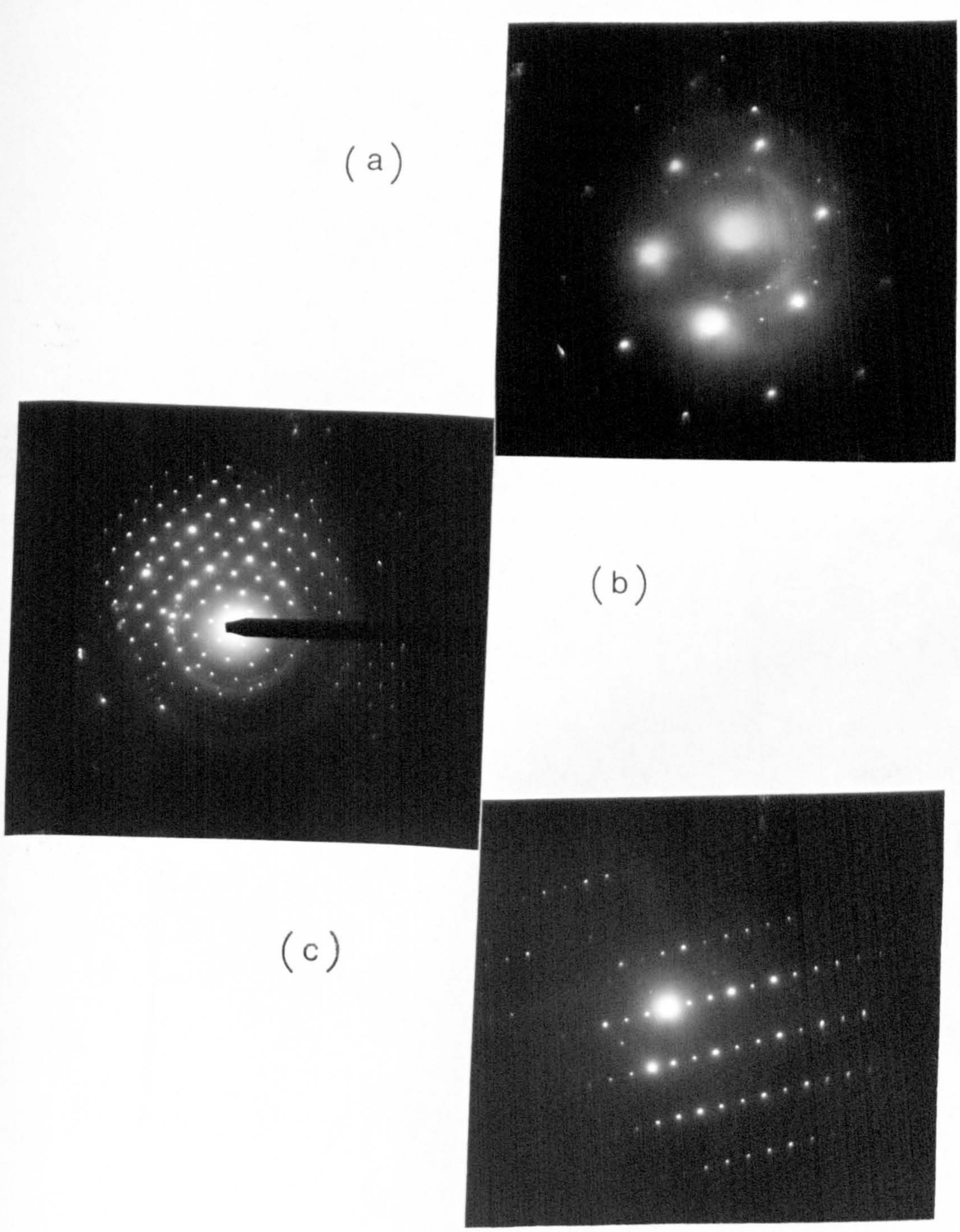


Fig.(25): Single crystal diffraction patterns of carbides present in annealed M42, which are similar to those in other steels examined.

(a) MC, zone axis $[\bar{1}11]$ (b) $M_6C$, zone axis [011]

(c) $M_{23}C_6$, zone axis $[\bar{1}23]$

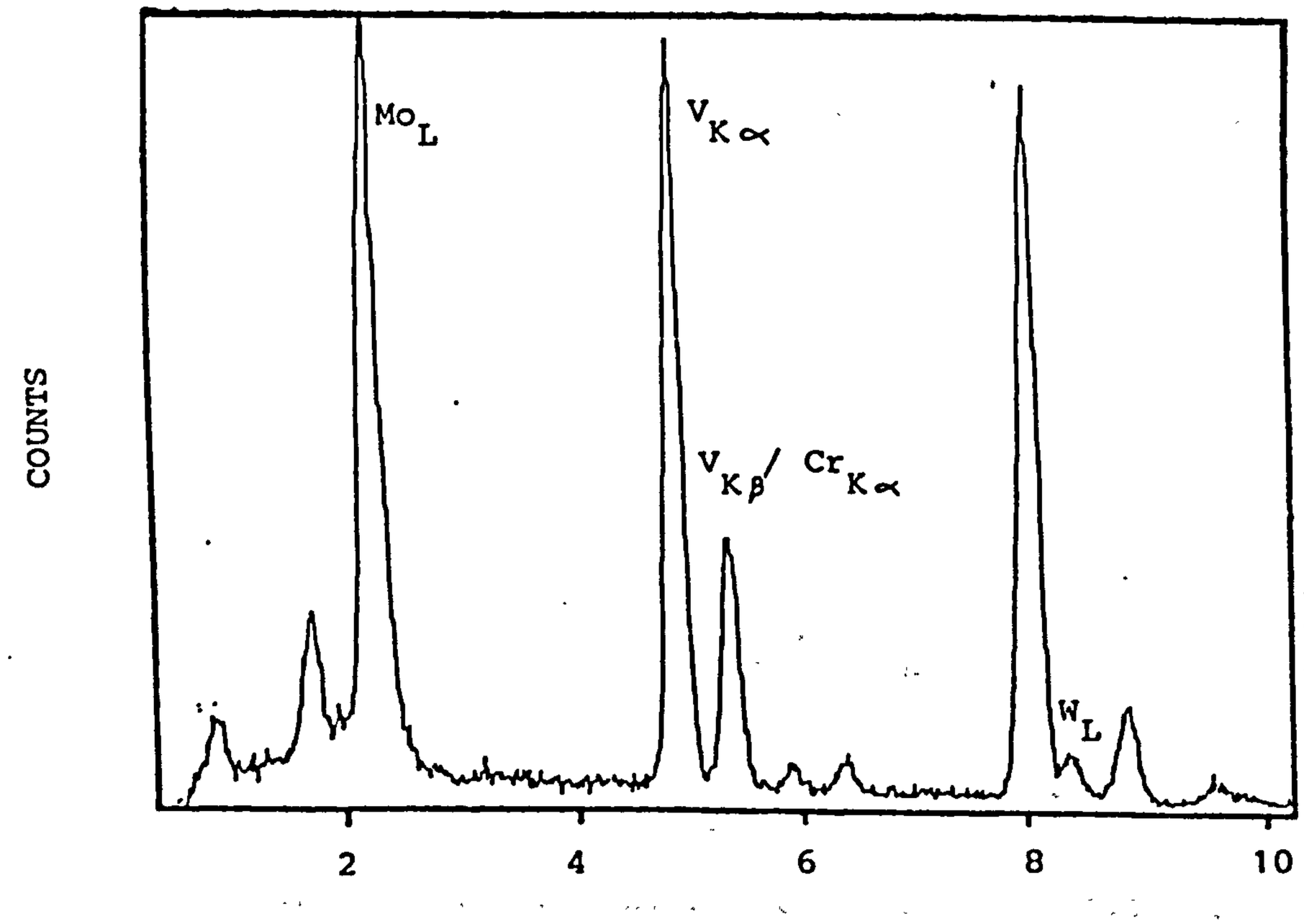


Fig.(26): Characteristic EDX spectrum obtained from secondary hardening carbide of M42.

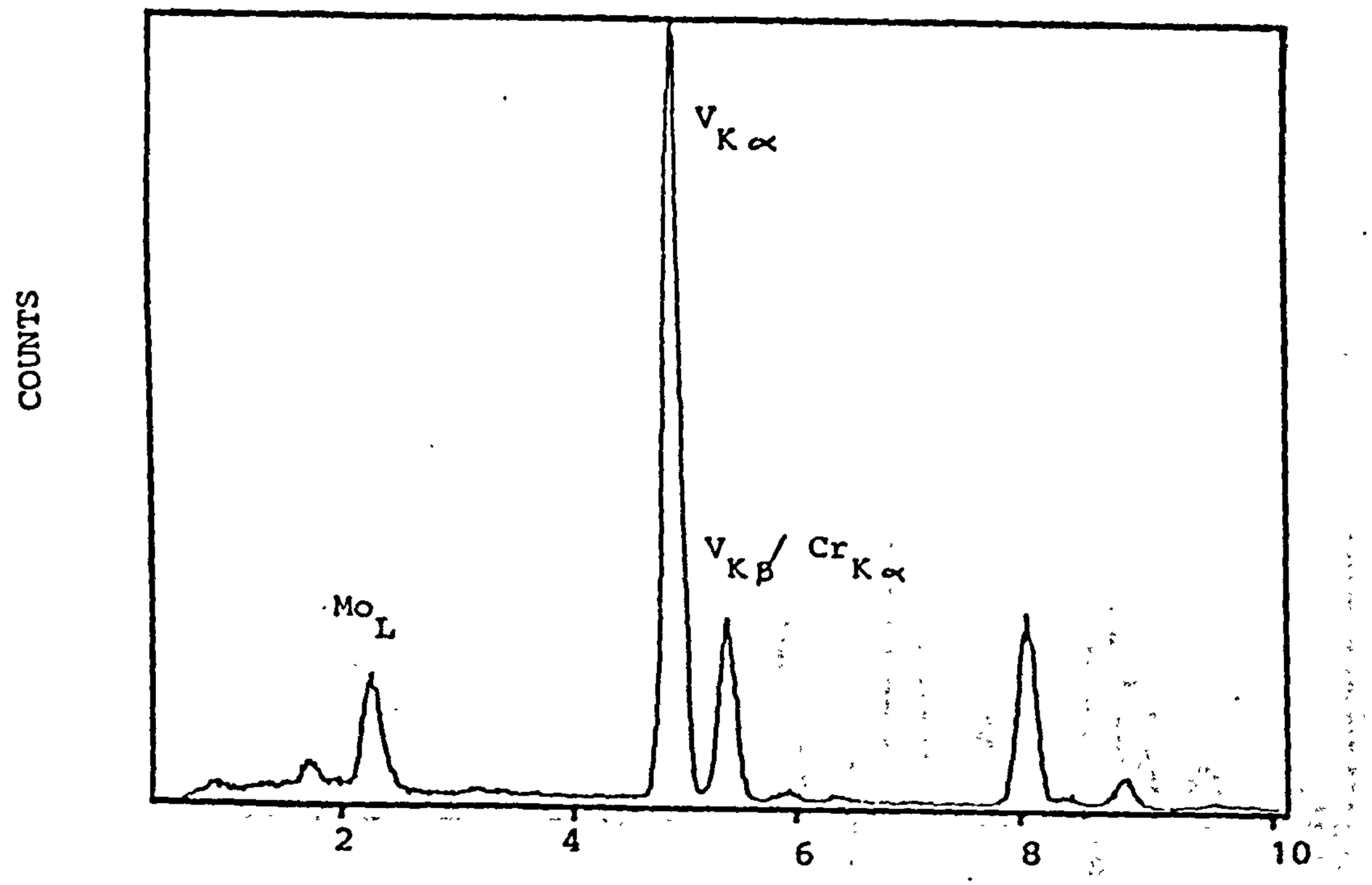


Fig.(27) : Characteristic EDX spectrum obtained from primary MC carbide extracted from M42.

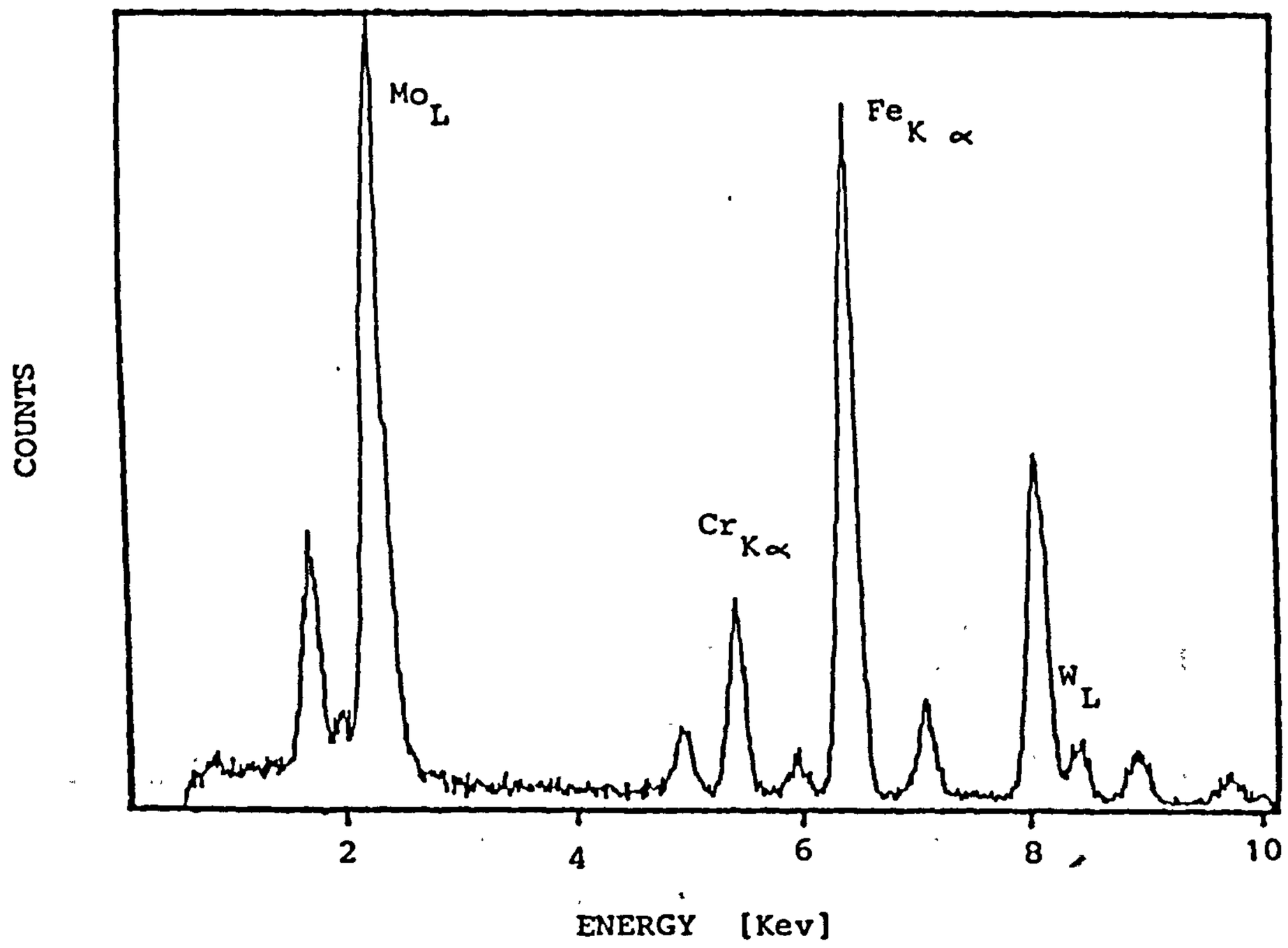


Fig.(28) : Characteristic EDX spectrum obtained from primary $M_6C$ precipitated in M42 .

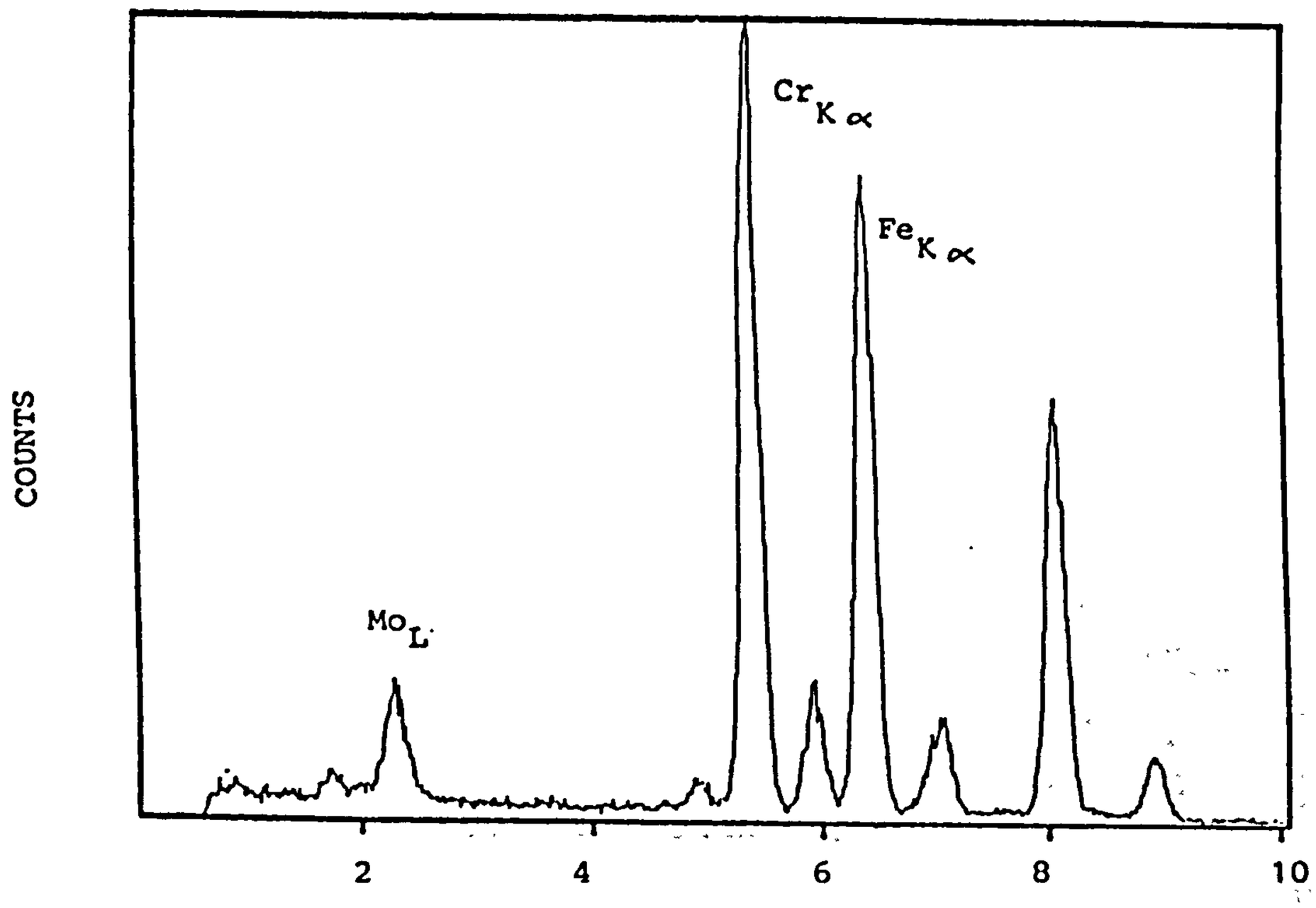


Fig.(29): Characteristic EDX spectrum obtained from $M_{23}C_6$ carbide precipitated in M42 .

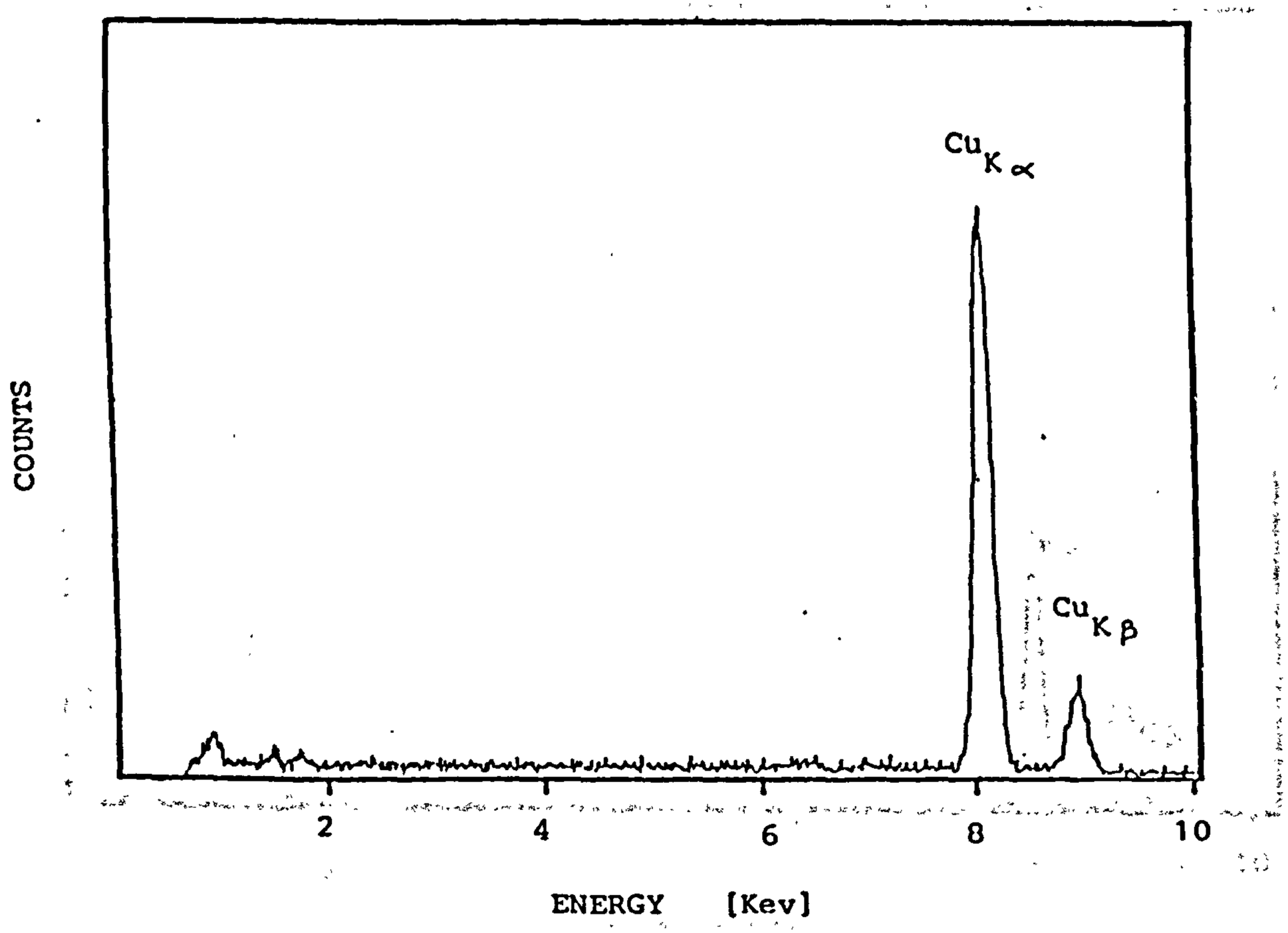


Fig.(30) : EDX spectrum showing the background of a carbon replica .

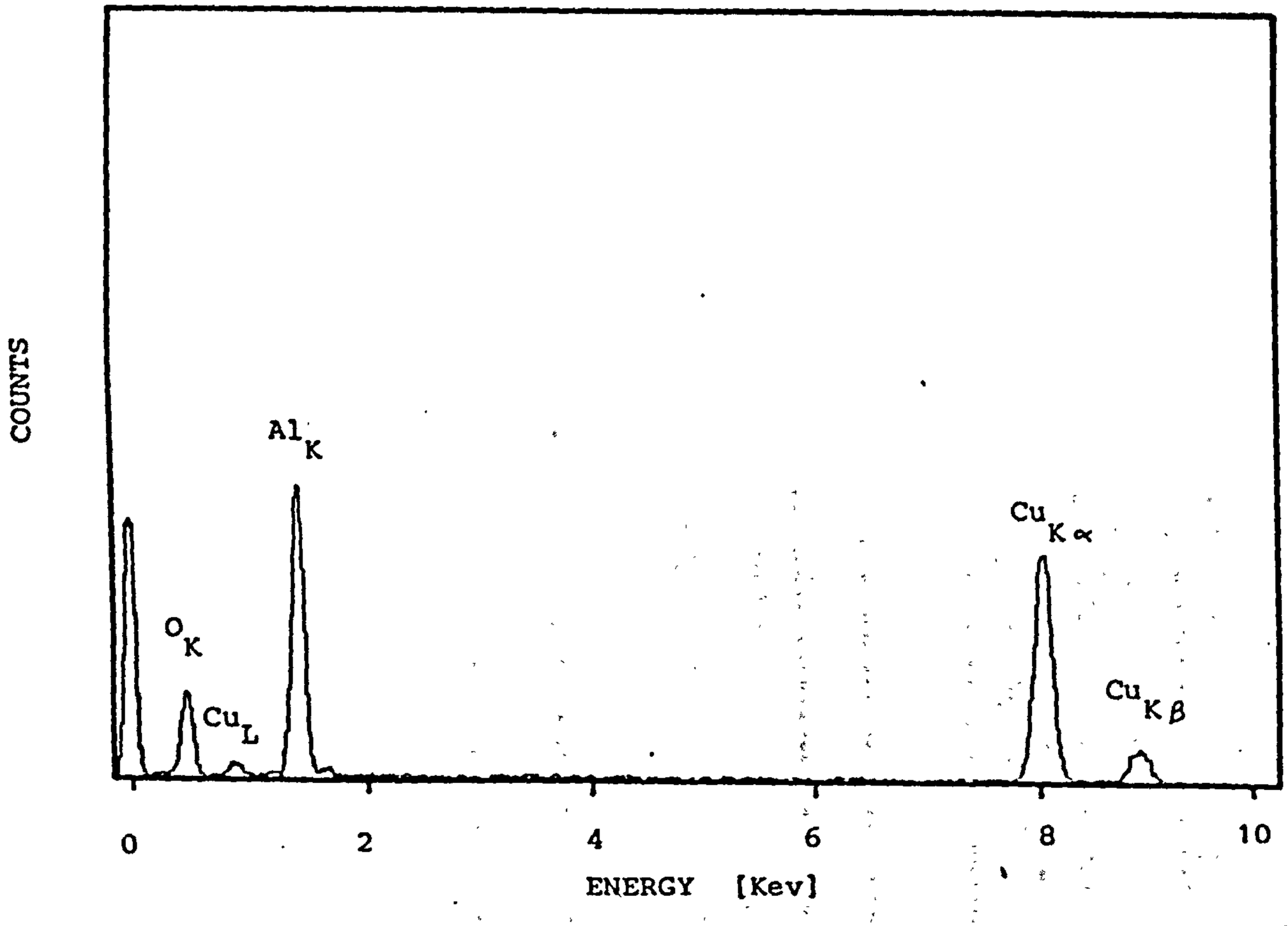


Fig.(31) : Window-less EDX spectrum showing the background of an aluminium replica .

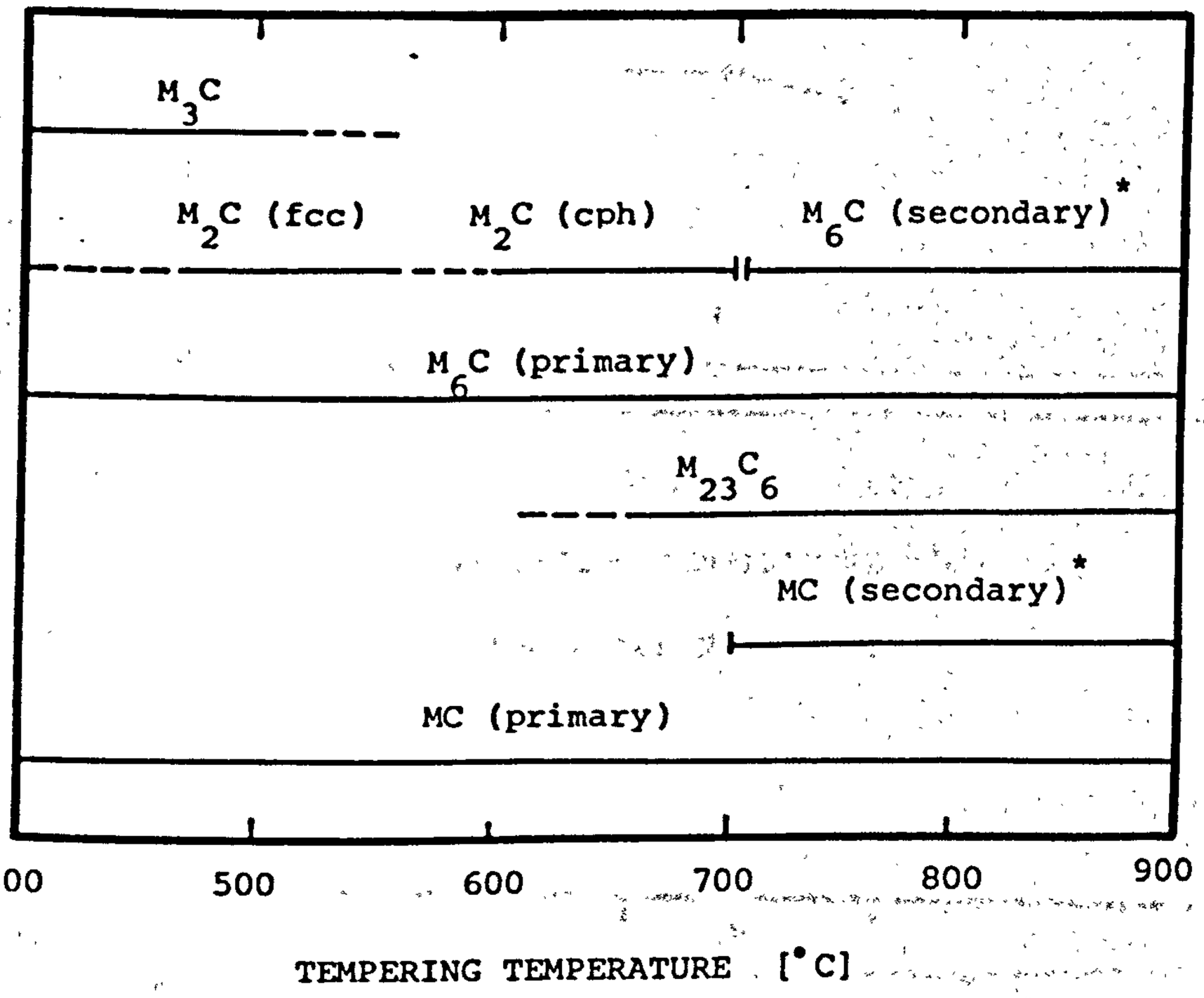


Fig.(32): Carbides produced in high speed steels after tempering for 2+2 h at different temperatures.

* ... detected after 24 hours.

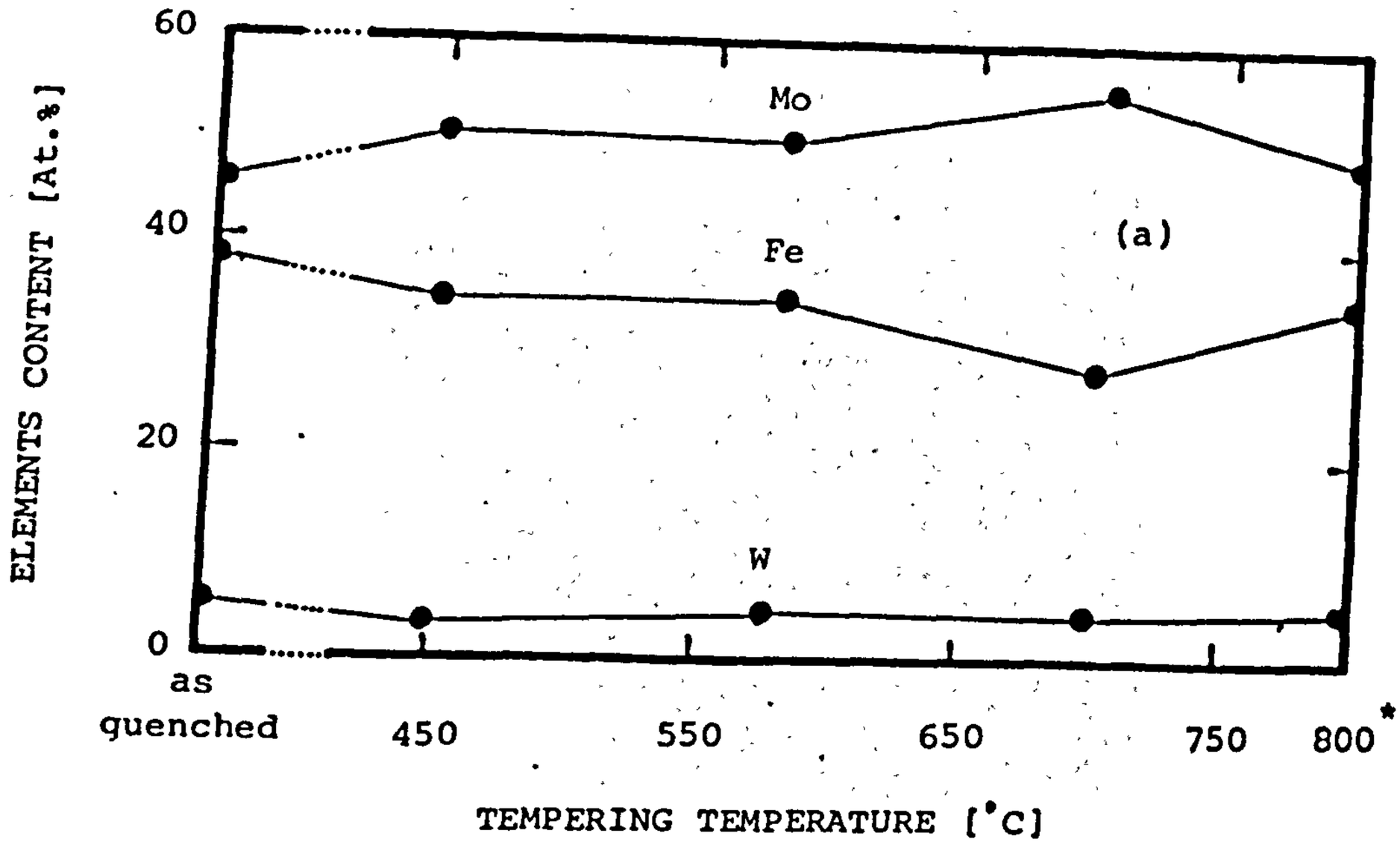


* .... detected after 24 hours.

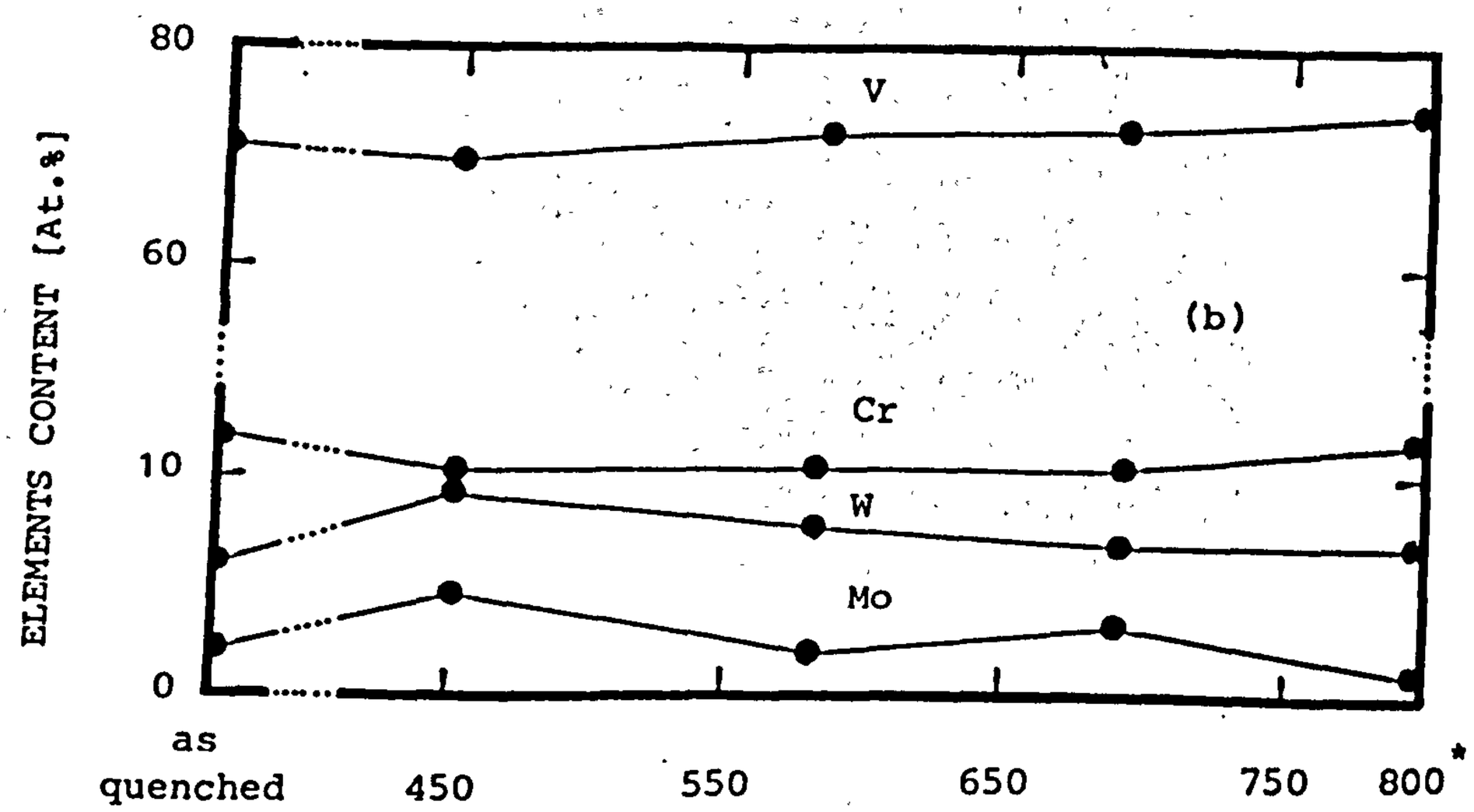


* .... detected after 24 hours.

Fig.(33): Variation of chemical composition of primary carbides with tempering temperatures.

(a) $M_6C$ carbide precipitated in M42.

(b) MC carbide precipitated in M15.

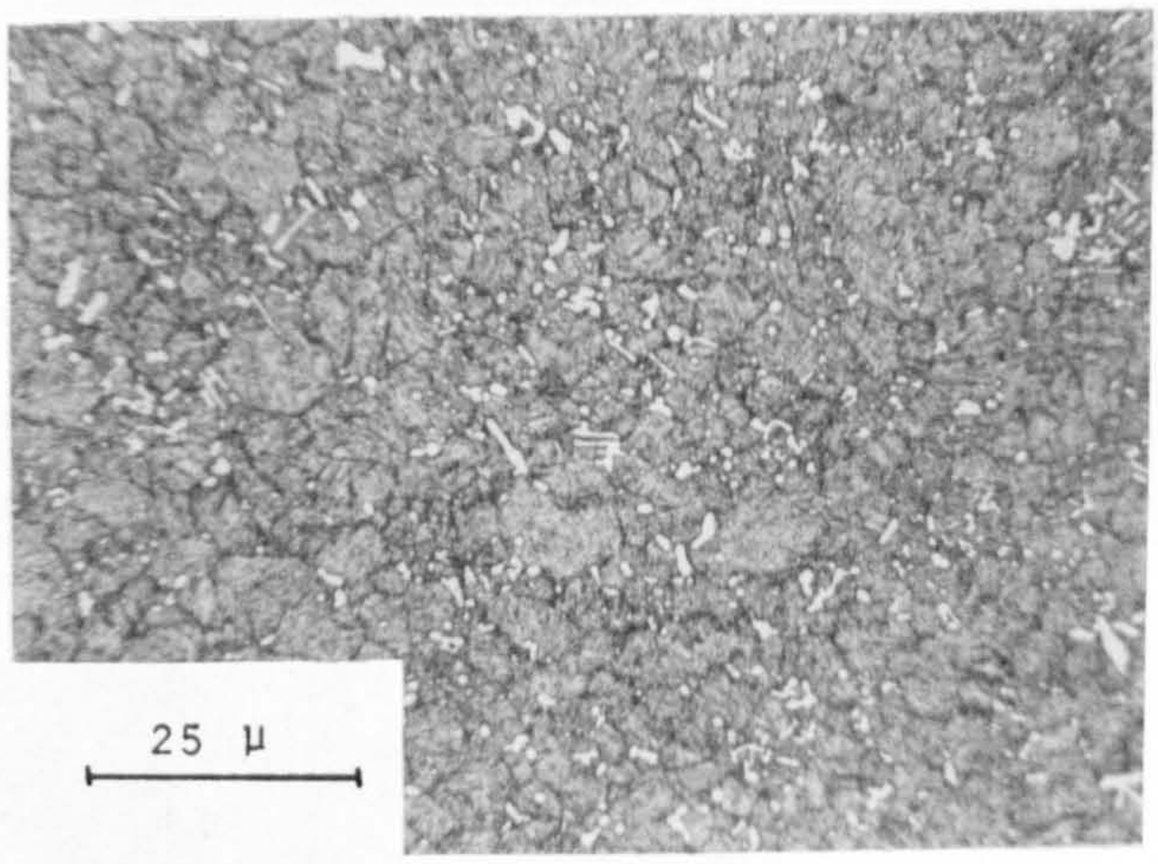


(a)

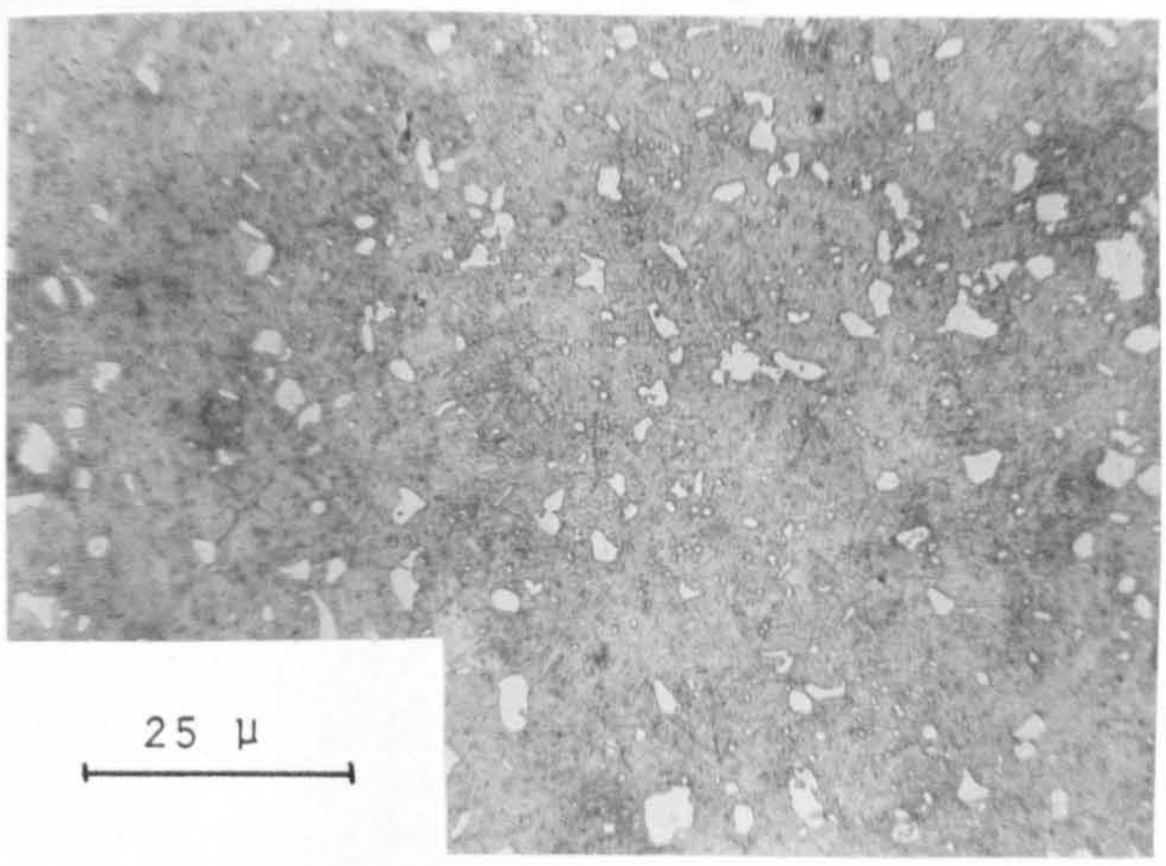


(b)

Fig.(34): Optical micrographs of tempered microstructure of :

(a) M42.

(b) M15.

(a)

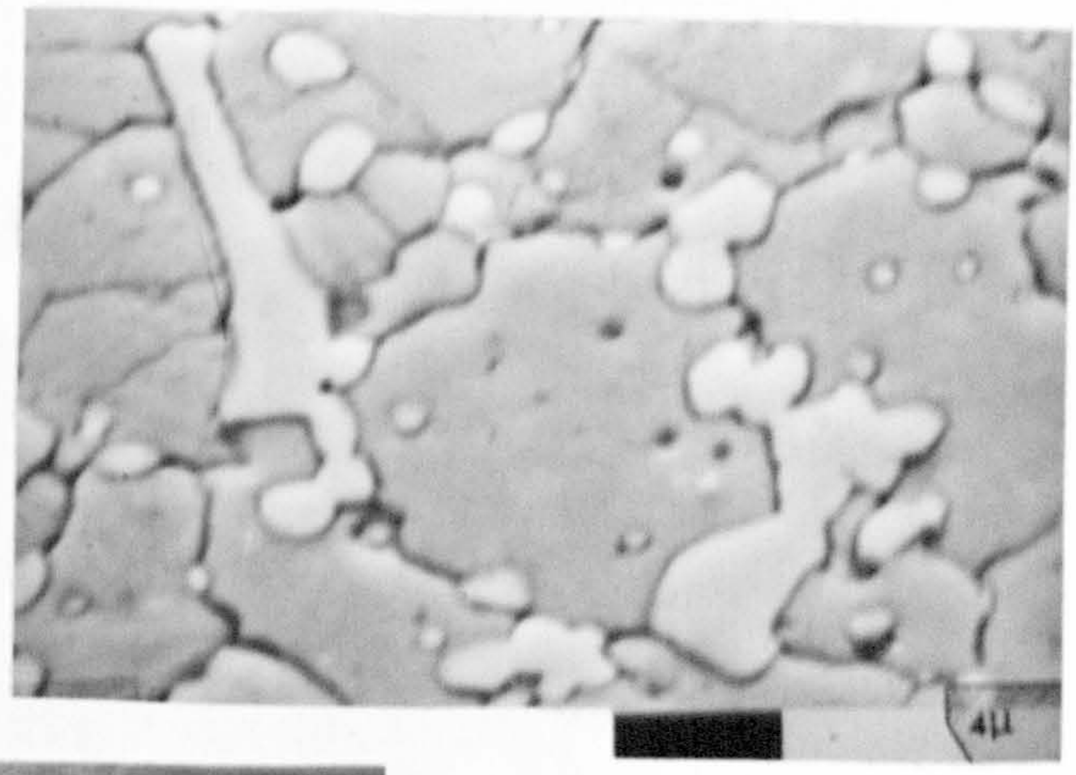


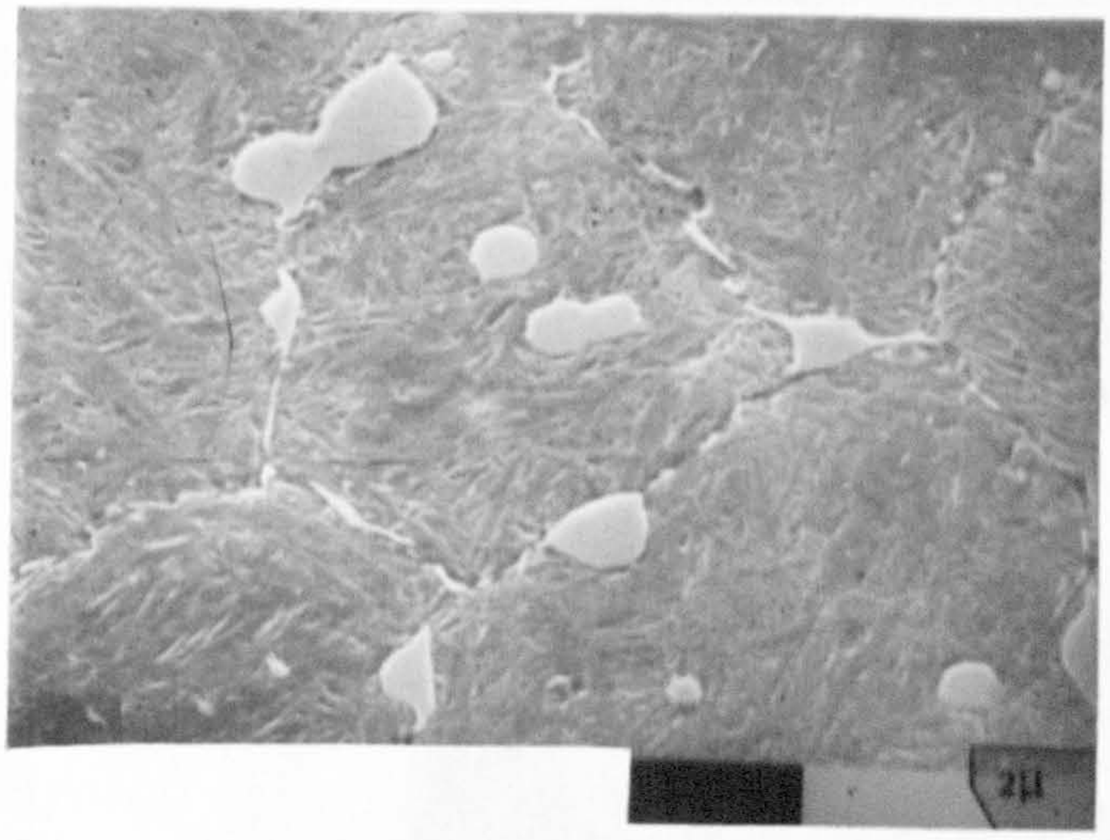


(b)

(c)

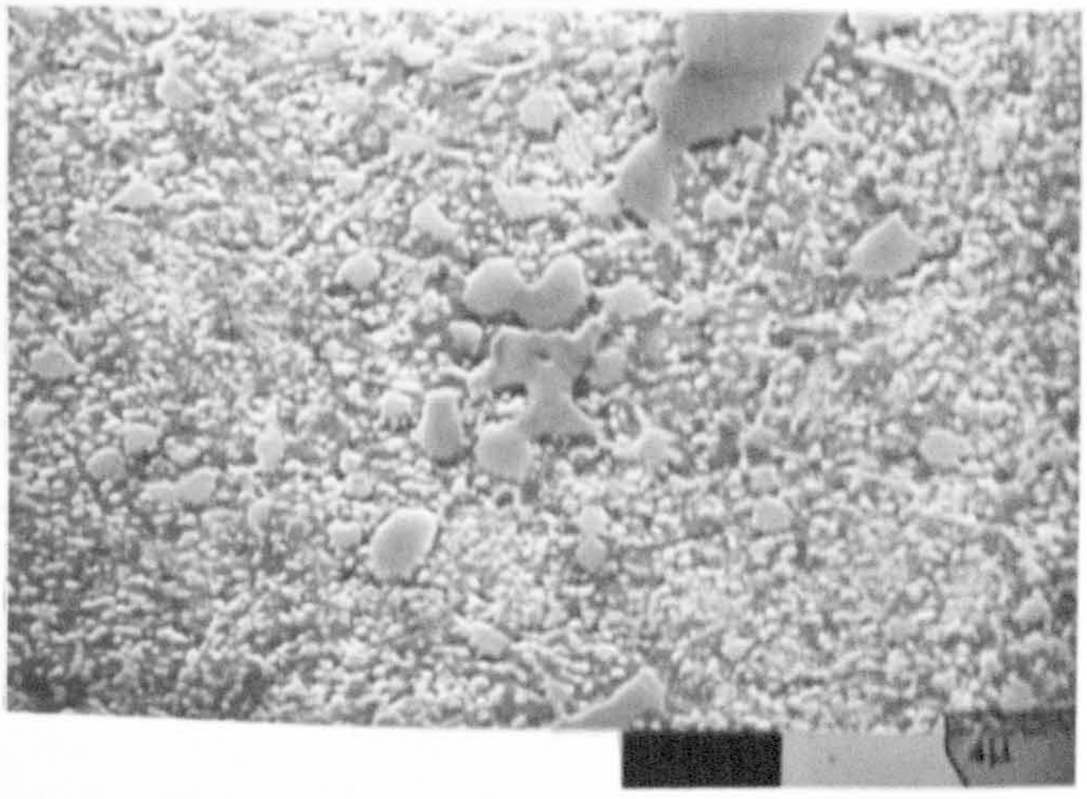


Fig.(35): SEM micrographs of M42 microstructure which is typical of that of other steels examined

(a) as quenched

(b) as tempered to peak hardness.

(c) as annealed.

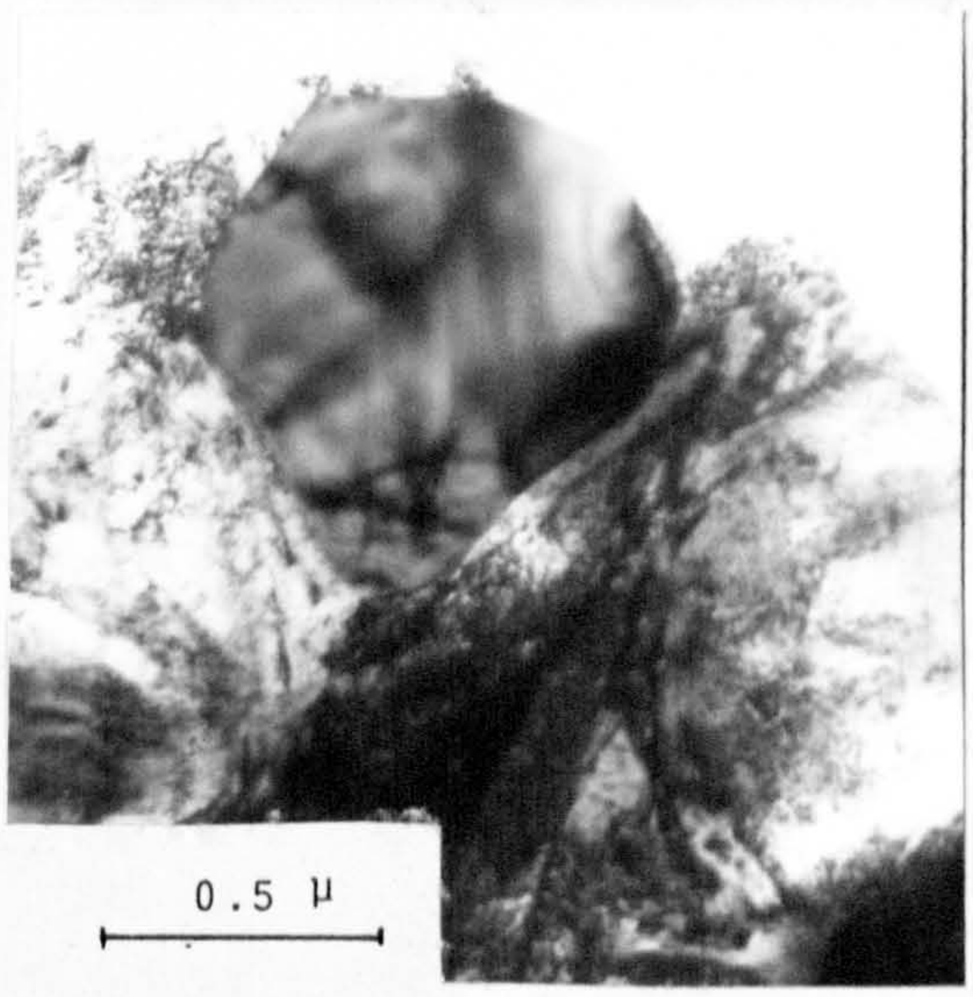


(a)

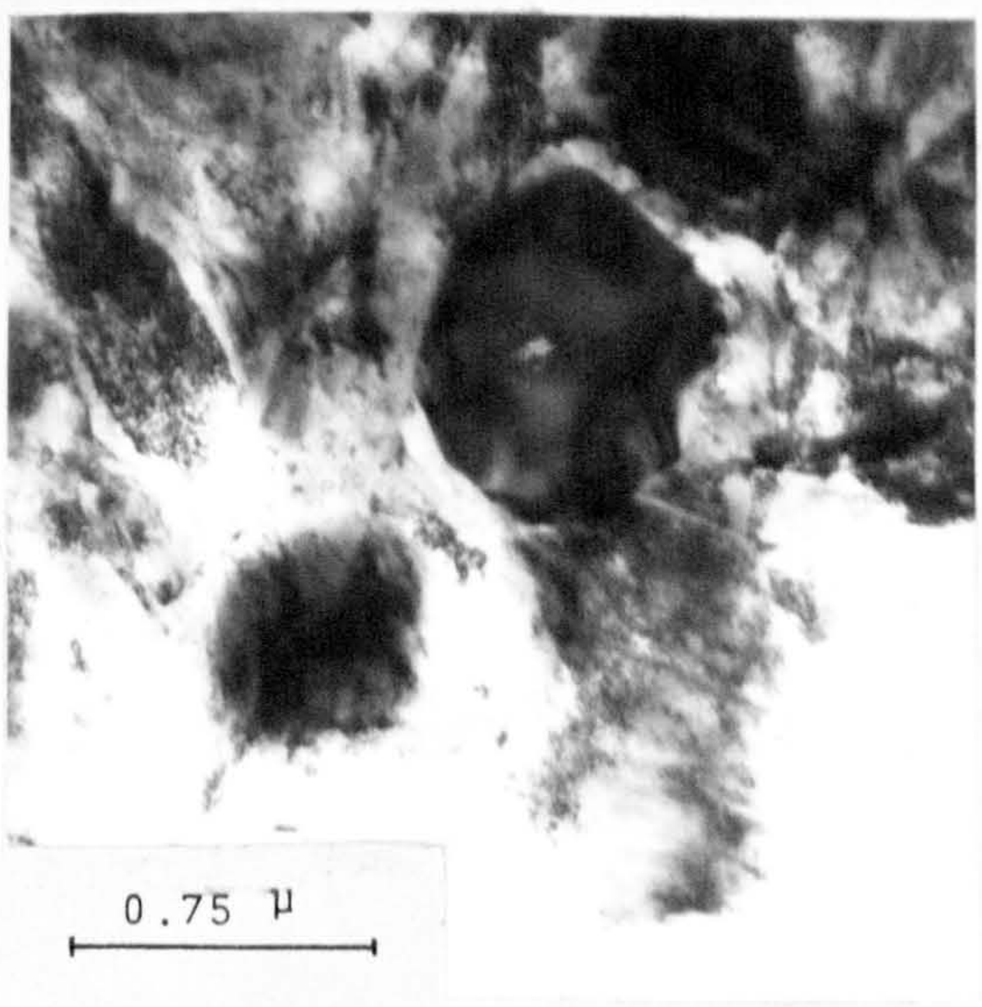


(b)

Fig.(36): Thin foil micrographs showing primary carbides,

(a) MC carbide in M15.

(b) $M_6C$ carbide in M42.

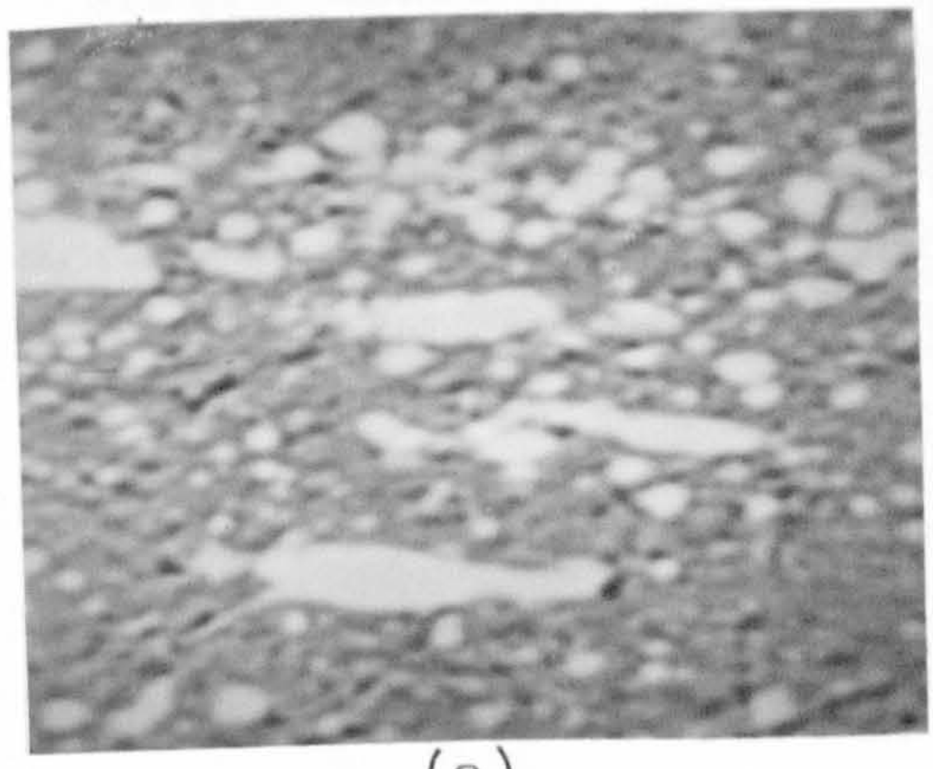


Fig.(37): EPMA X-ray scans showing alloying element distributions in tempered M42 specimen.

(a) microstructure x2000 (b) Mo

(c) V (d) Co (e) Cr

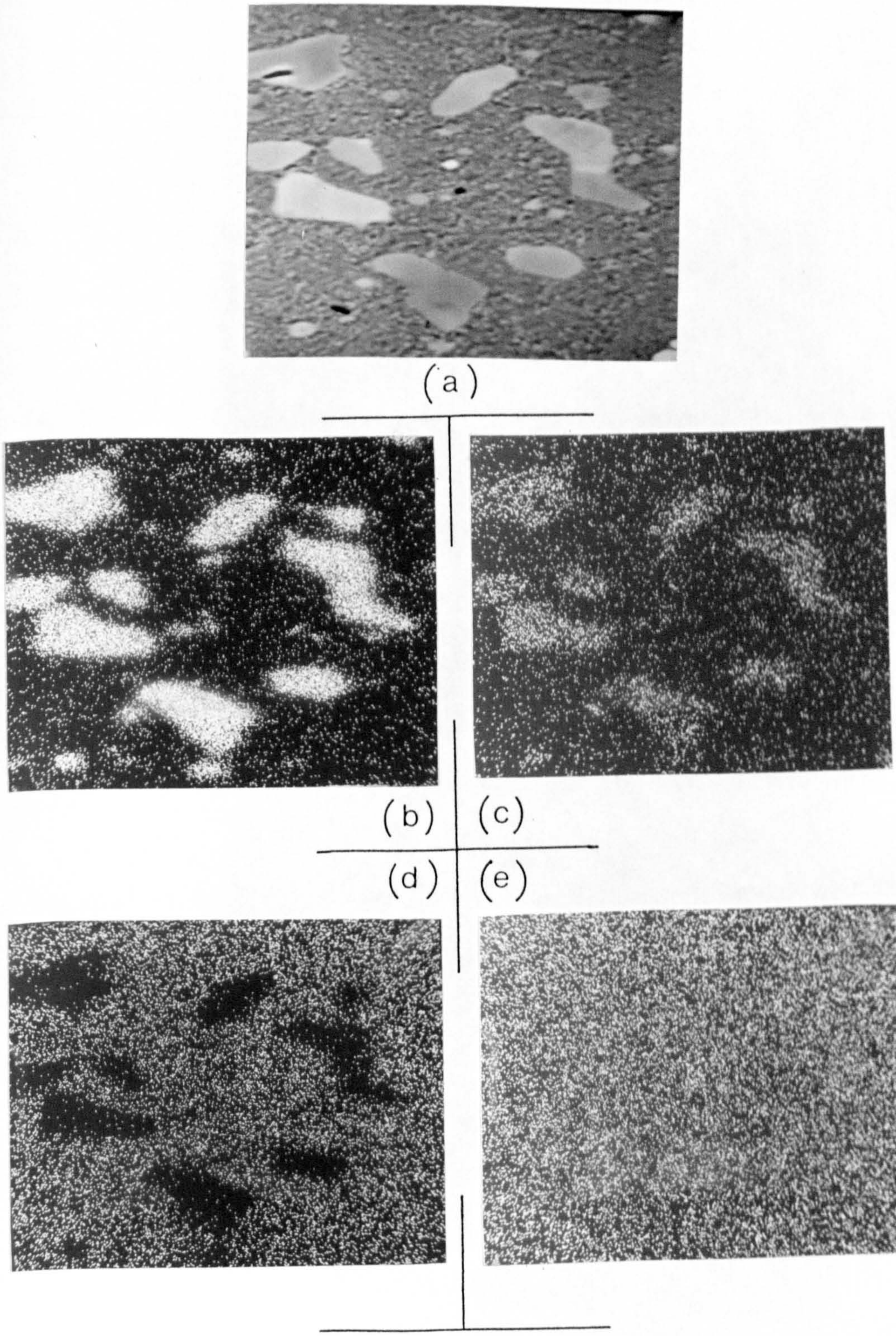


Fig.(38): EPMA X-ray scans showing alloying element distributions in tempered M15 specimen.

(a) microstructure x2000 (b) V

(c) W (d) Co (e) Cr

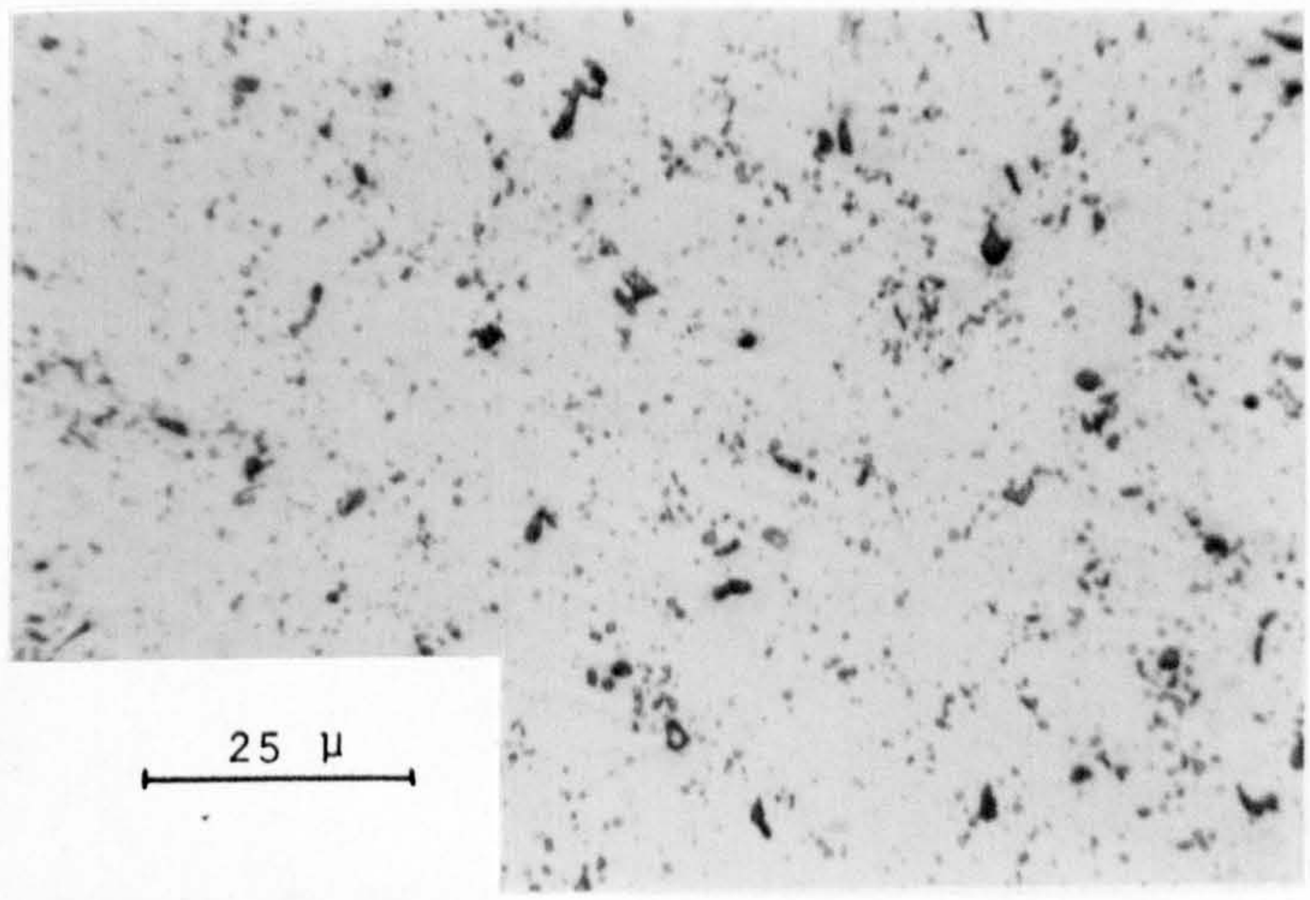


(a)

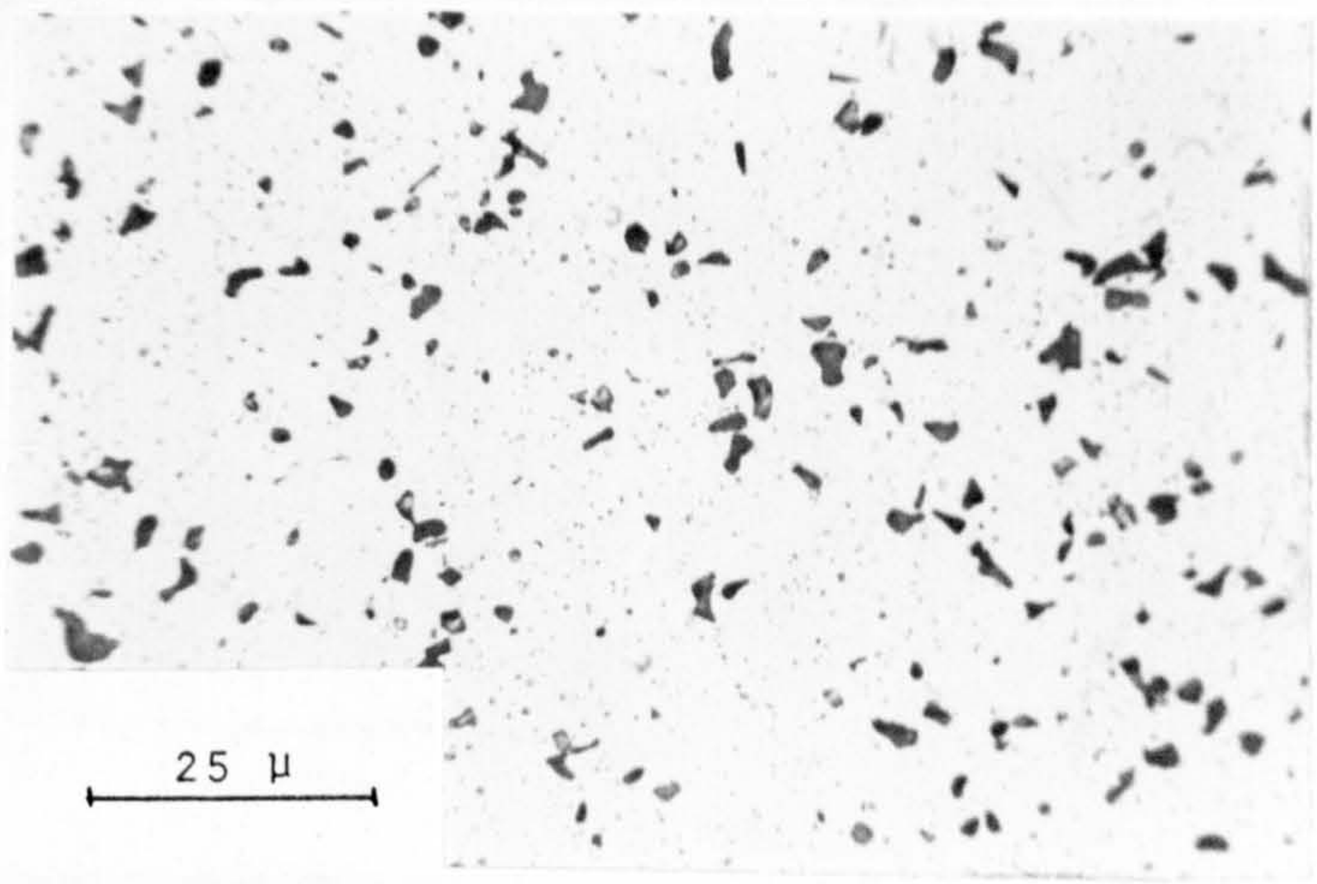


(b)

Fig.(39): Optical micrographs showing selective etching of carbides :

(a) M42 sample etched for $M_6C$ carbide.

(b) M15 sample etched for MC carbide.

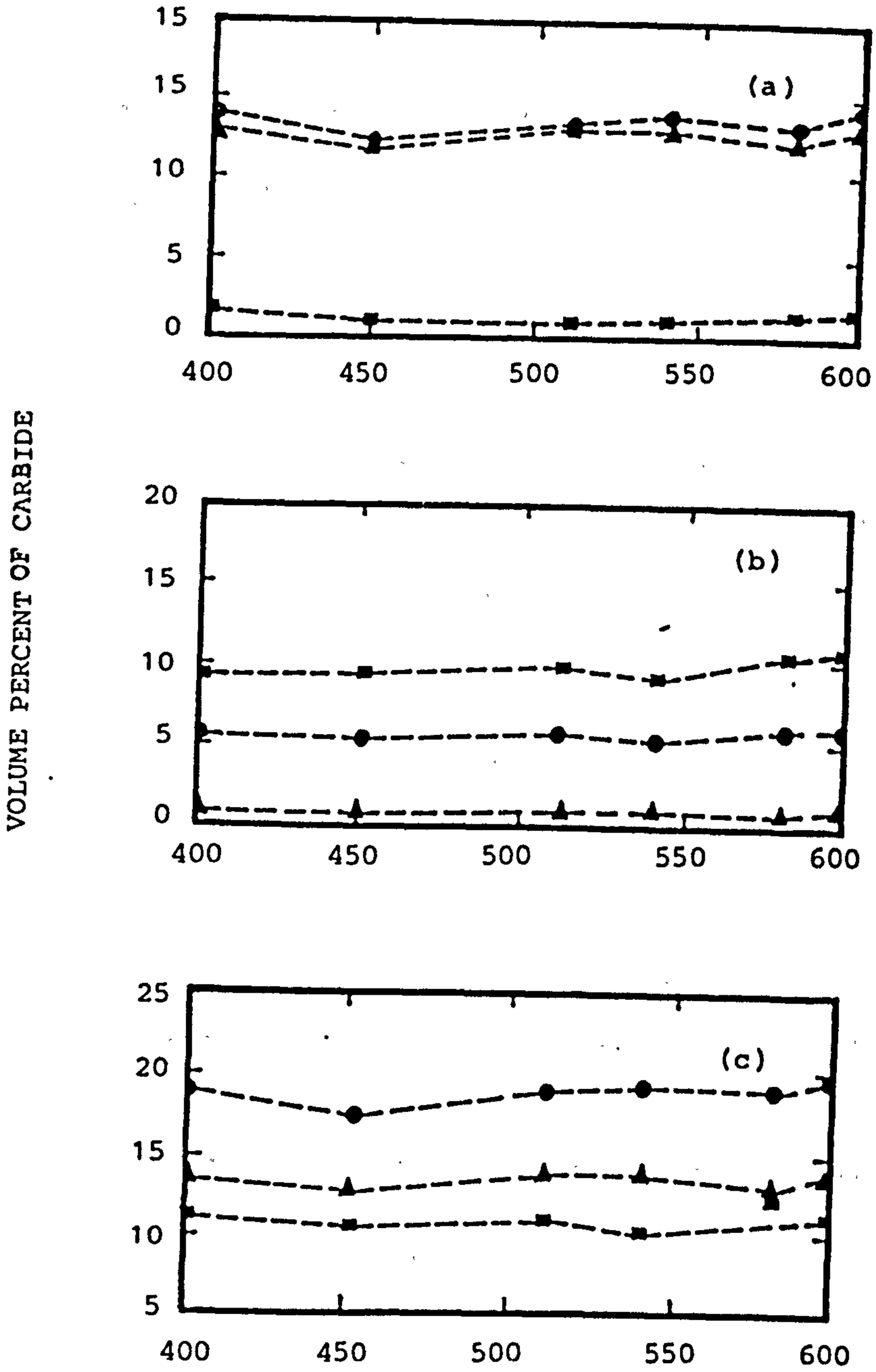


Fig.(40): Variation of carbides volume fraction with tempering temperature; (a) $M_6C$, (b) MC and (c) $M_6C$+MC .

● M42 ■ M15 ▲ M1

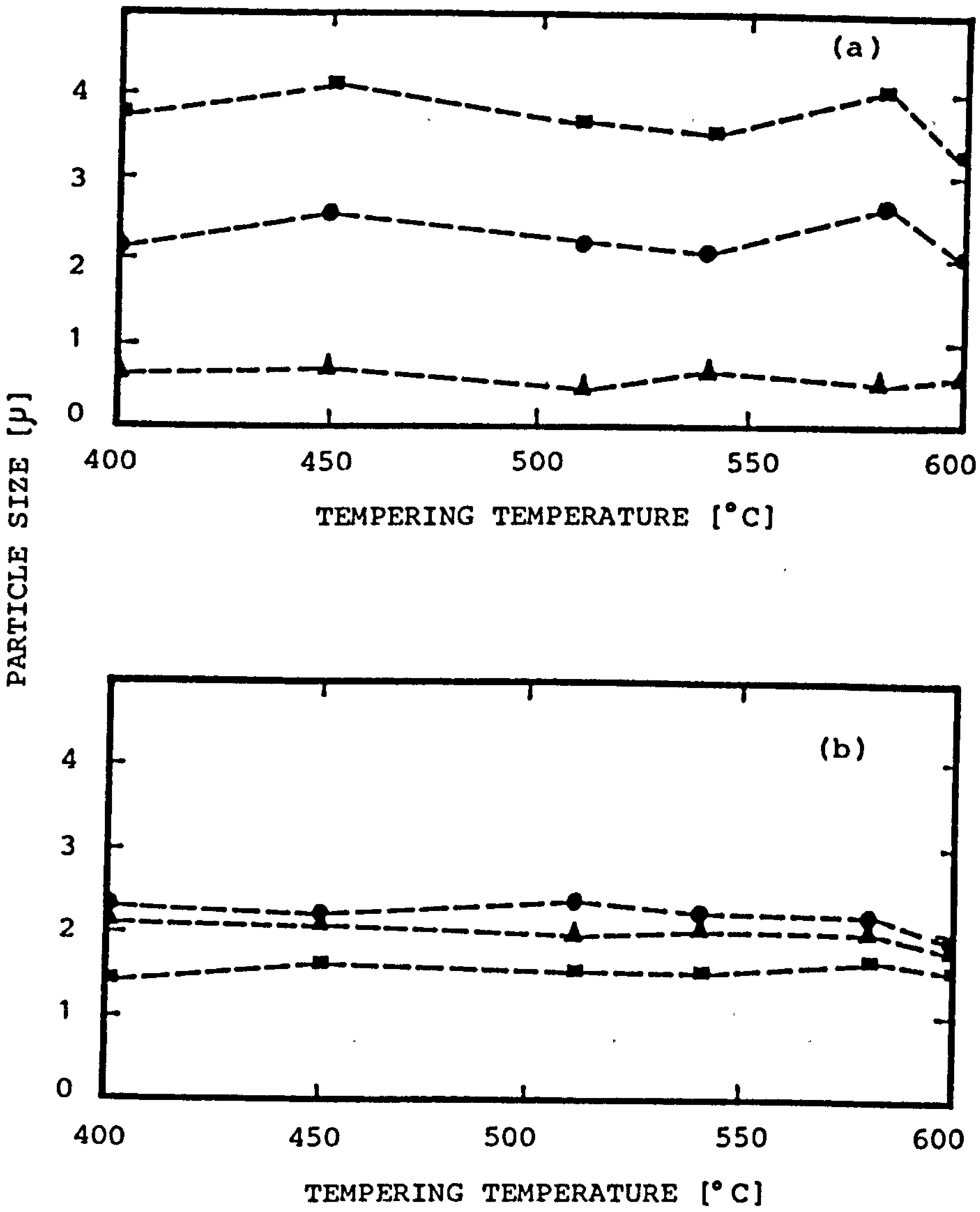


Fig.(41): Variation of average carbide particle size with tempering temperature for different steels. (a) MC carbide , (b) $M_6C$ carbide.

● M42 ■ M15 ▲ M1

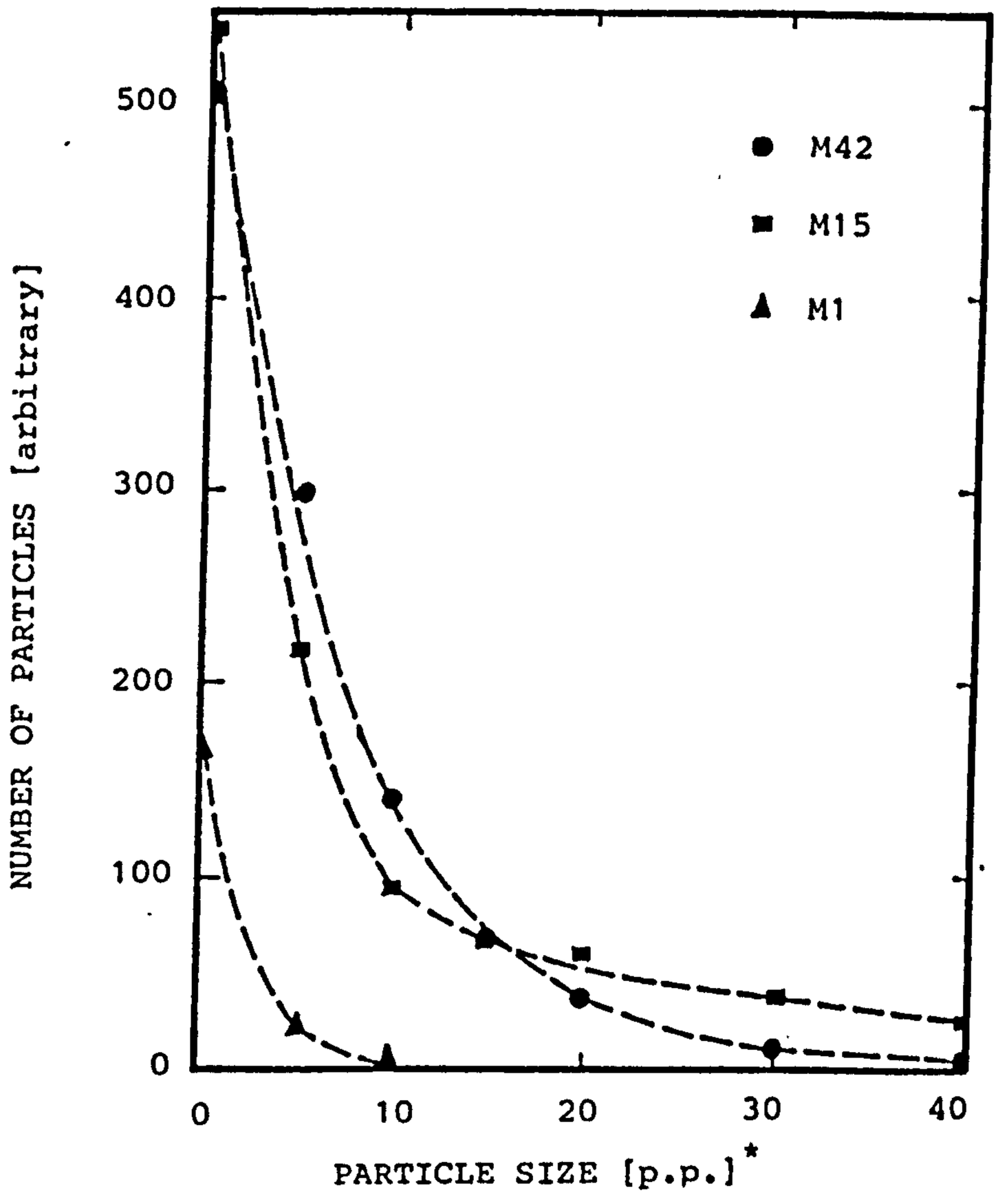


Fig.(42): Particle size distribution of MC carbide.

* 1p.p. = 0.28 μ

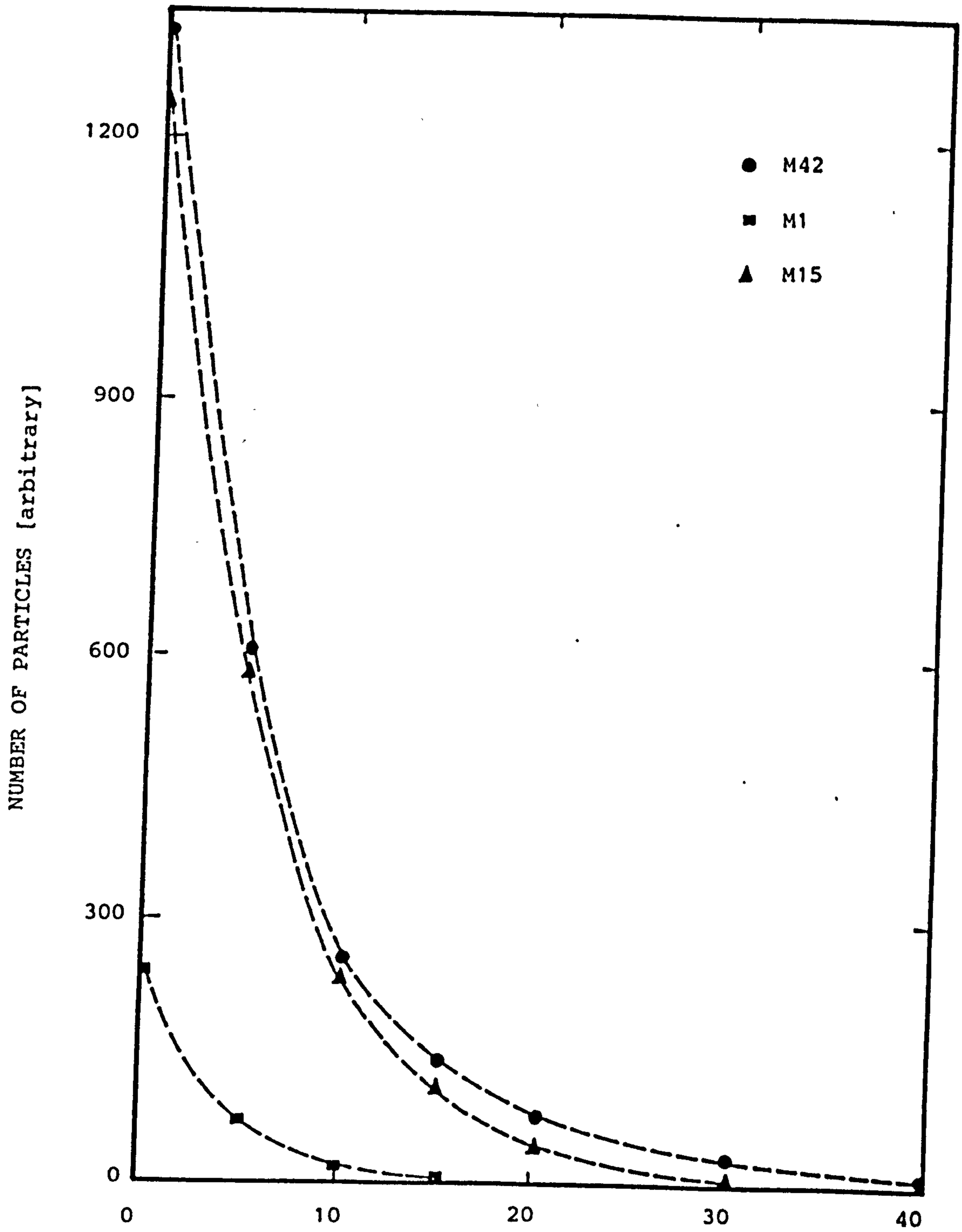


Fig.(43): Particle size distribution of $M_6C$ carbide .

* 1p.p. = 0.28 $\mu$

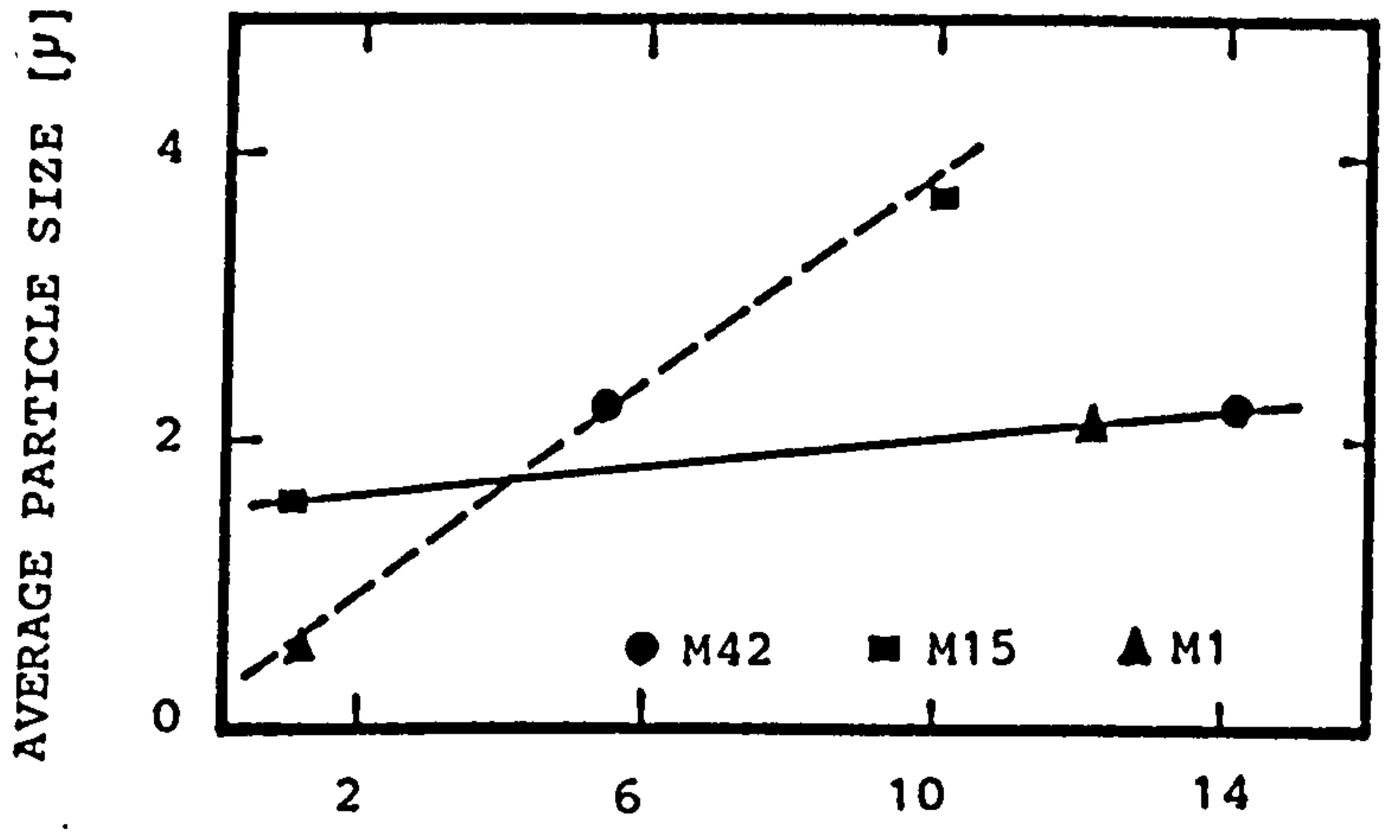


Fig.(44): Relation between average particle size and carbide volume fraction.

----- MC carbide

——— $M_6C$ carbide

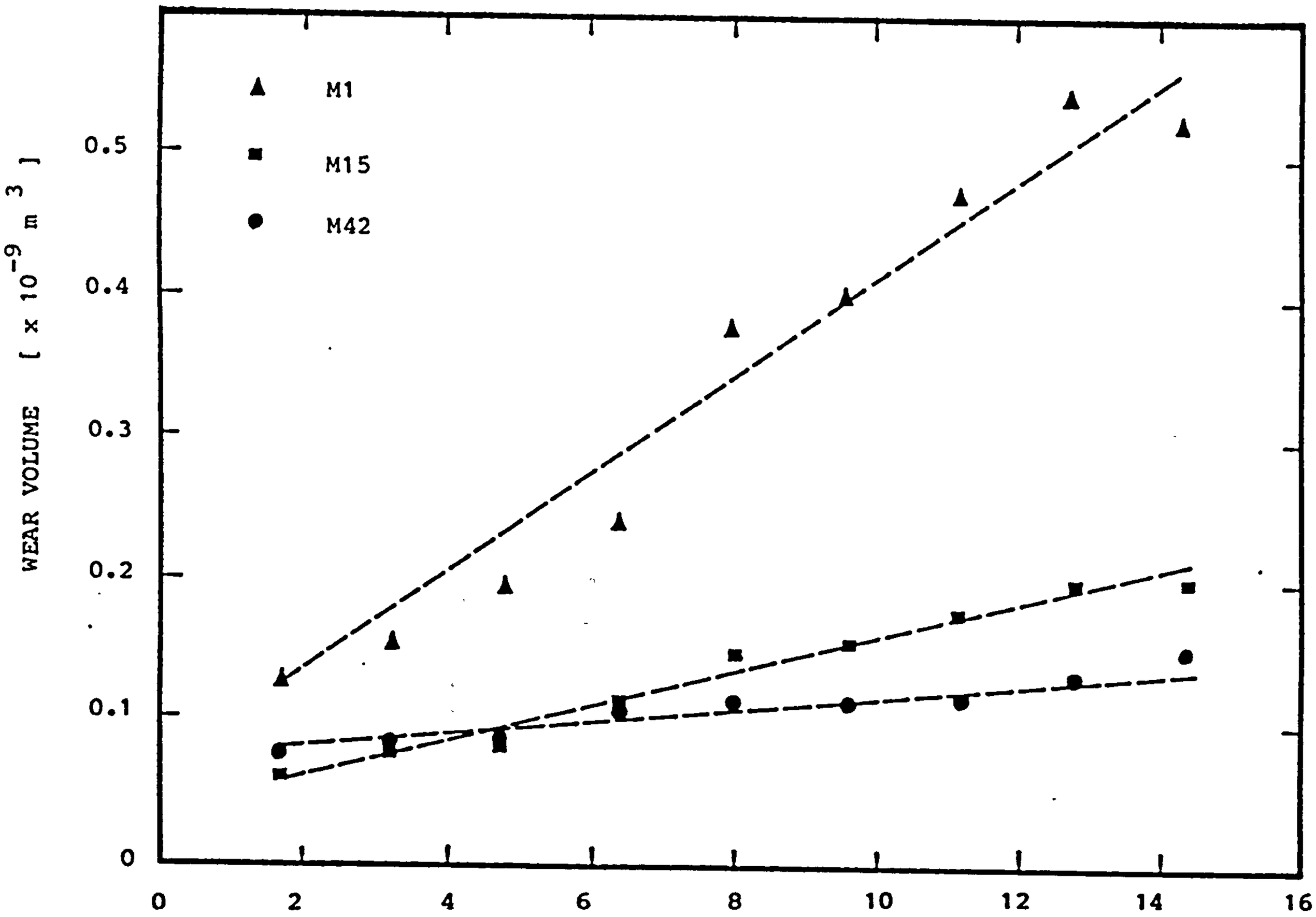


Fig.(45): Relation between wear volume and sliding distance , for samples tempered for 2+2 h at 530°C .

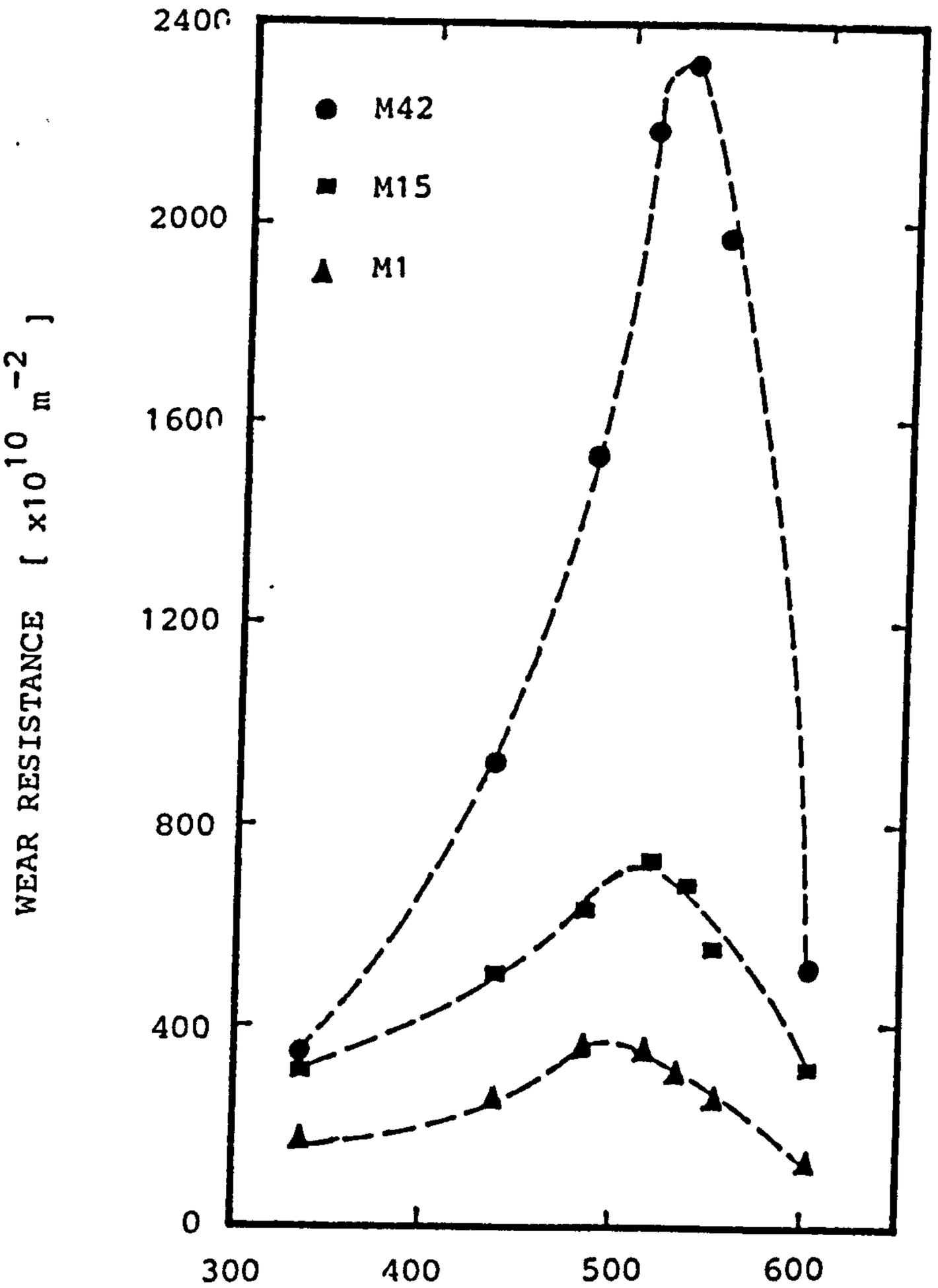


Fig.(46): Variation of wear resistance with tempering temperature.

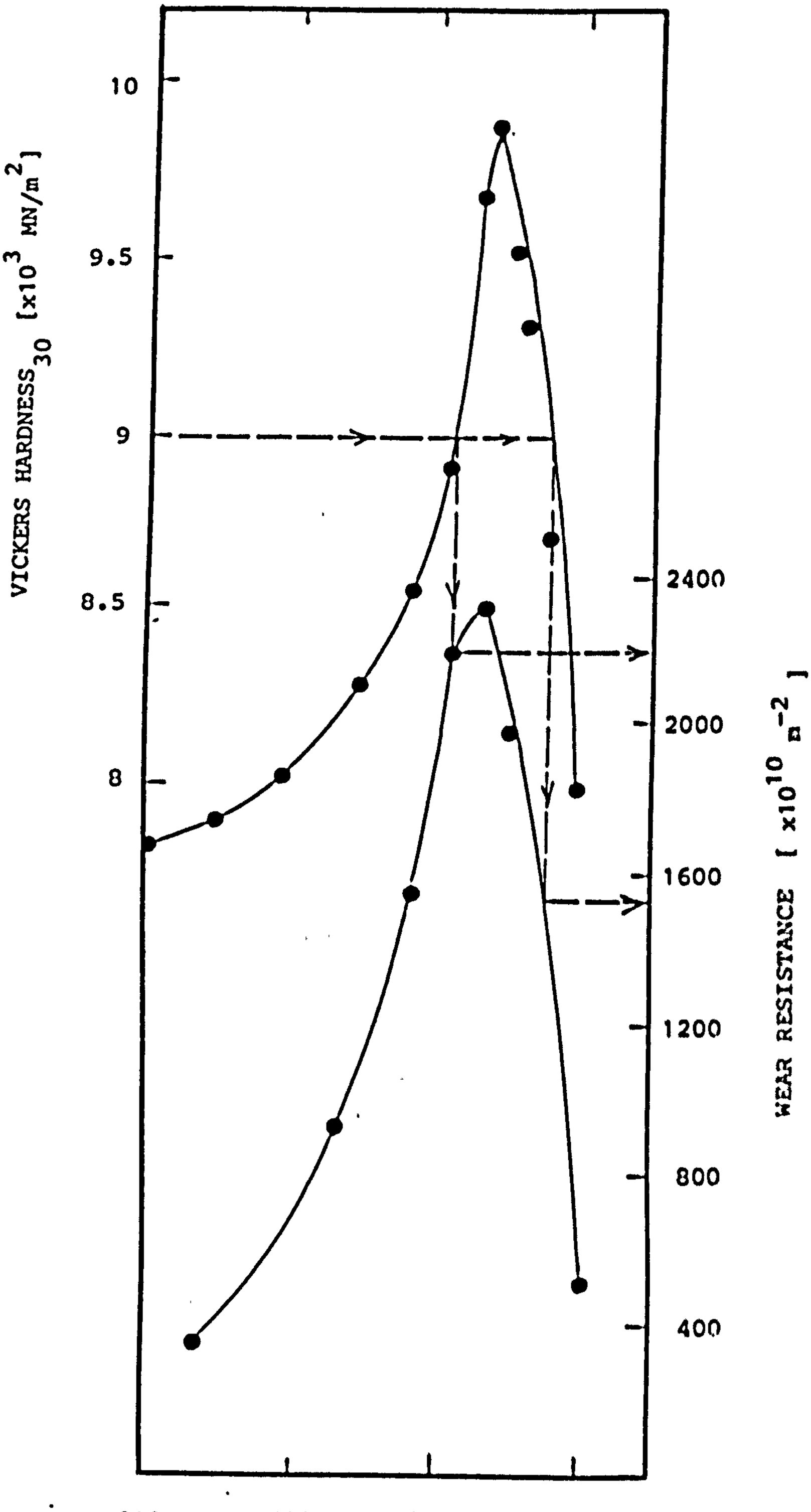


Fig.(47): Variation in hardness and wear resistance with tempering temperature for M42.

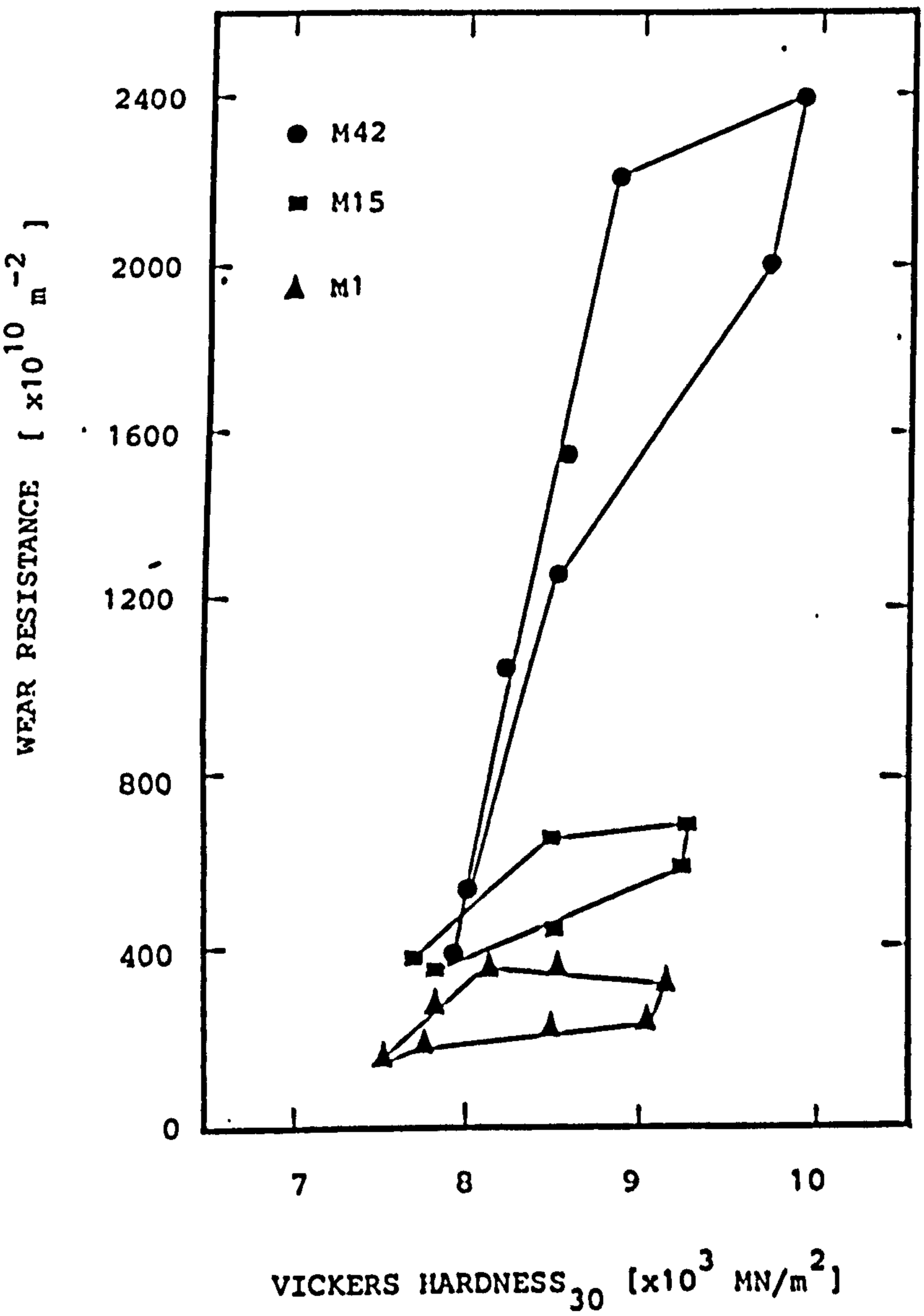


Fig.(48): Relation between wear resistance and hardness.

(a)

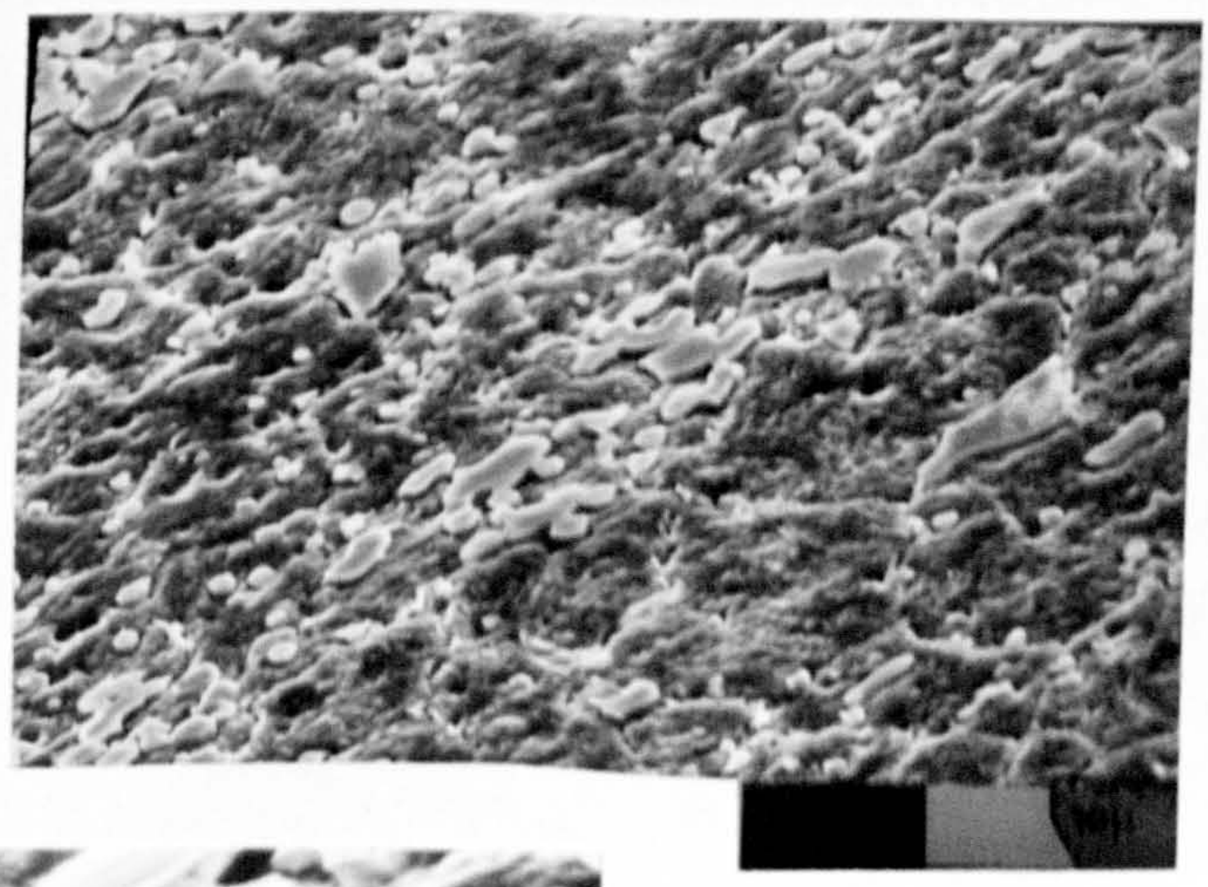

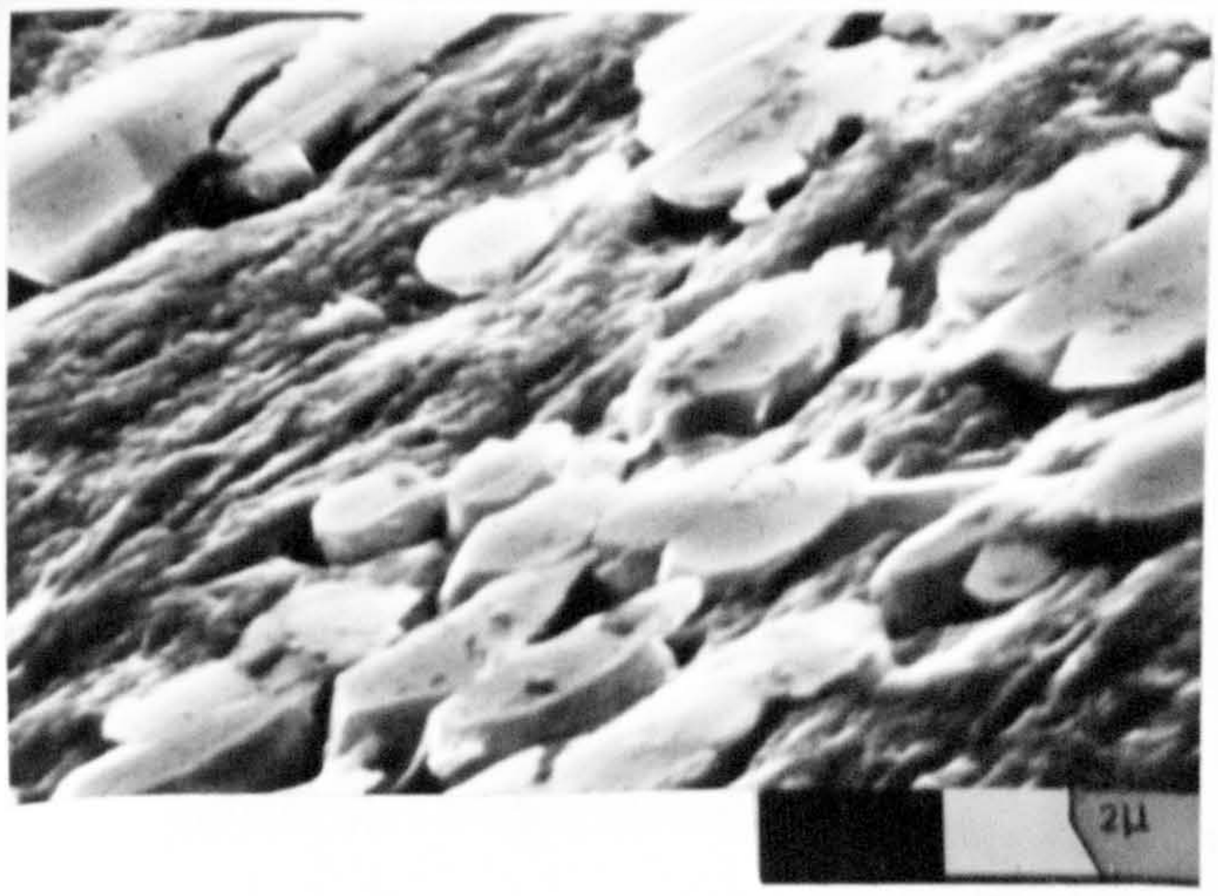


(b)

(c)

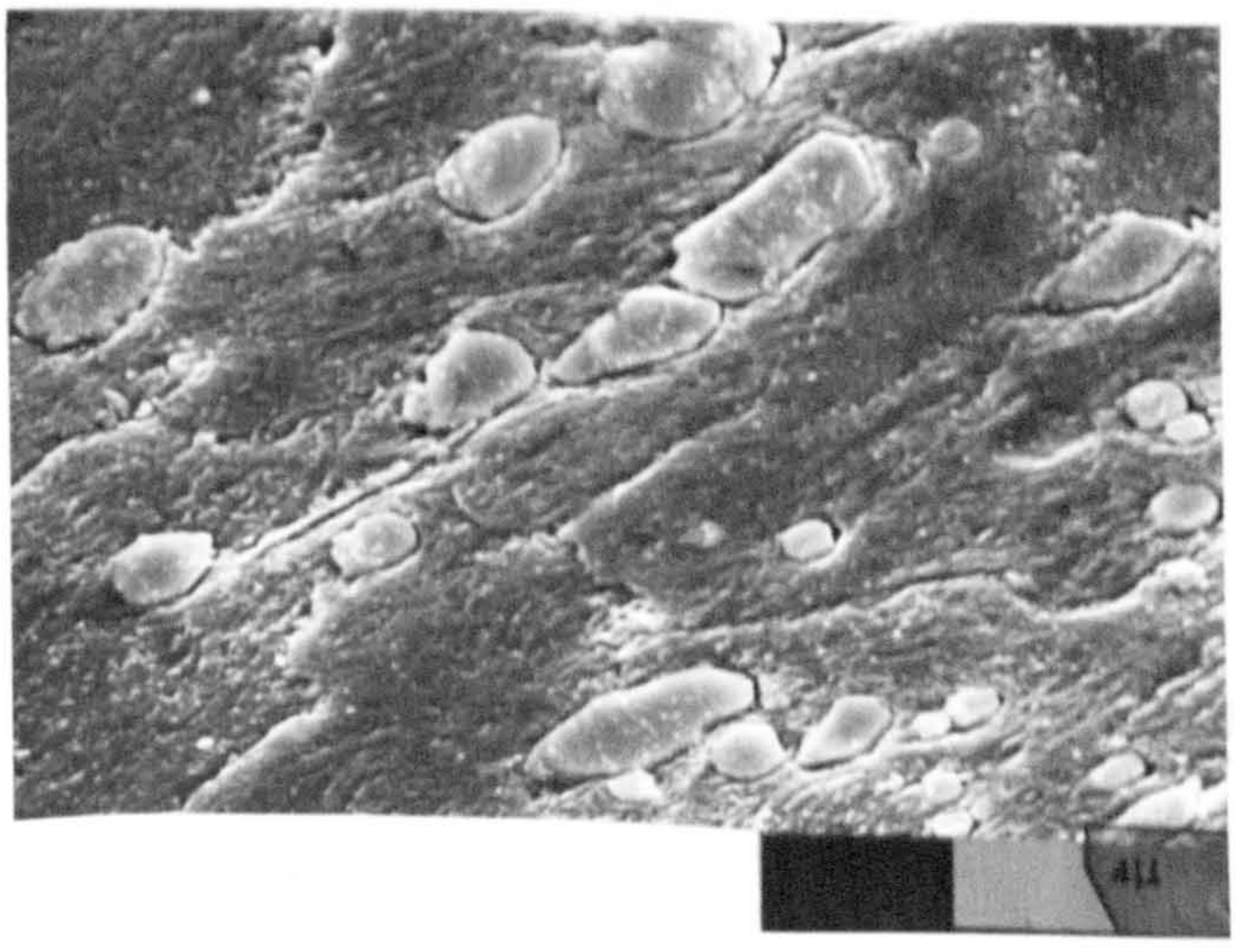

Fig.(49): SEM micrographs of wear surface of M42 tempered to peak hardness showing primary carbides fixed in their initial places.

(a),(b) etched samples (c) unetched sample .

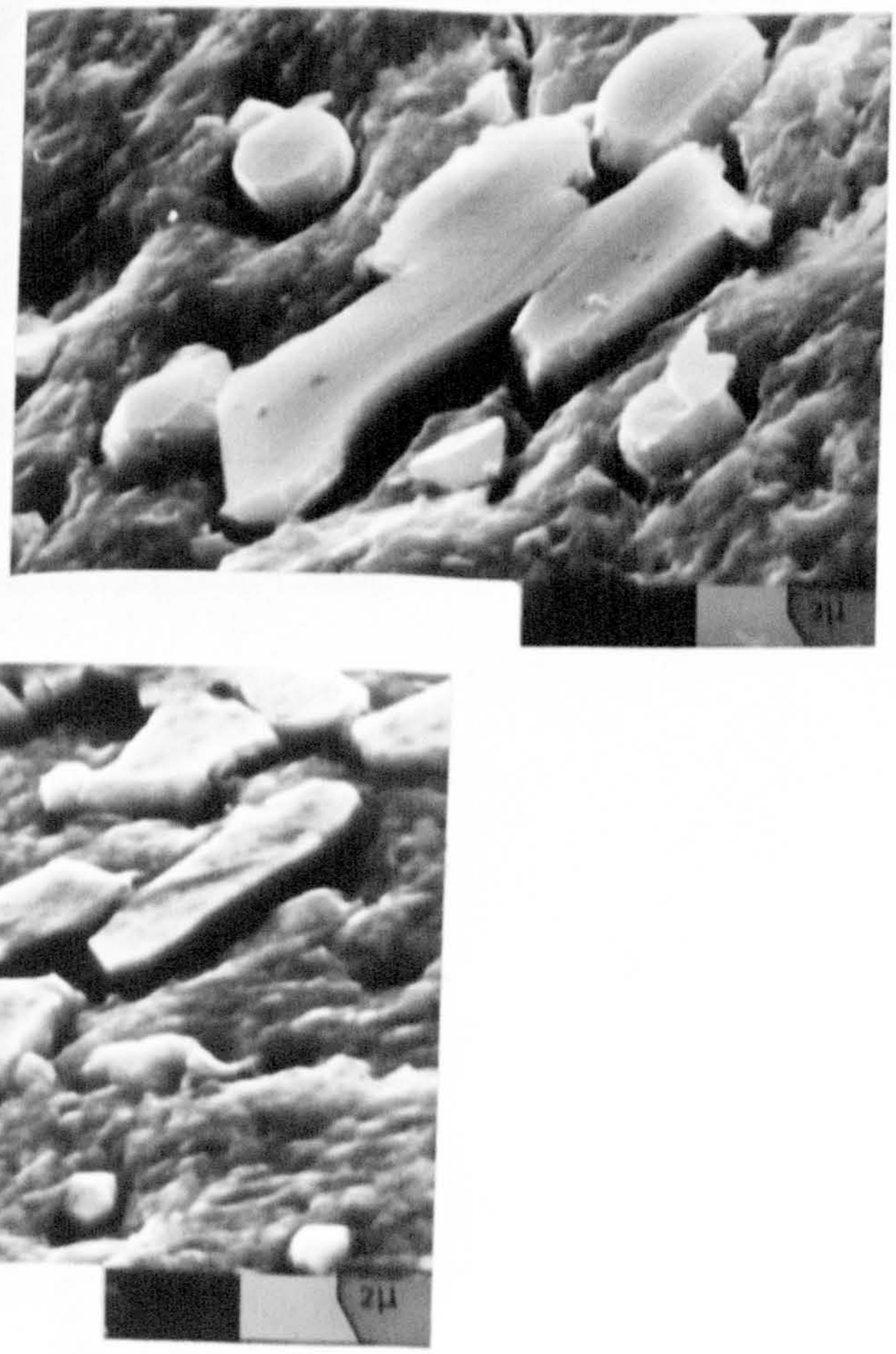


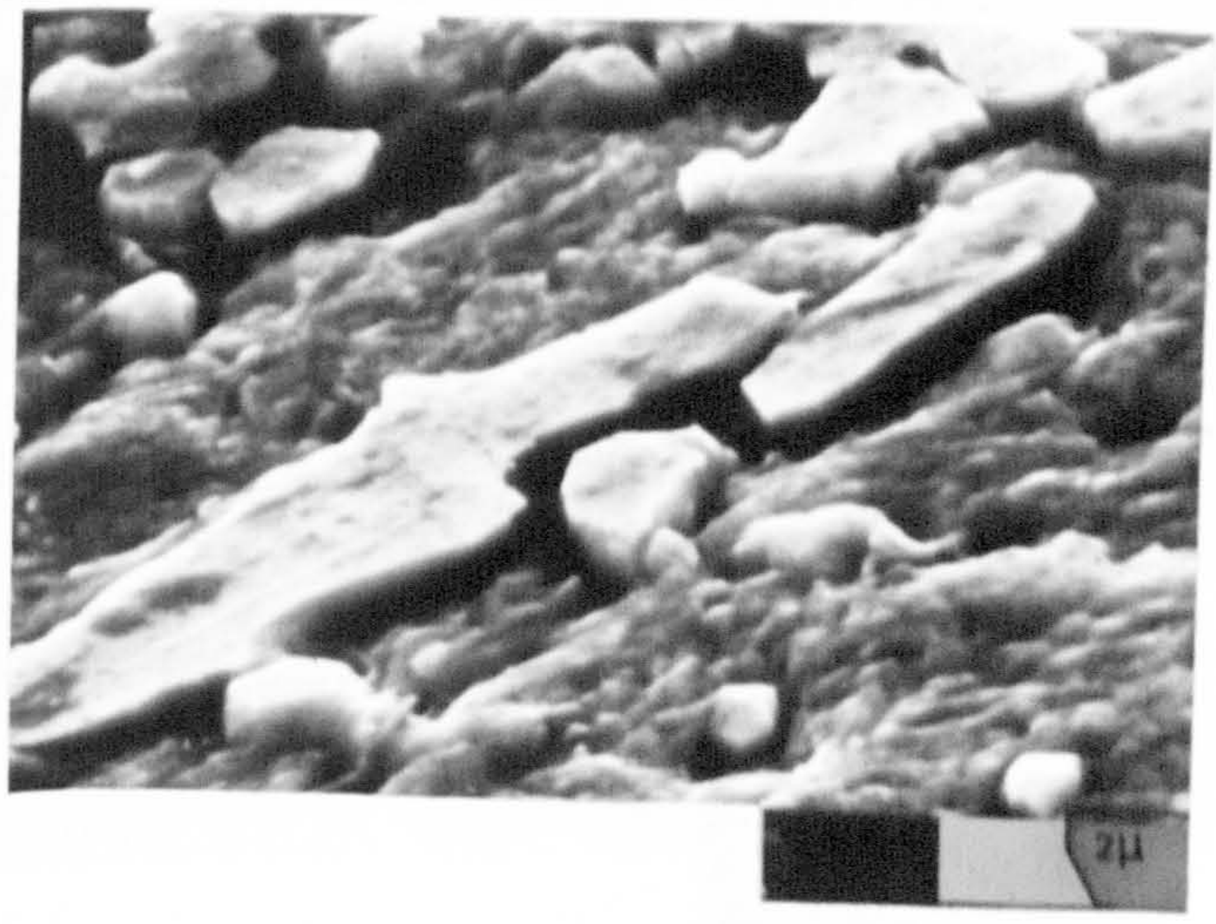


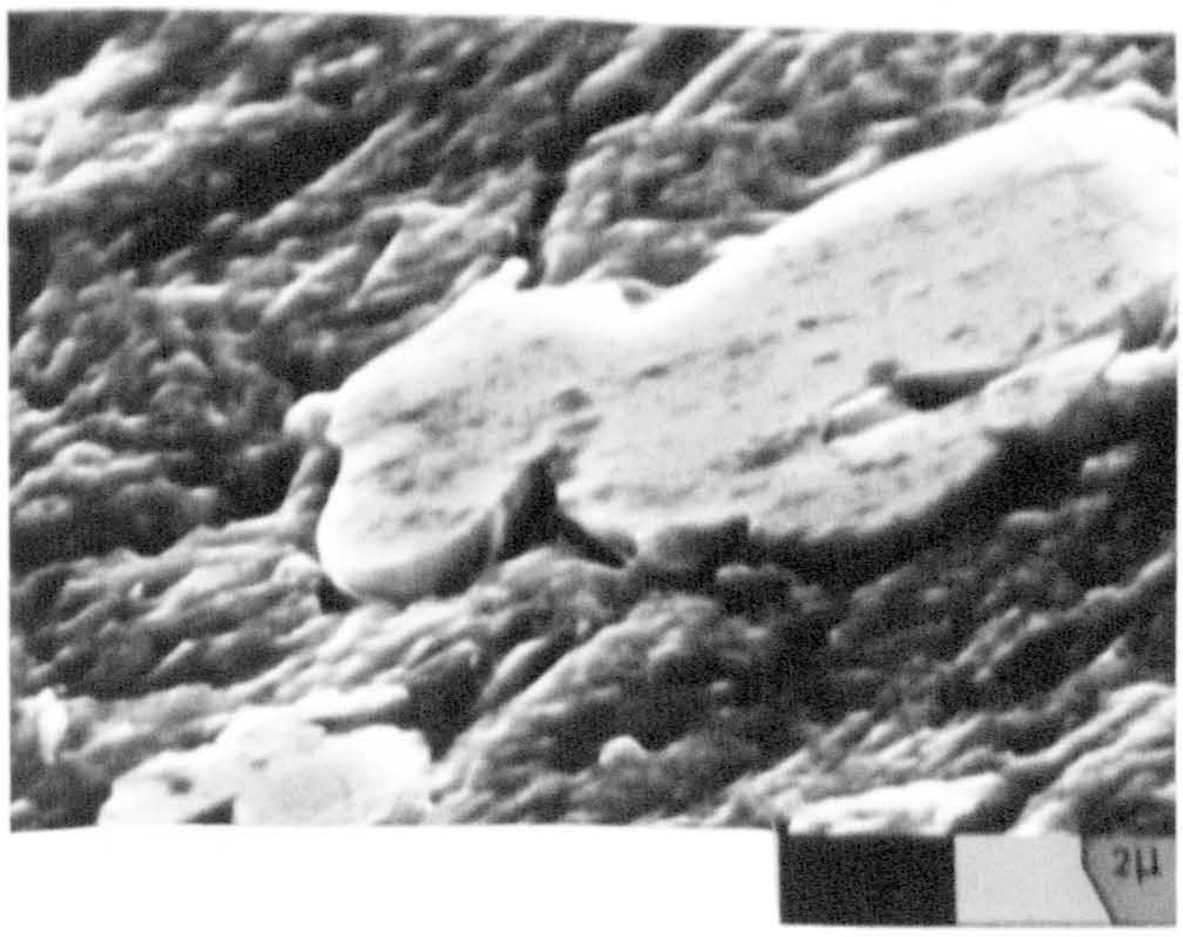


Fig.( 50): SEM micrographs showing flat surface of worn primary carbides in M42 sample tempered to peak hardness,worn surface being etched.

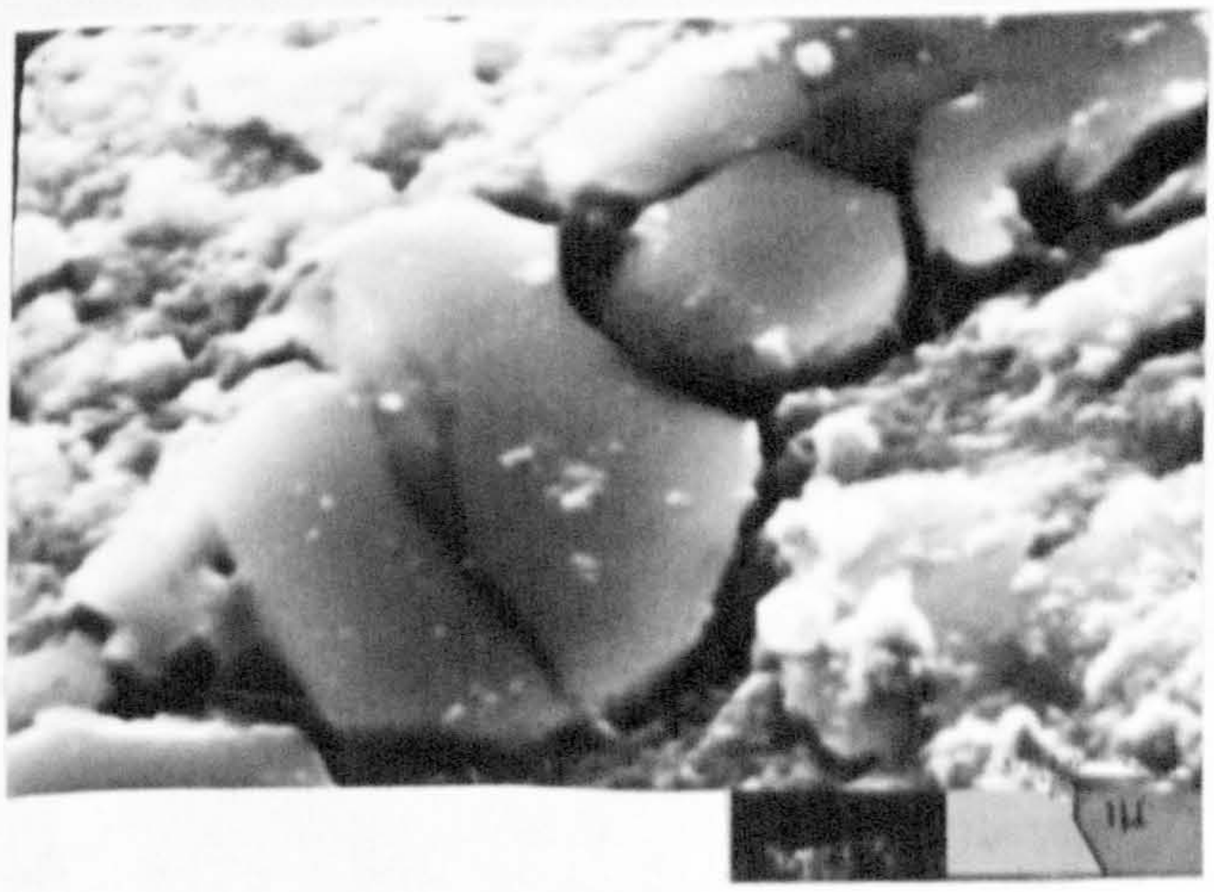

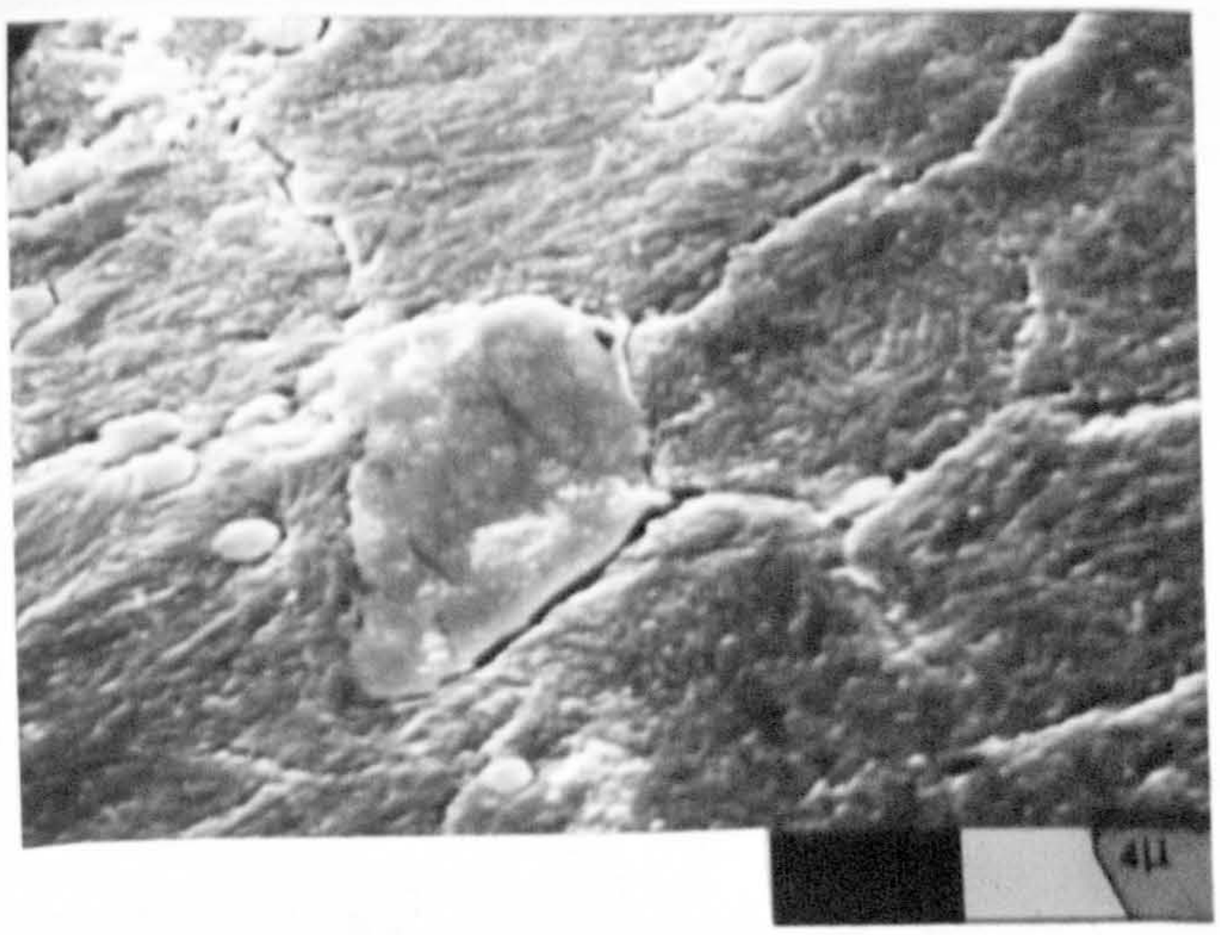

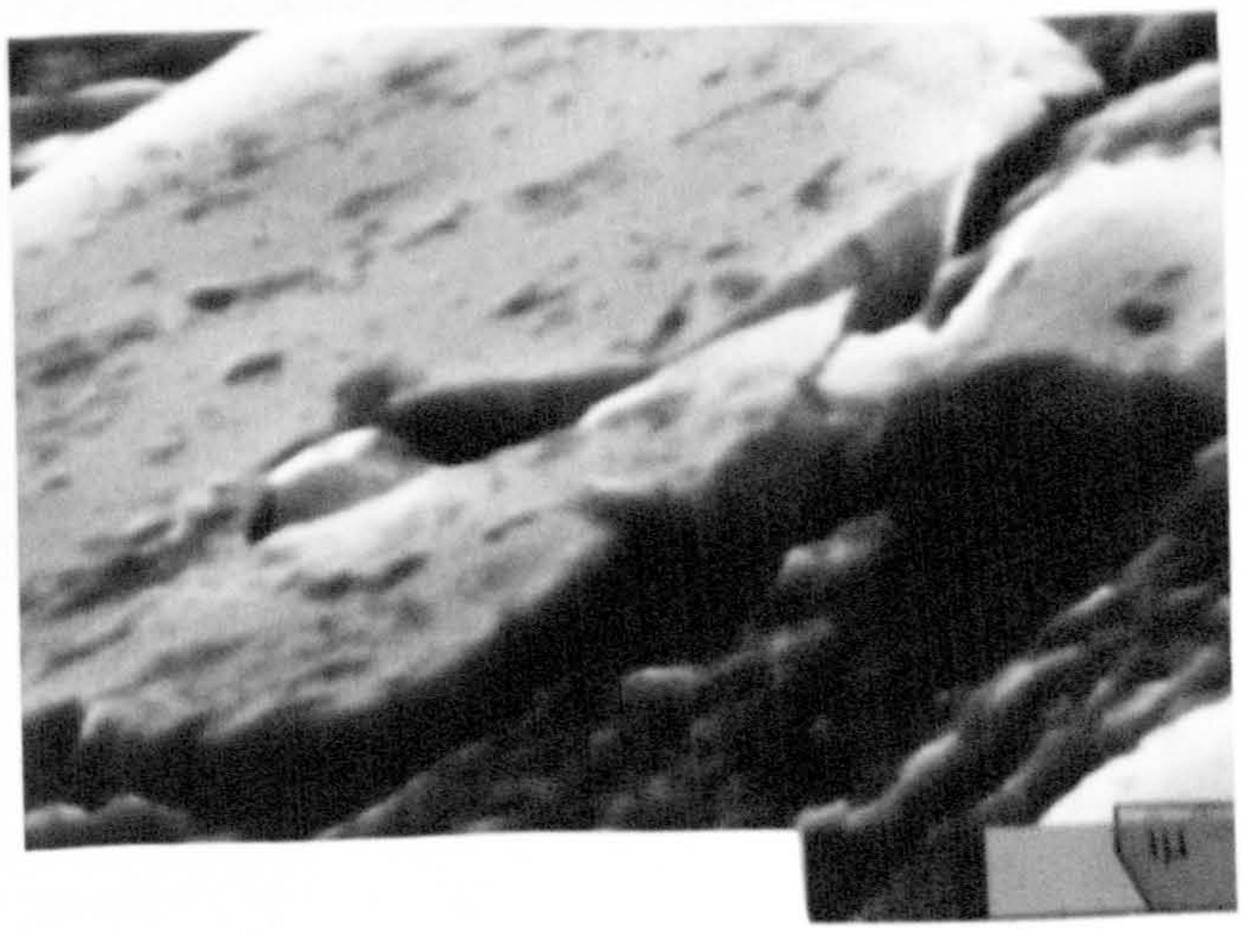

Fig.(51): SEM micrographs showing cracks in primary carbides in samples tempered to peak hardness.

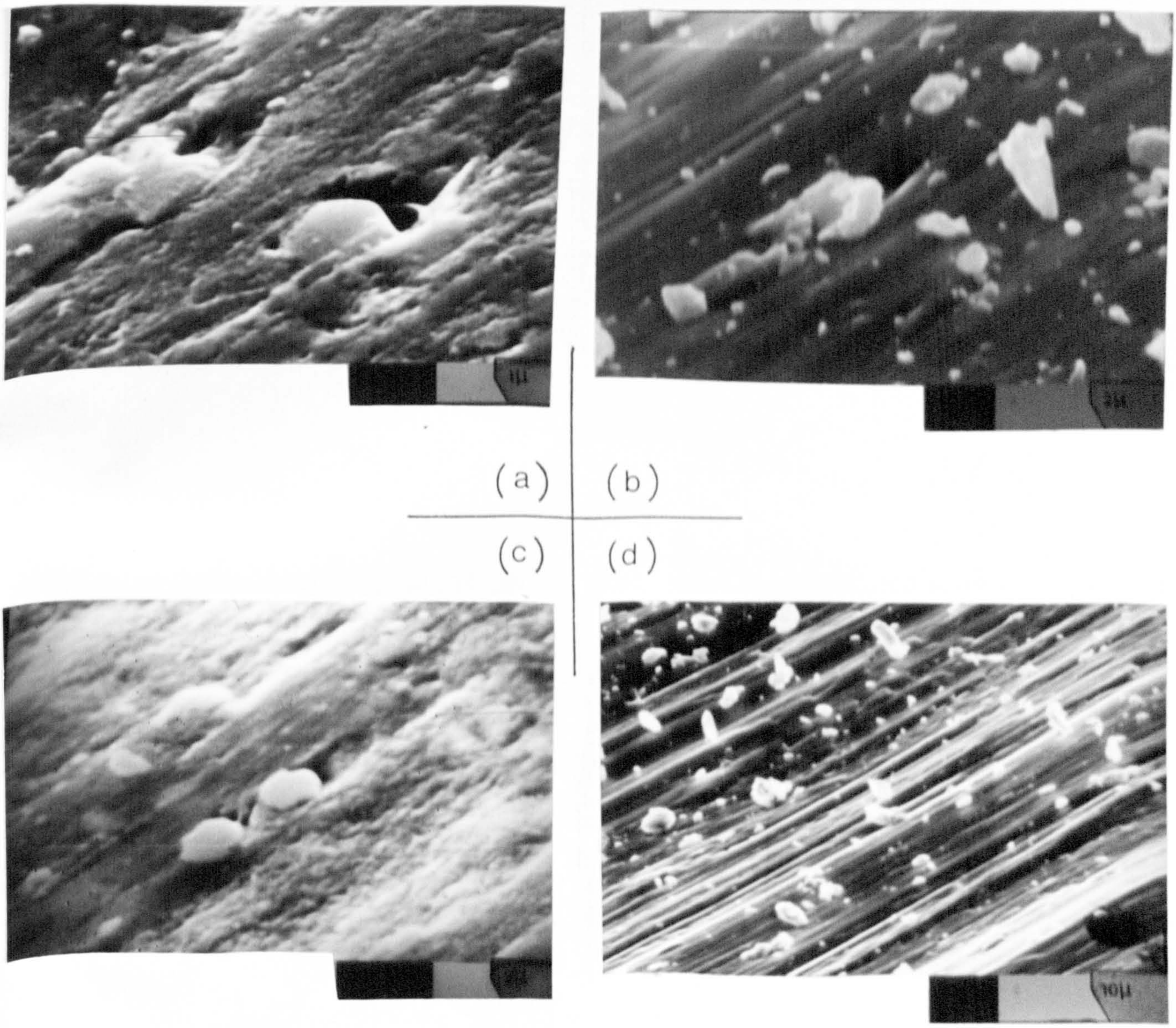


Fig.(52): SEM micrographs showing worn surface of over-tempered high speed steels.

(a) primary carbide torn off the surface.

(b),(c) primary carbides abrading the surface.

(d) loose primary carbides and the abraded surface.